NASA CR-134704
MTI 74TR20

NASA

DEVELOPMENT OF PROCEDURES FOR CALCULATING STIFFNESS AND DAMPING PROPERTIES OF ELASTOMERS IN ENGINEERING APPLICATIONS

PART II: ELASTOMER CHARACTERISTICS AT CONSTANT TEMPERATURE

by
Pradeep K. Gupta
Juergen M. Tessarzik
Loretta Cziglenyi

MECHANICAL TECHNOLOGY INCORPORATED

Prepared for

NATIONAL AERONAUTICS AND SPACE ADMINISTRATION

NASA – Lewis Research Center

Contract NAS3-15334

Robert E. Cunningham, Project Manager

1. Report No	2 Government Accession No.	3. Recipient's Catalog No.
NASA CR-134704		

4. Title and Subtitle	5. Report Date
DEVELOPMENT OF PROCEDURES FOR CALCULATING STIFFNESS AND DAMPING PROPERTIES OF ELASTOMERS IN ENGINEERING APPLICATIONS PART II: ELASTOMER CHARACTERISTICS AT CONSTANT TEMPERATURE	April 26, 1974
	6. Performing Organization Code

7. Author(s)	8. Performing Organization Report No.
Pradeep K. Gupta Juergen M. Tessarzik Loretta Cziglenyi	MTI 74TR20
	10. Work Unit No.

9. Performing Organization Name and Address	11. Contract or Grant No.
Mechanical Technology Incorporated 968 Albany-Shaker Road Latham, New York 12110	NAS3-15334
	13. Type of Report and Period Covered

12. Sponsoring Agency Name and Address	13. Type of Report and Period Covered
	Contractor Report
National Aeronautics and Space Administration Washington, D.C. 20546	14. Sponsoring Agency Code

15. Supplementary Notes

Project Manager, Robert E. Cunningham, Bearings & Mechanical Power Transfer Branch, NASA-Lewis Research Center, Cleveland, Ohio 44135

16. Abstract

Dynamic properties of a commercial polybutadiene compound have been determined at constant temperature of 32 C by a forced-vibration resonant mass type of apparatus. The constant thermal state of the elastomer was ensured by keeping the ambient temperature constant and by limiting the power dissipation in the specimen. Experiments were performed with both compression and shear specimens at several preloads (nominal strain varying from 0 to 5 percent) and the results are reported in terms of a complex stiffness as a function of frequency. Very weak frequency dependence is observed and a simple power law type of correlation is shown to represent the data well. Variations in the complex stiffness as a function of preload are also found to be small for both compression and shear specimens.

17. Key Words (Suggested by Author(s))	18. Distribution Statement
Dynamic Properties Vibration Test Rig Vibration Literature Survey Viscoelastic Models Analytical Prediction Methods Elastomers	Unlimited

19. Security Classif. (of this report)	20. Security Classif. (of this page)	21. No. of Pages	22. Price*
Unlimited	Unclassified	125	

* For sale by the National Technical Information Service, Springfield, Virginia 22151

FOREWORD

The work described herein was performed at Mechanical Technology Incorporated (MTI) under NASA Contract NAS3-15334 with Mr. Robert E. Cunningham, NASA-Lewis Research Center, as Project Manager. At MTI, Dr. Robert H. Badgley, Manager, Machinery Dynamics Center, was the Program Manager. The work reported is part of a continuing program whose objectives are, firstly, to develop, through analytical and experimental investigations, elastomer dynamics technology and, secondly, to reduce this technology to practical designer-oriented form, so that it may be used to calculate the dynamic mechanical properties of elastomeric damping materials.

TABLE OF CONTENTS

TABLE OF CONTENTS (concluded)

LIST OF ILLUSTRATIONS

LIST OF ILLUSTRATIONS (continued)

LIST OF ILLUSTRATIONS (concluded)

I SUMMARY

This report documents an experimental investigation to determine the dynamic properties of elastomer test samples at constant temperature. The objective of the investigation was to identify the influence of excitation frequency, preload, shape, and deformation amplitude on the dynamic properties under shear and compressive loading.

An existing forced-vibration resonant-mass-type test rig was refined to control the ambient temperature around the elastomer sample and monitor the power dissipated in the specimen. These two constraints ensure a constant thermal state of the elastomer. Polybutadiene, a broad temperature range (BTR) elastomer, was selected as the test material for this investigation.

Three compression specimens with varying shape factors were tested at preloads corresponding to a compression of 2-1/2 and 5 percent of the initial specimen thickness. The ambient temperature and power dissipation were monitored and controlled effectively such that the elastomer temperature was 32°C to within 1°C. The test frequencies were varied from 100 to 1000 Hz. Test results are presented as complex stiffness values for each specimen as a function of frequency. Changes in stiffness as a function of frequency or preload were found to be small for the compression specimens, and within the test frequency range a simple power law relationship was used to represent the variation with frequency.

Three shear specimens were tested at preloads corresponding to nominal strains of 0, 2-1/2 and 5 percent. The frequency band was also 100 to 1000 Hz. The complex stiffness in this case was somewhat higher than that observed with the compression specimens, but the difference is consistent with the difference in static stiffness as calculated by conventional shape factor formulas. Variations of complex stiffness with either frequency or preload were found to be small, and a simple power law relationship was again used to represent the variation with frequency.

The compression samples, although covering a four to one range of diameter-to-height ratio, were each designed to have similar stiffnesses by varying the

number of individual elastomer elements, and applying published shape factor values. The measured dynamic stiffnesses of the three compression samples were similar.

The shear samples were each designed to have similar stiffnesses by varying the number of elements in inverse proportion to the sheared area. The resultant dynamic stiffnesses were similar for each of the shear samples.

II. INTRODUCTION

Elastomeric dampers have been successfully applied in the control of mechanical vibration problems. Increasingly demanding applications, particularly to vibration problems of rotors and power transmission shafting, are being considered. However, the availability of design-oriented data for such applications is limited. Dynamic testing under accurately controlled conditions is the means to develop this data and to determine the influence of important geometrical, environmental, and chemical design parameters. Physical properties of elastomeric materials can then be evaluated and used in the selection of materials for particular applications.

Substantial advances have been reported in the development of experimental methods for dynamic testing, and the determination of the influence of chemical composition on the observed dynamic response of the material. Chiang, et. al., in Part I of this series [1]*, described procedures for testing elastomer specimens in a forced-vibration, resonant mass test rig. The ability of the resonant mass approach to obtain data over a wide range of frequencies, amplitudes, and preloads was demonstrated. In addition, the significance of uncertainties in temperature variation was identified.

A narrative account of various test methods and some of their refinements developed during the past two decades has been recently presented by Miller [2]. In addition to the measurements of frequency and amplitude of deformation, a major concern is with the temperature level and gradient in the elastomer. It has been suggested that the thermal state of the material is one of the prime candidates dominating its dynamic behavior. Hence, monitoring the temperature of operation and the energy dissipated in the elastomer becomes essential in an experimental setup for elastomer testing.

The significance of dynamic testing in comparison with simple static tests has been well established. Larsen [3] has demonstrated that the dynamic stiffness

*Numbers in brackets denote References listed at the end of this report.

is generally higher than the static spring rate. The temperature dependence of the two properties as reported by Larsen is even more interesting in that although the dynamic stiffness decreases with an increase in temperature, the changes in the long chain molecules as a result of higher temperature results in increased static stiffness.

Cardillo [4] used a force vibration type hydraulic tester to determine the stiffness and damping properties of a number of materials. The effects of frequency, amplitude, preload, and temperature were also considered. In the case of butyl stock, it was shown that increasing the carbon black content in the compound results in increased dynamic stiffness and damping characteristics. Meyer and Sommer [5] have considered compounds based on styrenebutadiene and polybutadiene elastomers in their investigation with regard to the effects of compositional and testing variations. Their results concerning the influence of carbon black content are in agreement with those reported by Cardillo. In a more recent work, Sommer and Meyer [6] have summarized the effects of variations in rubbers, fillers, oils, level of crosslinking and processing factors such as mixing, curing, and storage on the dynamic properties of elastomeric products.

The work reported herein was motivated by a need to further improve the dynamic test methods for elastomers with particular reference to thermal conditions. By controlling the ambient temperature and the power dissipated in the elastomer specimen, the uncertainties in the dynamic behavior of the test material are reduced to a minimum. The primary objective of the investigation is to identify the influence of excitation frequency, preload, shape factor, and deformation amplitude on the dynamic properties of elastomer specimens under conditions wherein the thermal state of the material remains unchanged.

A previously designed [1] forced vibration type of testing apparatus was modified to control the temperature of the two metallic plates holding the elastomer sample. Also, heating and cooling systems were designed to control the ambient temperature in a closed chamber in which the test specimens are located. An electronic circuit to monitor the power dissipation was designed

with the objective of limiting the temperature gradients in the elastomer specimens. Polybutadiene, being a known broad temperature range elastomer, was selected as the test material. The influence of excitation frequency, amplitude of deformation, preload, and shape factor were examined under a constant ambient temperature and very low and bounded temperature gradients in the test specimen. Both shear and compression loadings were considered with suitably designed specimens. The compression specimens were designed with varying shape factors with the objective of identifying the variations in the dynamic behavior of the elastomer as a function of specimen geometry under isothermal conditions.

The experimental details of the apparatus are described in detail in the next section, which is followed by a fairly comprehensive analysis of the dynamic response of the test rig. Experimental results for both compression and shear samples are then presented. A complete summary of these results is presented in a tabulated form. Finally, the dynamic behavior of the elastomer as a function of the experimental conditions described above is discussed.

III. EXPERIMENT DESIGN AND TEST PROCEDURE

A forced-vibration resonant mass type of apparatus was used to test the dynamic properties of the elastomer samples. A general description of the test rig is presented below before discussing the design characteristics. The details of selected material, test specimens, required instrumentation and the test procedure are also presented in this section.

A. Description of Elastomer Test Rig

The basic features of this test rig have largely been developed in the course of work conducted under a previous phase of the present NASA Contract. The test rig was designed to impose precisely measured uniaxial vibration amplitudes upon a selected elastomer sample at desired test frequencies and under selected force preloads.

The rig is capable of testing, through the base-excitation resonant-mass technique, elastomer samples of virtually any size and shape (test sample cavity is a cylinder approximately 12.7 cm (5 in.) high by 12.7 cm (5 in.) in diameter over a wide frequency range. Selection of the resonant mass to match elastomer sample properties permits testing at very high amplitudes at resonance, with correspondingly lower amplitudes at off-resonance conditions. Thus, maximum test amplitudes are limited by elastomer characteristics and shaker input power rather than by the test rig itself.

The vibration input to the test rig in all tests was obtained from a commercially-available electromagnetic shaker system* capable of delivering 66,700 N (15,000 lb) force in the sinusoidal mode of vibration.

Prior to the acquisition of the elastomer test data reported here, ambient temperature control facilities in the form of heating elements and cooling coils embedded in the sample base holder and circuitry to monitor the power dissipated in the specimen were added. Uncertainties due to temperature

*Ling Electronics, Model 335A Shaker With PP-35/70 VC Power Amplifier and SCO-100 Servo Control Center.

variations are now minimized by accurately controlling the ambient temperature, and by limiting the heat generated in the specimen. In addition, new holding plates for the elastomer samples were made; two different configurations provided shear and compression loading of the samples, respectively.

B. Design Characteristics of the Test Rig

A schematic of the elastomer test rig is shown in Figure 1 and a layout drawing of the same rig in Figure 2. Figure 3 shows the complete rig mounted on the shake table.

The test rig was designed to meet the following functional requirements:

1. Very low residual damping.
2. An inertia mass loading of the elastomer test sample with weights ranging from approximately 0.8 to 227 kg (1.8 to 500 lb).
3. A means for accurately controlling force preloading of the elastomer test sample.
4. Temperature control of the ambient air within the test specimen cavity.

The rig employs a unidirectional vibrating mass-spring system. In its simplest form, this concept might consist of an elastomer spring to which various amounts of inertia mass are bonded and the system could be completely free of residual damping or stiffness contributions from test rig elements. However, the practical requirements of balancing rather large inertia masses (up to 227 kg.(500 lb))on top of the elastomer spring and the desired mechanism to provide elastomer sample preloading at all test frequencies introduce additional elements which have finite stiffnesses and small amounts of parasitic damping.

Specifically, two radial guide bearings for the inertia mass and two air cylinders for the preloading of the elastomer samples are required. The stiffness and damping properties of these elements have an influence on the test rig response, but as described in Section IV, these properties are independently measured and accounted for.

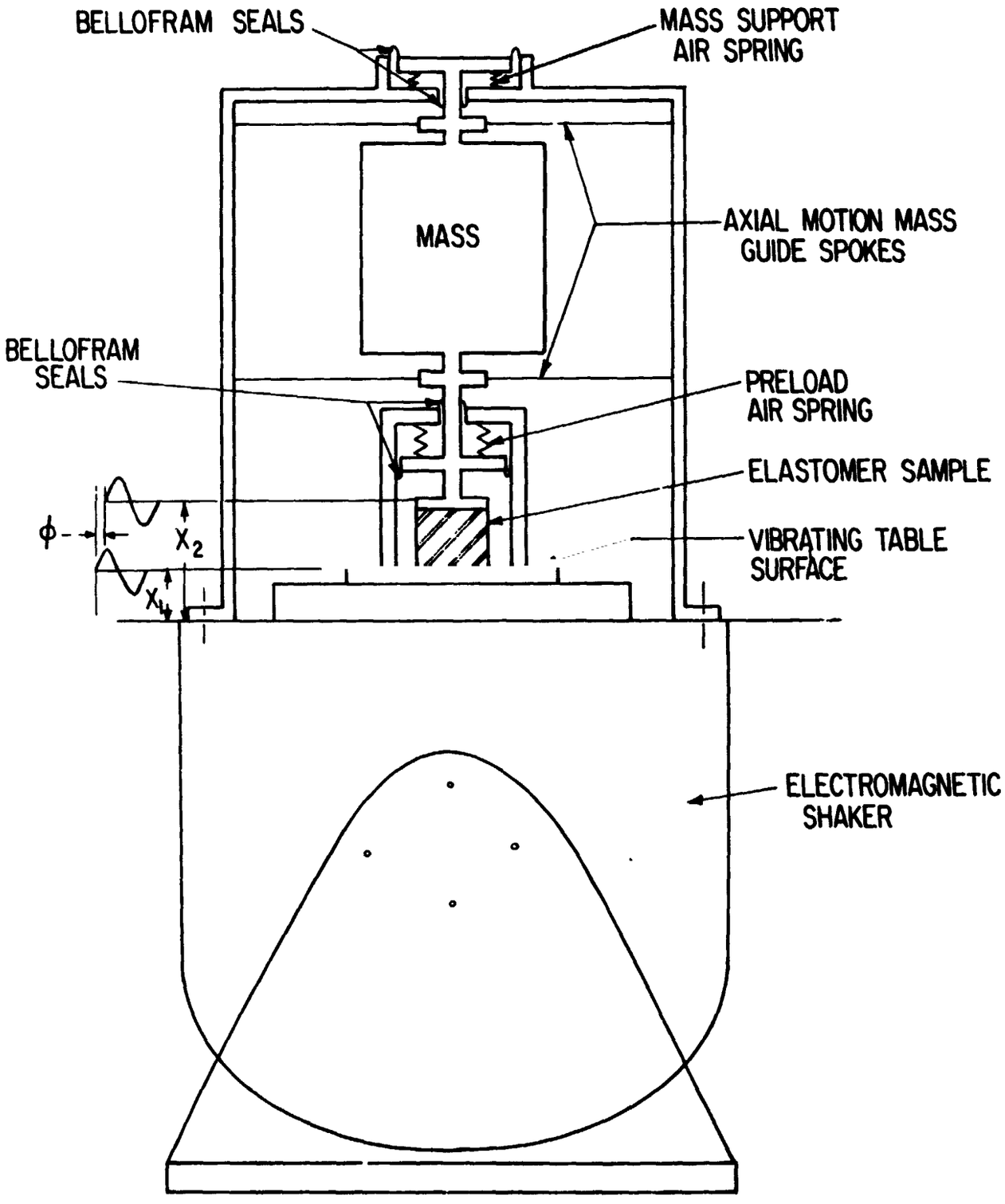

Fig. 1 Schematic of Elastomer Test Rig

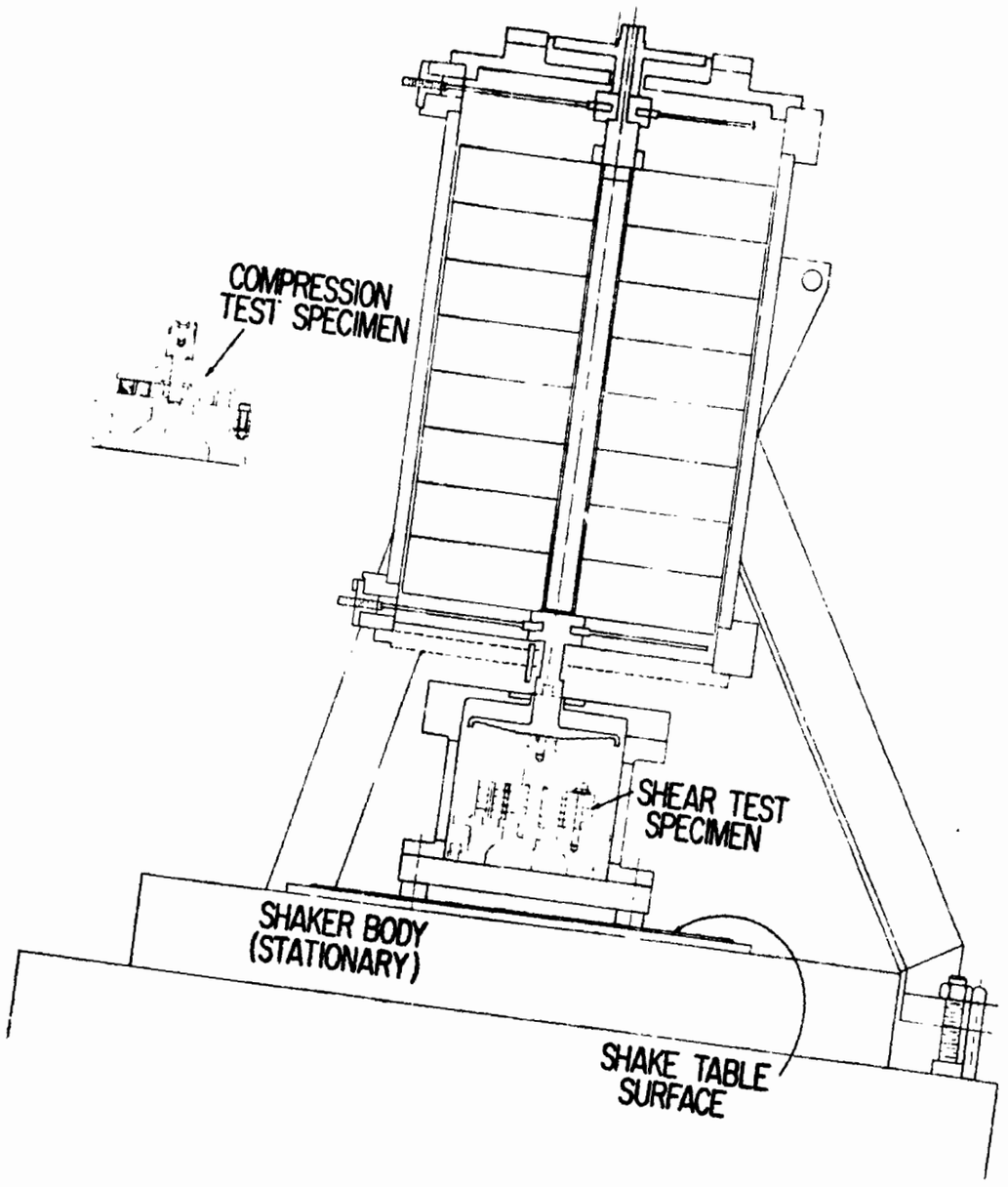

Fig. 2 Elastomer Test Rig Details

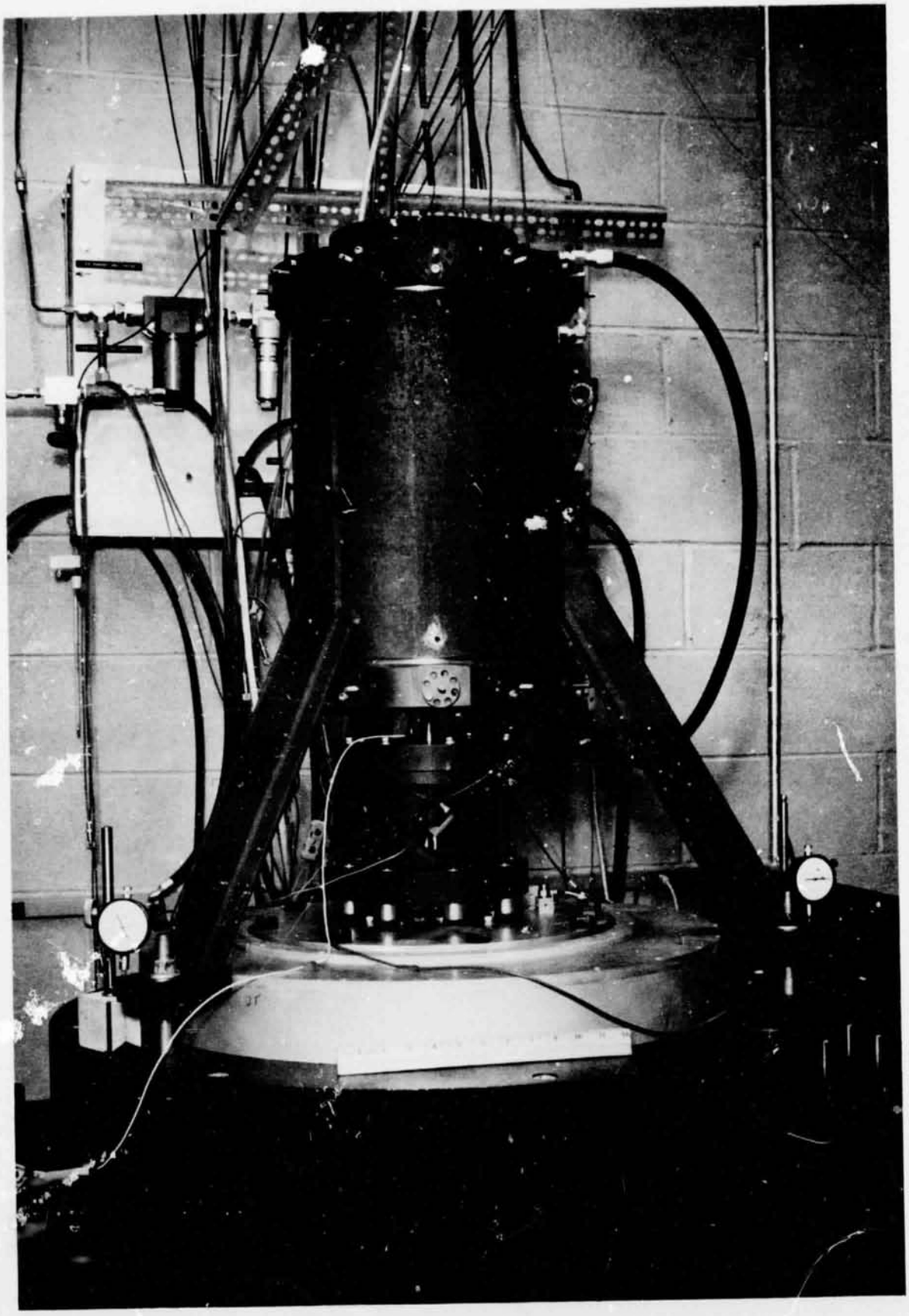

Fig. 3 Elastomer Test Rig Mounted on Vibration Table

The resonant mass bonded to the top of the elastomer specimens consists of a number of elements. For high frequency tests, in which only a minimum of mass is required, the resonant mass can be reduced to the top plate of the specimen holder and the preload piston. The top plate is made out of aluminum and the preload piston is made out of titanium for minimum weight. Increased mass for medium or low frequency testing is provided by rigidly attaching a long rod to the top of the preload piston, and adding steel weights. The weights are centered by the rod and are axially restrained by spacers of various lengths and a locknut near the upper end of the rod.

The rod itself receives radial support from two frictionless guide bearings (Figure 4 shows one of the dismounted bearings), each of which consists of a hub and 12 steel spokes. The hub is fitted over the end of the rod and is axially clamped to it. This kind of bearing arrangement provides good radial stiffness for reasonably high spoke tension, but provides only limited freedom for axial motion if overstressing of the spokes is to be avoided. Consequently, changes in preload on the test specimen must be accompanied by lowering or raising of the outer frame (to which the guide bearings are attached).

Preload of the elastomer test specimens is controlled by a pair of air cylinders. The lower cylinder is located directly above the test specimen. Its piston is attached to the specimen's upper holding-plate and exerts a downward force on the specimen. The upper cylinder is located at the top of the test rig and its piston exerts an upward force on the resonant mass. When the resonant mass is large, the desired preload is usually achieved by pressurizing the upper cylinder and partially supporting the weight of the mass. When the resonant mass is small, the desired preload is usually achieved by pressurizing the lower cylinder and exerting a downward force in addition to the weight of the mass.

The upper and lower preload pistons are sealed in their cylinders by two rolling diaphragm seals (Bellofram 3C-600-37-FPJ and 3-119-119-CBJ). The air cylinder inlet hole is 0.762 mm (0.030 in) in diameter, making each cylinder essentially a "closed" cavity under vibration conditions. A constant preload force on the test specimen is maintained through regulation of air pressure in the cylinders.

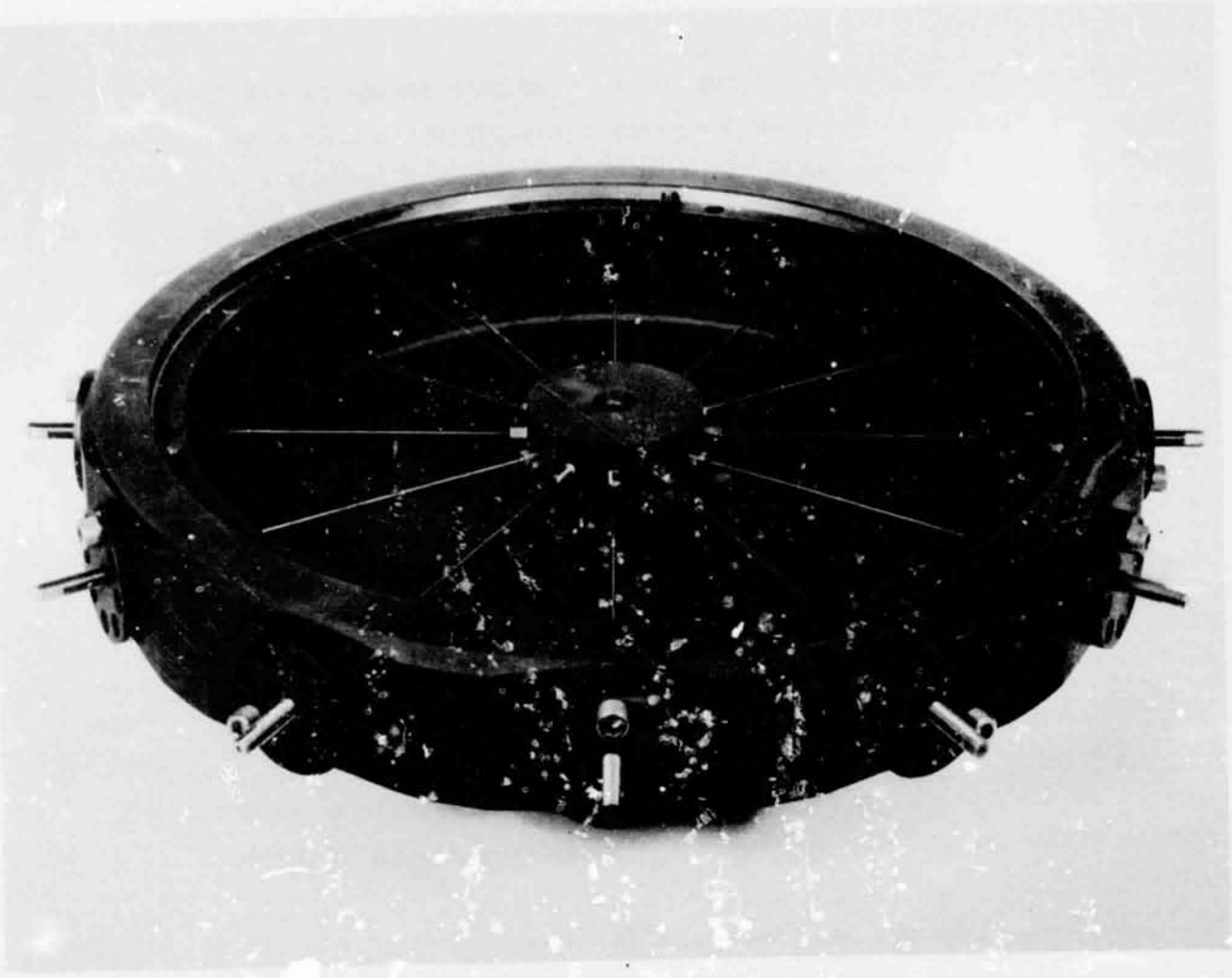

Fig. 4 Radial Guide Bearing

The ambient temperature within the elastomer test specimen cavity is controlled through the combined effect of electric heating cables and water-cooled tubes installed in the base plate below the test specimens (see Figure 5 for a photograph of the installed heating-cooling elements). The grooves in which the heating cable and the tubing are embedded have a reverse taper to ensure secure and rattle-free operation in a vibration environment. The electric heater is automatically controlled by a temperature controller, which obtains the necessary feedback from a thermocouple embedded in the metal of the base plate.

Details of the temperature control system and of the temperature recording system are shown in Figure 6.

C. Test Material Selection

As discussed above, the temperature variations are minimized by accurately controlling the ambient temperature and the heat generated in the specimen. To reduce the effects of any temperature variations which remain, a Broad Temperature Range (BTR) elastomer was selected as the test material. BTR elastomers are claimed to show reduced variation of material properties with temperature.

Two of the BTR-type elastomers under consideration for testing were silicones and polybutadiene. The final choice was polybutadiene, because of the difficulty, according to the manufacturer, of producing batches of silicone materials with consistent material properties. As with most elastomers, polybutadiene may be produced with various material hardness and damping rates, according to proprietary manufacturers' formulas. The polybutadiene chosen for the test described in this report carries the manufacturer's (Nichols Engineering, Inc., Shelton, Connecticut) designation NE X156G, with a nominal hardness of 70 durometer (or Shore A Hardness) and 21 percent of "critical damping". This material had the highest hardness and damping of those available from the manufacturer.

The individual polybutadiene test specimens were bonded with a cyanoacrylate adhesive (Eastman 910 HMP) to their respective aluminum support plates. The choice of bonding agent was based upon the manufacturer's recommendations and upon

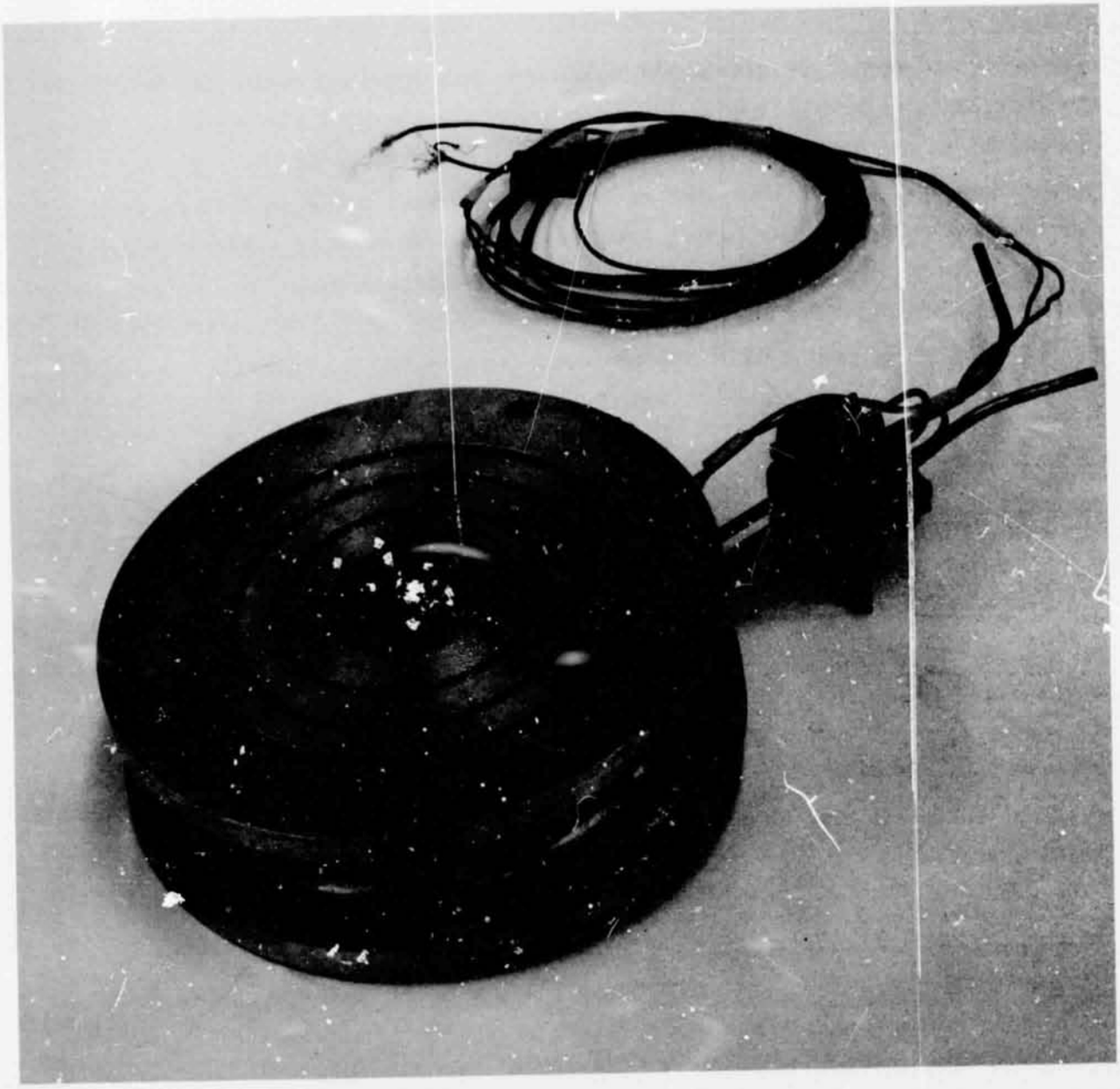

Fig. 5 Elastomer Test Sample Support Base With Cooling Coils and Heating Cables Installed

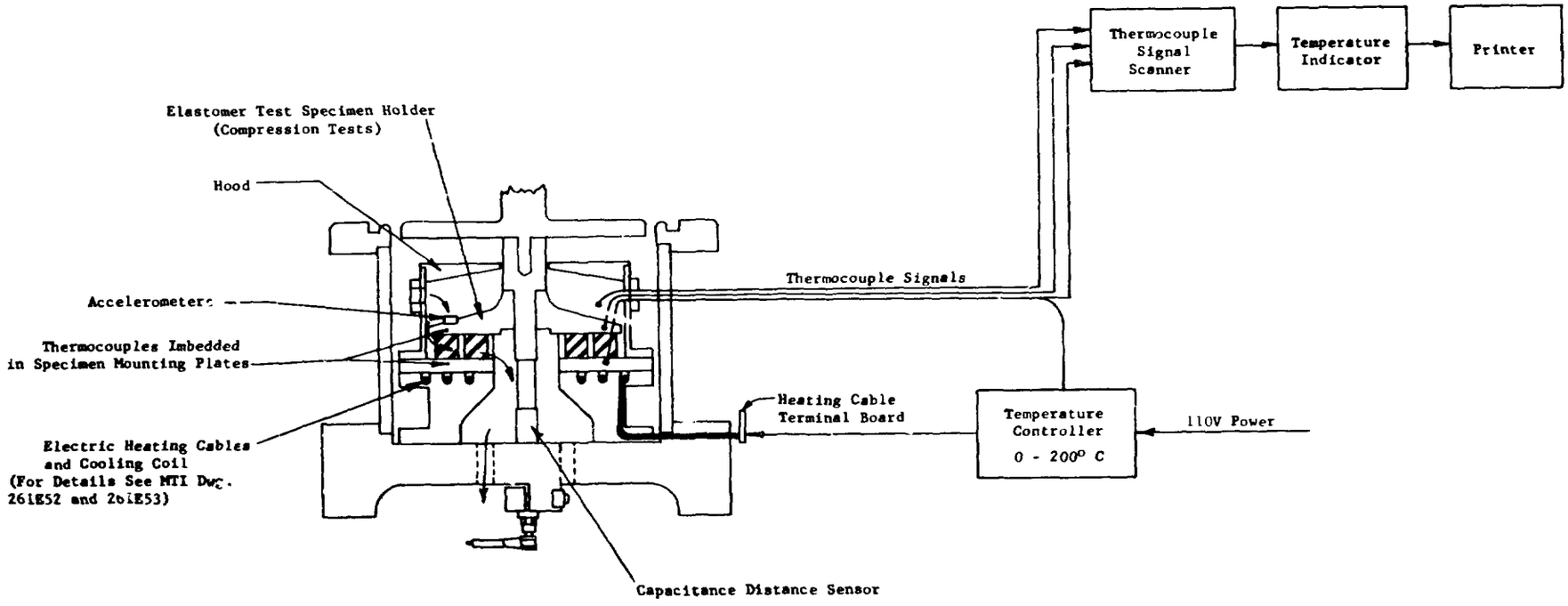

Fig. 6 Temperature Control System for Elastomer Tests

sample tests, which showed the epoxy (HYSOL AS7-4323) which was previously used for the bonding of neoprene and urethane elastomer specimens to steel and titanium surfaces yielding unsatisfactory results. It was found that successful bonding with Eastman 910 HMP is dependent upon smooth bonding surfaces, a thin film of adhesive and rapid application of a considerable clamping force to the bonded surfaces.

D. Shear Test Samples

The shear test specimens were molded as sheets 15 cm by 15 cm (6 in. by 6 in.) with a thickness of 3.2 mm (0.125 in.). Individual test specimens of the following quantities and sizes were knife-cut from these sheets:

1. Four strips - 25.4 mm high x 48.8 mm long (1.0 x 1.92 in.)
2. Eight strips - 12.7 mm high x 48.8 mm long (0.5 x 1.92 in.)
3. Twenty strips - 5.1 mm high x 48.8 mm long (0.2 x 1.92 in.)

In the case of the first sample configuration, the four individual strips were glued with one of their large faces to the sides of a square aluminim block and with their other large face each to one additional aluminim holding block (see Figure 7 for a photograph of the assembly of the four-strip shear test sample). In the assembly of the test fixture, the four holding blocks were bolted to the shake-table, while the elastomer-supported center block was attached to, and therefore became part of, the resonant mass.

The second shear test sample in its assembled configuration (Figure 8) was very similar to the first one, except that each of the assemblies was only of half the height. The two assemblies, placed on top of each other, then fitted into exactly the same space in the test fixture as the first test sample. The eight strips, deflecting in unison, were designed to have the same stiffness against deflection of the center mass relative to the mounting blocks, as the four strips in the first assembly (see Appendix A).

The convenience associated with the assembly of individual four-specimen sub-assemblies becomes quite apparent upon inspection of the third shear test

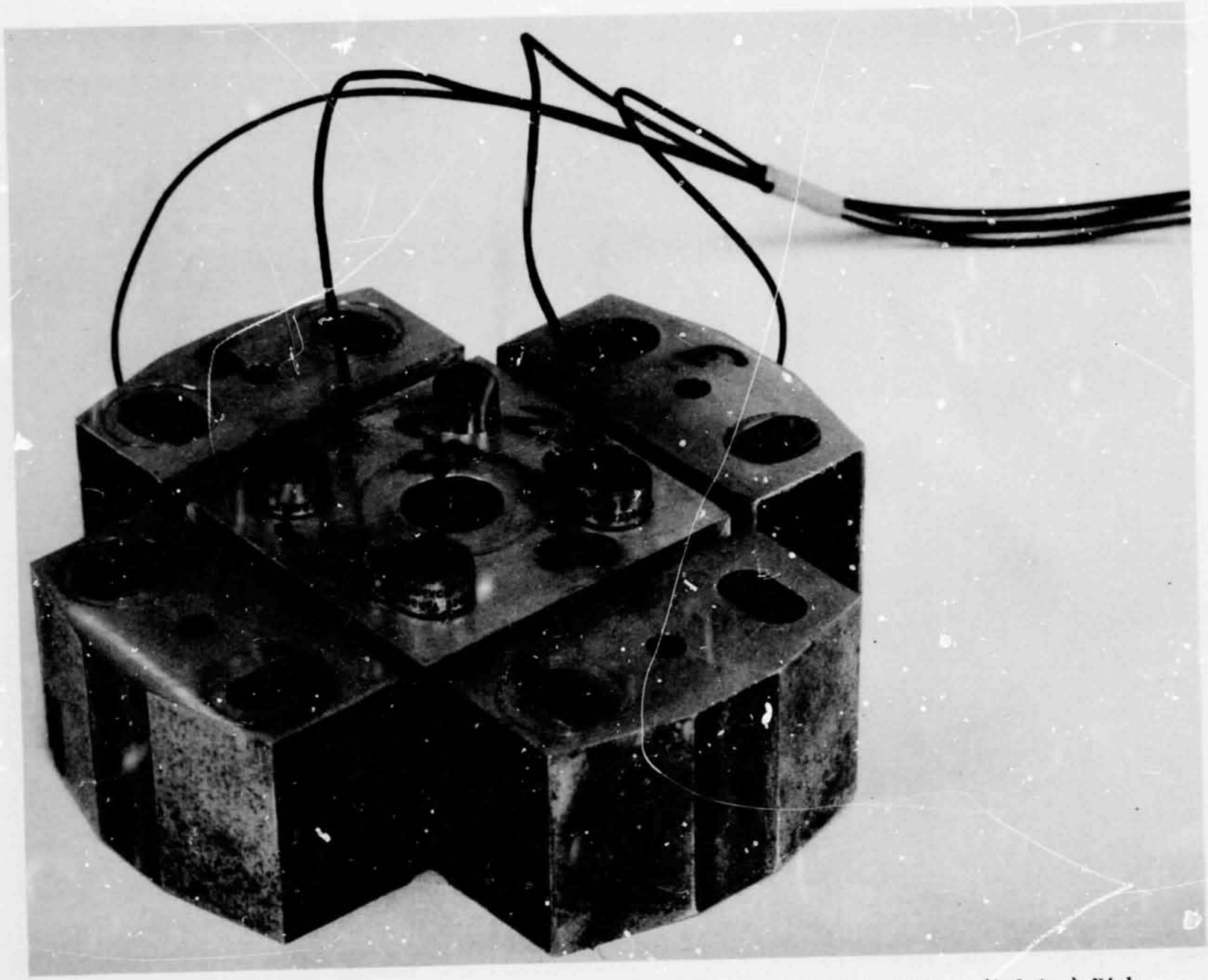

Fig. 7 Test Assembly of Four Elastomer Shear Specimens, Each 2.54 cm (1.0 in.) High

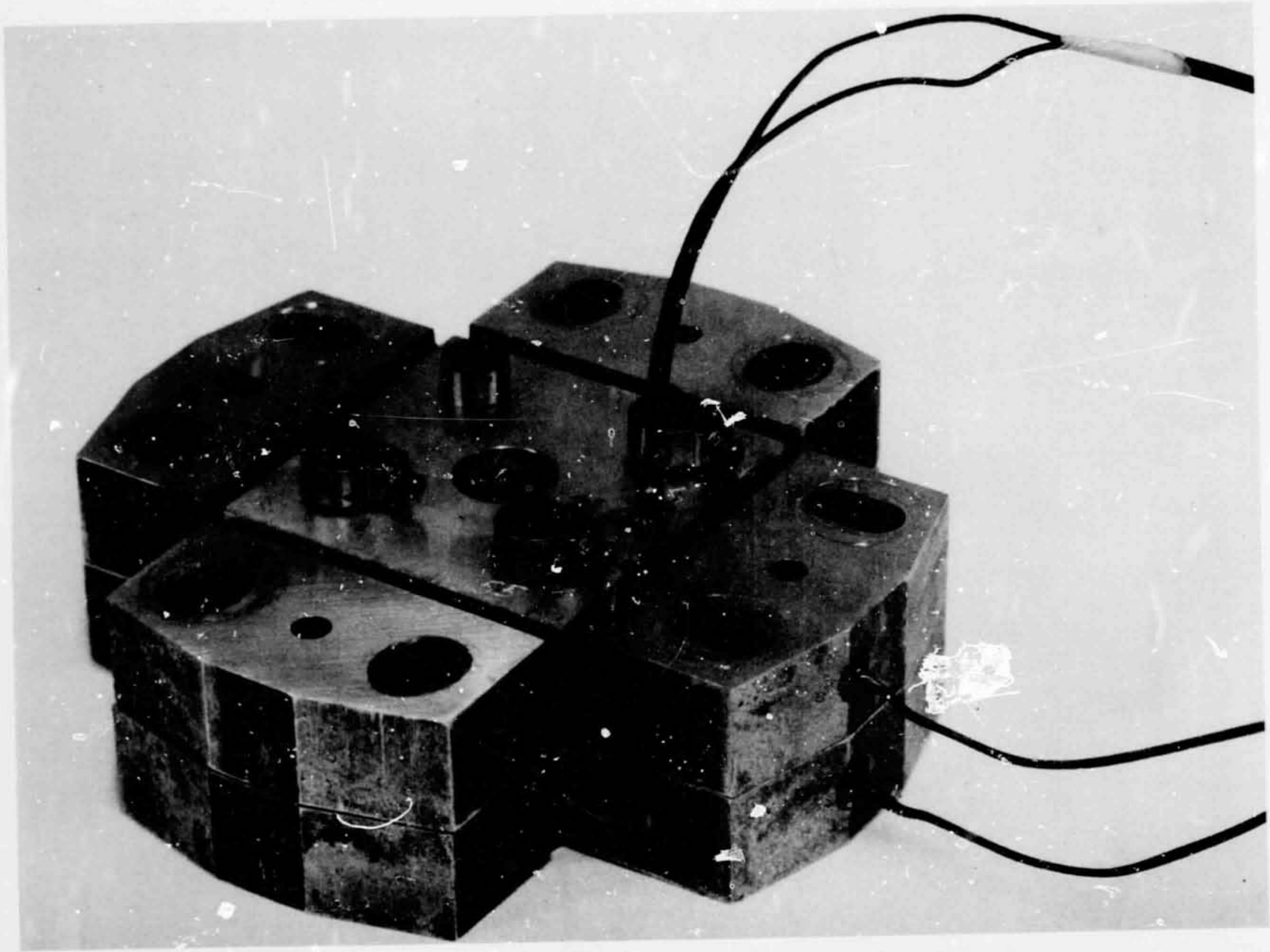

Fig. 8 Test Assembly of Eight Elastomer Shear Specimens, Each 1.27 cm (0.5 in.) High

sample (Figure 9). To maintain the same stiffness of the assembly with shear strips only 5.1 mm (0.2 in.) high, a total of twenty were needed. Since the individual strips were required to be free of interference by the strips above or below it, they were glued to aluminum blocks 6.4 mm (0.25 in.) high. When assembled in a stock of five, there is a height separation of 1.3 mm (0.05 in.) between the individual strips.

E. Compression Test Samples

Individual compression test specimens were shaped as cylinders of various heights. The cylinders were molded to a uniform height of 12.7 mm (0.5 in.) and later cut and ground to the desired height. From individual specimens the following three test samples were assembled:

1. Thirty cylinders - 12.7 mm diameter by 12.7 mm height (0.5 x 0.5 in.)
2. Ten cylinders - 12.7 mm diameter by 6.4 mm high (0.5 x 0.25 in.)
3. Three cylinders - 12.7 mm diameter by 3.2 mm high (0.5 x 0.125 in.)

The compression test specimens were assembled to circular plates, with the bottom plate anchored to the shaker table and the top plate connected to the resonant mass. The assembly of the thirty 12.7 mm (0.5 in) high cylindrical specimens is shown in Figure 10.

As with the shear samples, the compression samples were each designed to provide similar stiffnesses. Appendix A discusses how the shape factors for the different height cylinders lead to selection of the above numerical combinations.

F. Instrumentation

The measurement requirements for the experimental investigation of the elastomer dynamic properties were as follows:

1. Displacement measurement of elastomer support plate attached to the vibration table, relative to ground;
2. Displacement measurement of elastomer support plate attached to the resonant mass, relative to ground;

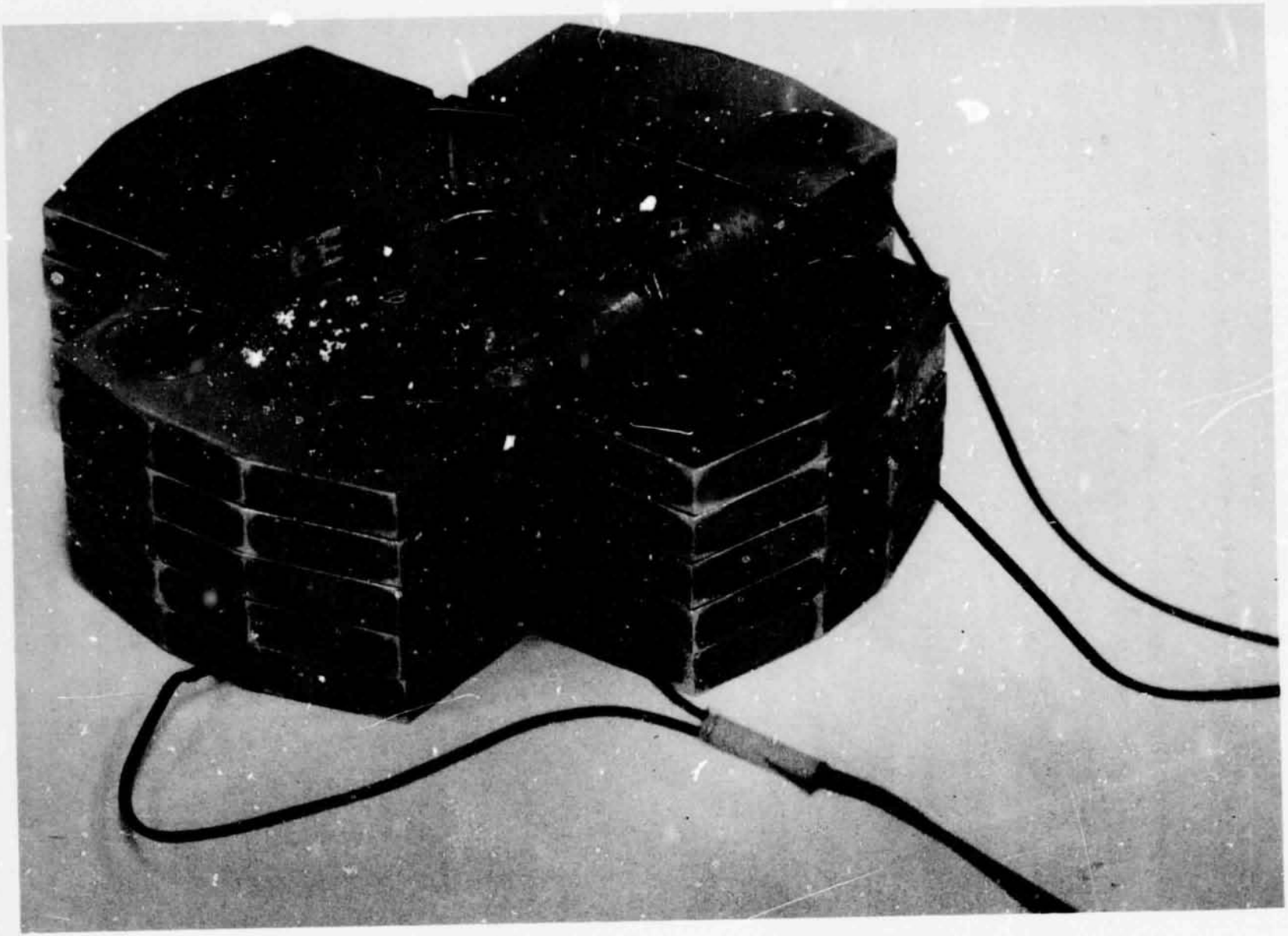

Fig. 9 Test Assembly of Twenty Elastomer Shear Specimens, Each 0.5 cm (0.2 in.) High

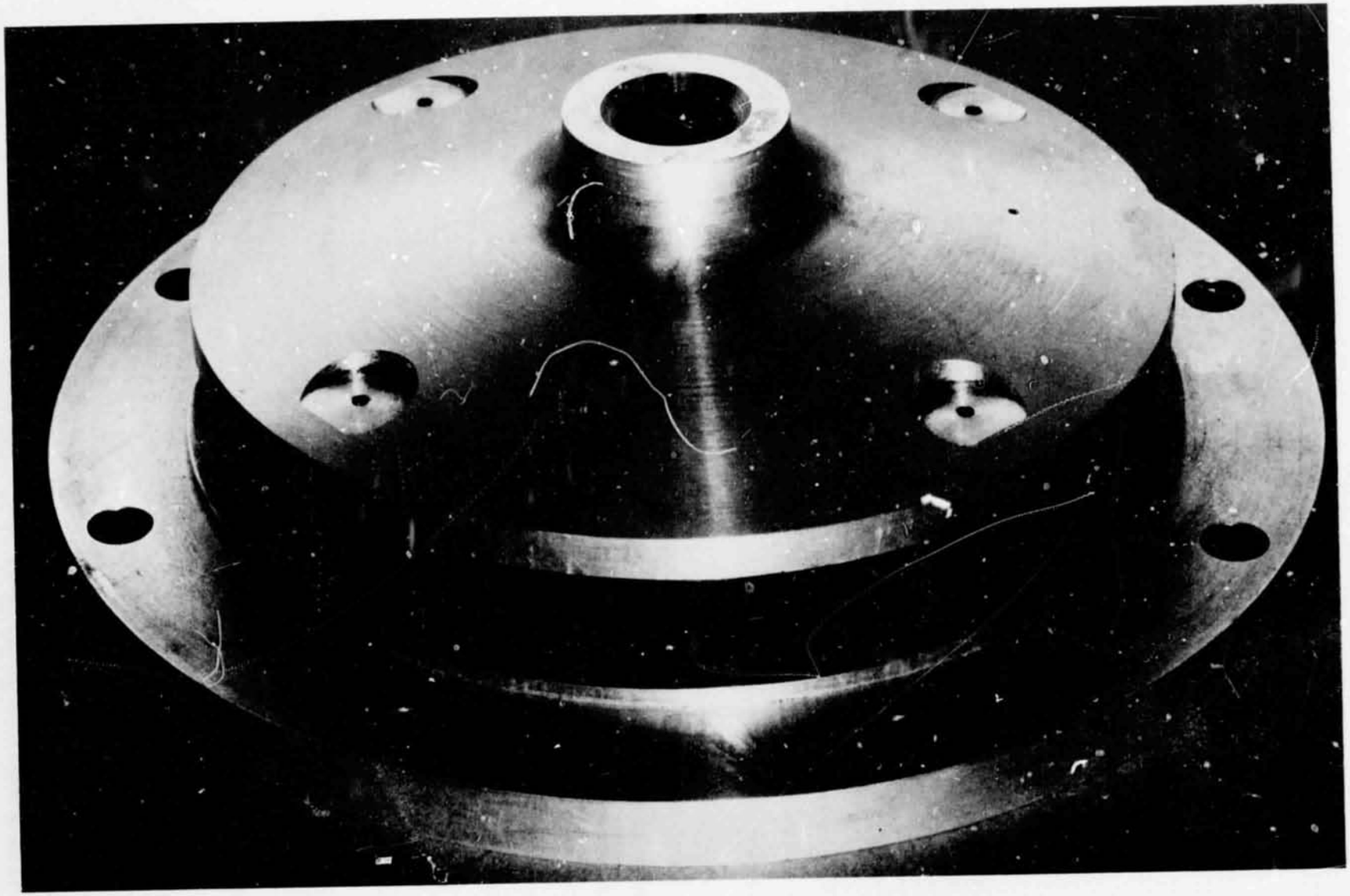

Fig. 10 Test Assembly of Thirty Elastomer Compression Specimens, 1.27 cm Diameter by 1.27 cm High (0.5 x 0.5 in.)

3. Phase angle measurement between displacement measurements (1) and (2) above;

4. Displacement measurement between two elastomer support plates, relative amplitude across the elastomer;

5. Vibration frequency;

6. Temperature of elastomer support plates and ambient air temperature in test specimen cavity;

7. Vibrational power dissipation across the elastomer test sample.

For convenience, acceleration was measured in (1) and (2) instead of displacement, but since the motions were sinusoidal the displacements were directly derivable from the accelerations. The very low level of motion of the shaker body (from which the shaker table is isolated by air springs with a very low resonant frequency) was also measured by accelerometers.

The input acceleration (1) was measured by an accelerometer located on the support base for the elastomer test samples. Output acceleration on the resonant mass (2) was determined from three accelerometers mounted directly to the top plate attached to the elastomer specimens. The use of three accelerometers, spaced 90 degrees apart, with their output signals displayed on one oscilloscope screen, permitted immediate detection of nonaxial motions of the resonant mass. When nonaxial motions of the resonant mass occur, they manifest themselves either as amplitude or phase angle variations among the three signals, or as a combination of both (testing experience revealed that only the compression specimen having three cylindrical specimens was susceptible to nonaxial motions at certain test frequencies).

The displacement measurement (4) between the two elastomer support plates (relative amplitude across the elastomer) was accomplished with a noncontacting capacitance-type sensor.

Chromel-Alumel type thermocouples were used to measure the temperature at the midface location of two shear specimens in each test assembly. The thermocouples were embedded in small holes in the aluminum holding plates at a

distance of approximately 1.6 mm (1/16 in.) from the elastomer surfaces. The compression test samples contain thermocouples directly above and below the center point of the flat surfaces of three individual cylinders. Again, the thermocouples were separated by approximately 1.6 mm (1/16 in.) of metal from the elastomer surfaces. (See Figure 11 for typical thermocouple installation in compression test sample.)

Displacement and acceleration data, together with temperatures from individual thermocouples were displayed visually in digital form for monitoring purposes. As a permanent record, this data was also recorded on a digital printer, with one thermocouple reading automatically printed with each amplitude data point. The two types of data were cycled independently by their own scanner-switches, and thus a given vibration sensor output did not always appear on the same line as a given thermocouple output. This is illustrated in Figure 12.

Amplitude signals, either acceleration or displacement, were sequentially switched by an analog scanner into a two-channel tracking filter, which provided a visual readout of vibration frequency and of two filtered amplitude signals. The base amplitude signal (acceleration) was fed at all times into one of the two channels of the tracking filter and from there into a phase meter where it served as a reference signal for the measurement of the phase angle of the resonant mass amplitude signal (one of the accelerometer signals). The d-c values proportional to phase angle and amplitudes from the phase meter and the tracking filter were then converted into digital form in digital voltmeters and printed on paper by a 21-column printer at a rate of approximately two lines per second (manually activated). Each line additionally contains the vibrational test frequency and the temperature indication from one thermocouple. (see Figure 12 for a typical data printout, Figure 13 for a photograph of the instrumentation console and Figure 14 for a schematic of the data acquisition system).

To monitor the power dissipation in the test sample during testing, a power meter was specially designed and built. This meter utilizes available

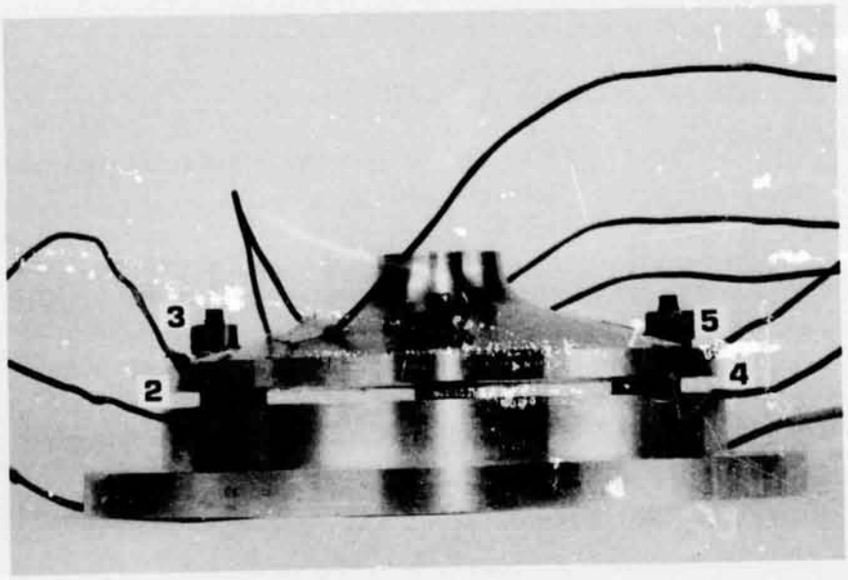

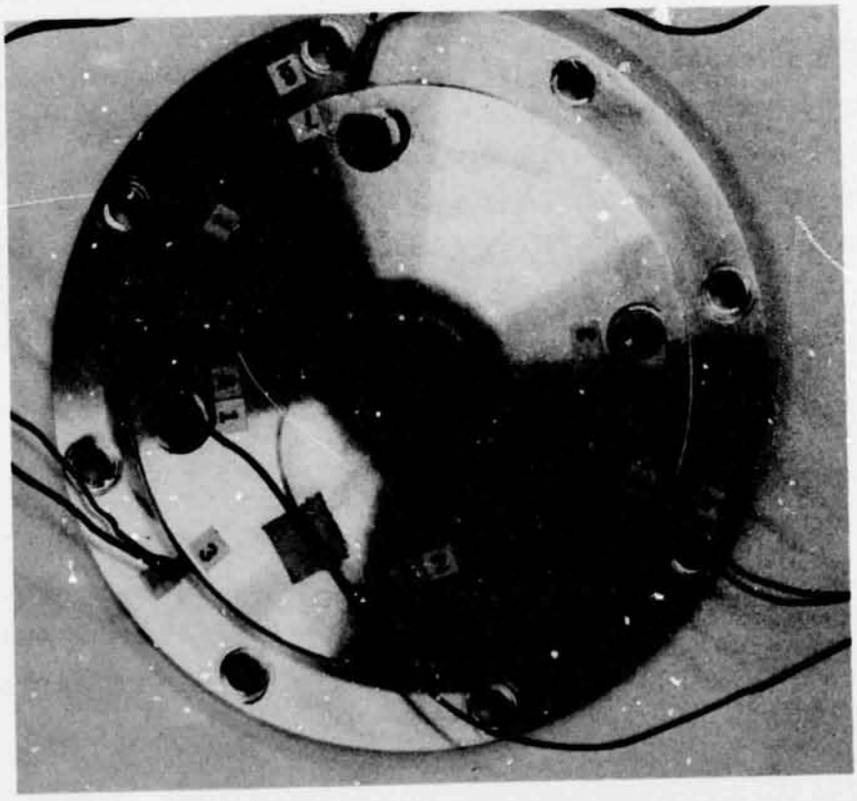

Fig. 11 Location of Thermocouples and Accelerometers on the Three Specimen Elastomer Test Sample (Compression)

Signal Identification (1)	Scanner Data Channel (2)	Frequency Hz	Temp. °C	Phase Angle (Channel 4 Ref.) (3)	Thermocouple Ident. No. (4)	Amplitude Signal (5)	
	6	00142	035.0	-025	3	1.3144	dcV
	5	00142	033.6	-013	2	0.5227	dcV
	4	00142	034.8	+000	1	2.0955	dcV
	3	00142	----	-010	0	4.5322	dcV
	2	00142	034.9	-010	6	4.4944	dcV
	1	00142	----	-012	5	4.9544	dcV
Relative Displacement Between Table And Mass	6	00142	033.5	-026	4	1.3044	dcV
Accelerometer Signal From Top Of Mass	5	00142	034.9	-013	3	0.5225	dcV
Table Amplitude	4	00142	033.7	+000	2	2.0911	dcV
Resonant Mass Amplitudes (7)	3	00142	034.9	-011	1	4.5800	dcV
	2	00142	033.6	-010	0	4.4655	dcV
	1	00142	033.7	-011	6	4.9622	dcV

Compression test sample, 0.125 in., 2-1/2 % preload
Mass: 24.3 lb. (6)

NOTES: (1) Mass amplitude and table amplitude signals (Data Channels No. 1,2,3,4,5) were accelerometer signals. Displacement probe signal of Channel No. 6 designated relative displacement between the table and the vibrating mass.

(2) Printout occurred in 1-2-3 sequence from bottom upward.

(3) Phase angle was measured with Channel 4 (base amplitude signal) as reference. Readings associated with Data Channels 1,2,3 are the desired phase angle between mass and table amplitude signals. The reading for Data Channel No. 6 is of no interest here, since it indicates the angle between signals ($X_2 - X_1$) and the base amplitude signal.

(4) Location of thermocouples 0 through 6 is shown in Figure 12 for this test sample.

(5) Individual calibration factors apply.

(6) Identification of test run was recorded by hand.

(7) Location of resonant mass accelerometers is shown in Figure 12 for this test sample.

Fig. 12 Typical Data Printout

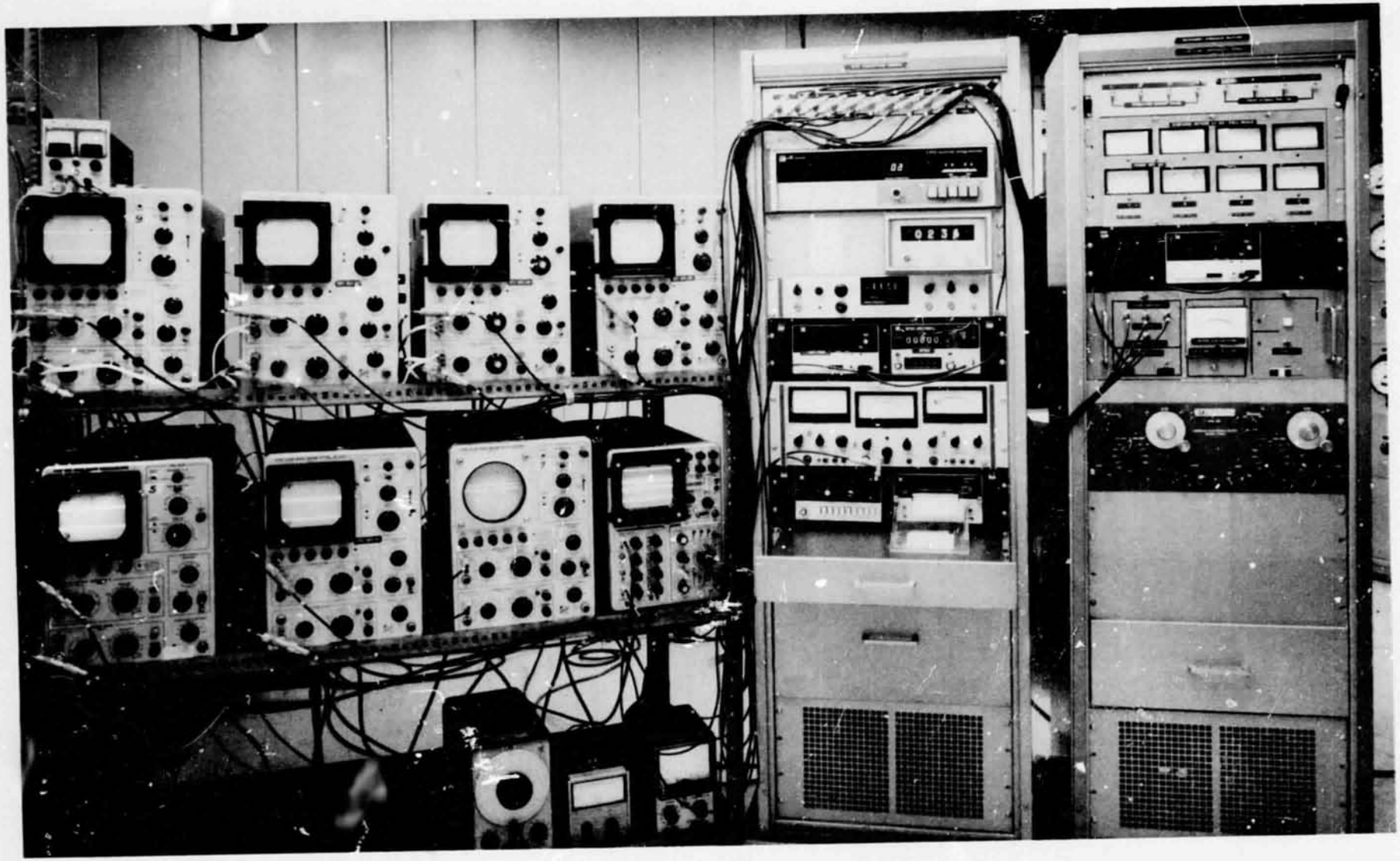

Fig. 13 Instrumentation Console

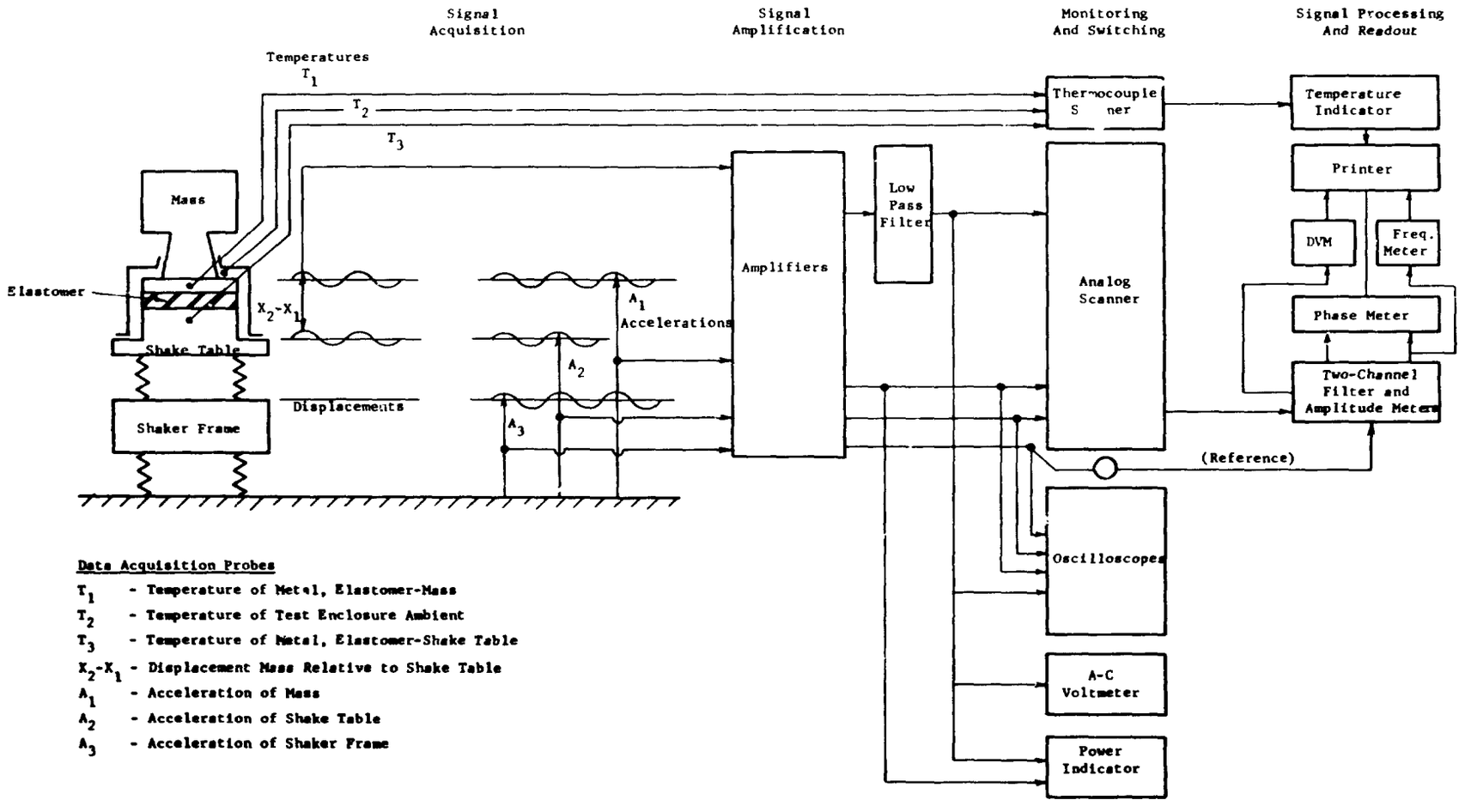

Fig. 14 Schematic of Data Acquisition System for Measurement of Elastomer Dynamic Properties

acceleration and displacement signal inputs. The three (unfiltered) accelerometer signals from the top plate of the specimen holder (resonant mass signals) are averaged, to give a signal proportional to the net force on the resonant mass. This signal is therefore almost equal to that portion of the force acting through the elastomer sample which is due to dynamic displacement (differing only by the small guide spoke and air cylinder forces due to their dynamic displacement.) The displacement signal which indicates relative motion across the sample is differentiated to give a signal proportional to rate of deformation (relative velocity). The force and velocity signals are multiplied together to give the instantaneous power. The instantaneous power consists of a d-c (average) component and a sinusoidally varying component and, by filtering out the sinusoidally varying component, the average power dissipation is obtained.

During test, the average power dissipation was held to a value which, by heat transfer analysis, gave a temperature rise in the specimen of less than $1^{o}C$.

G. Testing Procedure

One of the major features of the current test program was the performance of the scheduled tests at near-resonance conditions. Since phase angle between base excitation and resonant mass response is an accurate indicator of the amount of damping in the region of resonance, measurements should preferably be made in the phase angle range between approximately 15 and 165 degrees (see Appendix B). This requires that the test frequency be approximately 0.9 to 1.5 times the critical frequency of the elastomer-resonant mass system. Coverage of the full test frequency range of 100 to 1000 Hz with sufficient test points therefore necessitates changes in the size of the resonant mass. Typically between seven and nine different mass arrangements ranging from 0.8 Kg (1.8 lb.) to 51 Kg (113 lb.) were found sufficient to cover the desired test range. The smallest mass consisted of the elastomer test sample top plate and the preload cylinder piston, with no additional weight attached. The next three combinations were obtained by attaching weights of up to 1.9 Kg (3.5 lb.) directly to the preload piston cylinder without the use of the spoke guide bearings. For the last five mass arrangements both guide bearings were used.

Once any one of the six elastomer test samples has been mounted on the shake table and the necessary instrumentation installed and connected, a typical test sequency proceeded as follows:

1. A resonant mass was selected and installed.

2. The elastomer sample was statically preloaded. (For zero preload cases, the static loading on the elastomer by the resonant mass was relieved through an appropriate pressurization of the top air cylinder. If the preload requirement exceeded the static deflection of the elastomer obtained from the resonant mass, pressurized air was admitted in the lower cylinder to produce the desired preload. Elastomer deflections were determined by readout from the capacitance probe installed in the lower base plate of the elastomer specimen holding fixture.)

3. The elastomer test sample cavity was enclosed and the temperature control system given time to adjust ambient temperature to the desired value.

4. With low vibration levels applied to the base of the elastomer holding fixture, frequency scans were conducted until the approximate resonant frequency of the system was found. Subsequently, an exact determination of the system resonant frequency was made by tracing, on an X-Y plotter, the d-c value proportional to the resonant mass acceleration amplitude as a function of the base excitation frequency. It may be noted here that, for a base-excited single degree of freedom spring-damper-mass system, resonance occurs at an angle smaller than 90 degrees. The deviation from 90 degrees is essentially determined by the amount of damping in the system as shown in Appendix B.

5. While the predetermined vibrational power dissipation level in the elastomer test sample was maintained by adjustment of the shaker power input level, the vibration frequency was reduced until the phase angle decreases to a value between 15 and 25 degrees. Provided none of the oscilloscope monitored acceleration and displacement signals showed signs of abnormalities (distortions, or indications of nonaxial motion of the resonant mass),

a data point was recorded. The recording of one data point consisted of either one or two complete printouts of all amplitudes (up to seven individual signals), associated phase angles and test frequency, and all temperatures from the thermocouples located in the test specimen holding plates.

6. Stepwise increases in vibration frequency were imposed and between six and ten data points were recorded until the phase angle reached approximately 165 degrees.

7. Shake table power was turned off and the preload on the elastomer sample was increased to the next higher value.

8. Steps 4 through 7 were repeated until data at all desired preloads was obtained.

9. Shaker table power was turned off, and all preload on the elastomer sample removed. The elastomer test sample was then given time (up to one hour) to recover its original, uncompressed height (as indicated by displacement probe readings).

Tests, comprising steps 1 through 9, were then repeated with each of the remaining masses in turn, each mass giving a dynamic system with a different resonant frequency.

The complete set of results obtained for each test specimen was reduced to yield stiffness and damping values over the range of frequency covered by the tests. The analysis upon which this data reduction was based is described in the following sections of this report.

H. Test Rig Response

With the forced vibration type of testing described in this section, the dynamic characteristics of the elastomer are basically determined by measuring the motions of the resonant mass and knowing the stiffness and damping characteristics of all elements of the test rig. It was, therefore, necessary to analyze the dynamic response of the test rig with the objective of determining the characteristics of the various system components, viz., lower cylinder, upper cylinder and guide bearings.

A dynamic model of the test rig is shown in Figure 15 where the system components are denoted by a spring or a combination of a spring and a dashpot depending on their physical characteristics. Both cylinders and the guide bearings have been designed such that their stiffnesses are negligibly small compared to the stiffness of the elastomer. Hence, very little precision is required in determining these stiffness values. However, damping introduced by the use of rubber seals in the cylinders needs careful attention since these damping coefficients may be quite comparable with that of the elastomer specimen.

In order to determine the dynamic response of the test rig, each component was tested individually and its relevant characteristics were measured. When assembly does not introduce any appreciable changes, the complete dynamic response of the test rig is determinable by the characteristics of each of the system elements. The most likely elements, whose response may depend on the assembly, are perhaps the rubber seals in the cylinders since their damping coefficients may depend on their proper alignment to a certain degree. With the primary objective of precisely determining the dynamic response of the test rig, the elastomer specimen was replaced by a mechanical spring shown in Figure 16, whose stiffness and equivalent mass are measured experimentally. Along with the testing of each system element separately, the total response of the test rig with the mechanical spring was measured as a function of air pressures in the cylinders. Although the stiffness of the various elements may be determined by the experiments performed with each of the system elements, it was found that the damping of the cylinders was best determined by performing a least squares analysis of the measured response of the assembled test rig.

The details of the analyses described above are presented in Appendix B. The results are summarized below.

Numerical Values for Dynamic Characteristics of Test Rig Elements

Guide Bearing Stiffness	k_s	$= 3.675 \times 10^4$ N/m (210 lb/in)
Lower Cylinder Damping	c_ℓ	$= 1.02 \times 10^2$ N-sec/m (0.583 lb-sec/in)
Upper Cylinder Damping	c_u	$= 2.45$ N-sec/m (0.014 lb-sec/in)

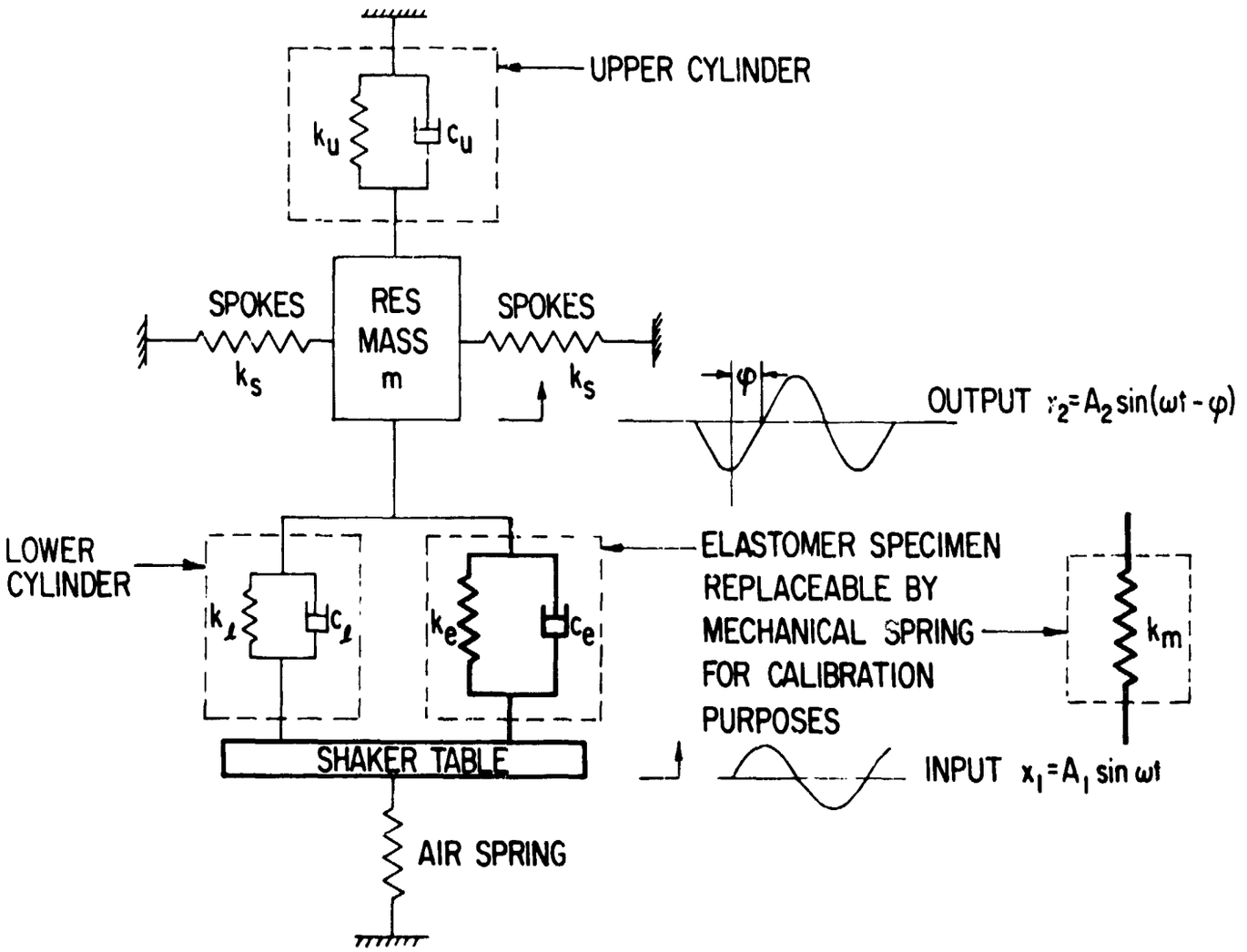

Fig. 15 Dynamic Model of the Elastomer Test Rig

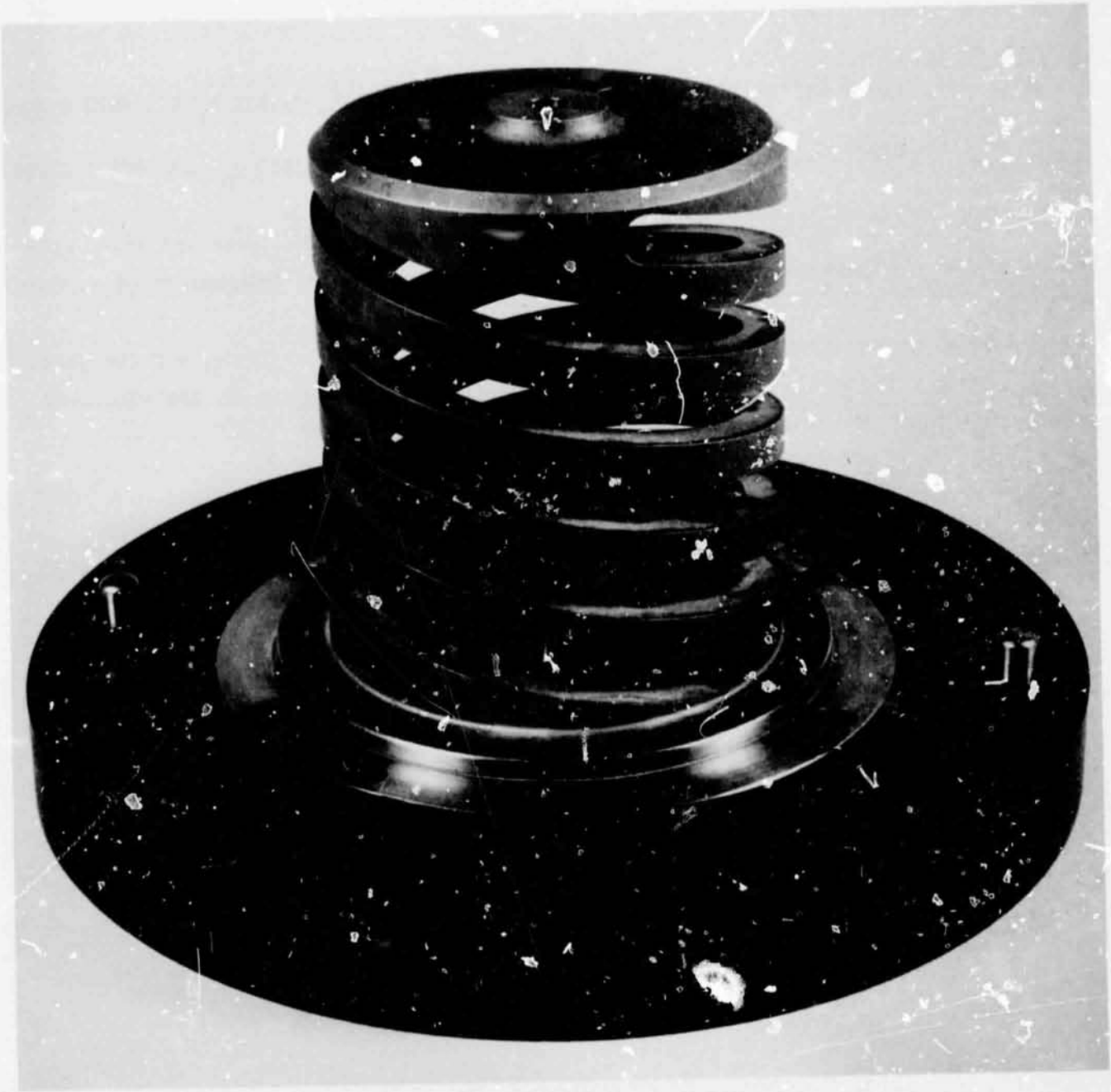

Fig. 16 Mechanical Spring Used for Determining the Test Rig Dynamic Response

Lower Cylinder Stiffness $k_\ell = 1.642 \times 10^5 + 1.023\ p_\ell$ N/m (938 + 40.25 p_ℓ lb/in

Upper Cylinder Stiffness $k_u = 9.0 \times 10^4 + 1.525\ p_u$ N/m(515 + 60.00 P_u lb/in)

where p_ℓ and p_u are pressures in N/m^2 or lb/in^2 gage in the lower and upper cylinders respectively. Note that all the above values are independent of frequency.

As shown in Appendix B, when the elastomer specimen is in place, and the phase angle p and ratio of output to input amplitude. α, is measured, the elastomer stiffness and damping (Ke,Ce) are calculated as follows:

$$Ke = -K_\ell + \frac{(ku + 2ks)\alpha(\cos\phi-\alpha)+\omega Cu\alpha Sin\phi-m\omega^2(\alpha\cos\varphi-\alpha^2)}{\alpha^2 - 2\alpha\cos\phi + 1} \qquad (1)$$

$$Ce = -C_\ell + \frac{Cu\alpha(\cos\phi-\alpha)+m\omega\alpha Sin\phi(1-\frac{ku + 2ks}{m\omega^2})}{\alpha^2 - 2\alpha\cos\phi + 1}$$

All the data for damping of the elastomer is presented as the imaginary part of the complex stiffness (ωCe).

IV. EXPERIMENTAL RESULTS

Dynamic response data for several elastomer samples was obtained over a range of excitation frequencies. The power dissipated in the elastomer was monitored within the present experimental procedures to establish an upper bound on the temperature distribution within the elastomer sample. The ambient temperature around the elastomer was maintained constant. Under such conditions, the data obtained determines the elastomer behavior at fixed temperature.

A. Operating Conditions and Data Range

Three compression and three shear samples as described earlier were tested. The preloads for the compression samples were set to 2.5 and 5 percent of the height of the specimens. Under all operating conditions, the elastomer was never subjected to tension in the compression experiments. In the case of the shear samples, three different preload, viz., 0., 2.5, and 5 percent of the specimen thickness were used. The frequency range for all experiments was 100 to 1000 Hz. The ambient temperature around the elastomer was maintained to $32^{\circ}C$ within $1^{\circ}C$. Also, the total power dissipated in the lower air cylinder and the elastomer sample was held constant to establish an upper bound on the temperature gradients in the elastomer sample. The conditions were adjusted such that the maximum temperature rise within the elastomer specimen was less than $1^{\circ}C$ as discussed below.

B. Temperature Gradient in the Elastomer

Since the elastomer sample and the lower air cylinder act in parallel, the total measured power dissipation is divided between the cylinder and the elastomer specimen, depending on their relative damping characteristics. This total power per unit of the elastomer volume was maintained constant at about 0.022 watts/cm^3 in all the experiements. For the purpose of computing an upper bound on the temperature rise from either end to the center of the specimen, it may be assumed that the entire power is dissipated in the elastomer and, hence, writing the energy equation gives

$$\frac{d^2T}{dx^2} = \frac{-q}{F_k}$$

where T is the temperature (^{o}C), q is the dissipation (watts/cm^{3}), F_k is the thermal conductivity (watts/^{o}C cm) and x is the coordinate as shown in Figure 17.

Since the temperature at the two ends is held constant at say T_o, the above equation may be integrated to determine the temperature T_c in the center of the specimen.

$$T_c - T_o = \frac{q}{8F_k} a^2$$

where a, height of the specimen is 1.27 cm (0.5 in.) for the worst case. Assuming the thermal conductivity to be 0.002 watts/^{o}C cm [7] the temperature rise for a dissipation of 0.022 watts/cm^{3} will be

$$T_c - T_o = \frac{0.022}{8 \times 0.002} \times (0.50)^2$$

$$= 0.344^{o}C$$

Thus, under all operating conditions for the entire experimental data, the temperature rise within the elastomer is less than 1^{o}C. Since the ambient temperature was monitored to be constant at 32^{o}C to within 1^{o}C, it may be concluded that the measured elastomer response is under isothermal conditions.

C. Reduction of Experimental Data to Complex Stiffness

The experimental variables measured included the input and output acceleration, relative phase angle, relative amplitude of elastomer displacement and the dissipated power. When the damping coefficient for the lower cylinder is a constant, then the dissipation in the cylinder at any frequency is proportional to the relative displacement amplitude. Thus, when the total dissipation (cylinder plus elastomer sample) is held constant, the displacement amplitude is an indicator of elastomer dissipation. From the measurement of the input and output acceleration, and the observation that all motions are sinusoidal, the system transmissibility α, which is the ratio of output to input amplitudes, may be determined. From the measurement of the phase angle φ and the computed α, Equations (1) and Table 1 may be used to compute the elastomer stiffness k_e and damping coefficients c_e.

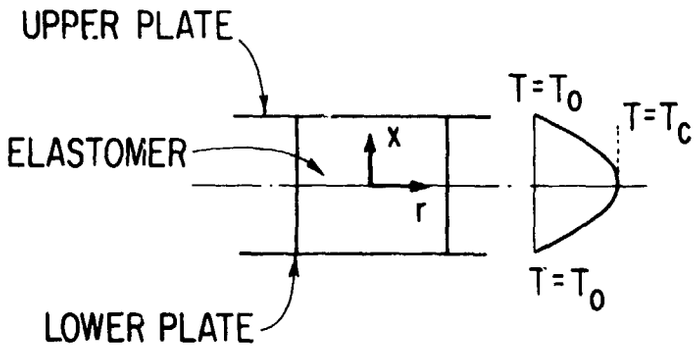

Fig. 17 Schematic of Thermal Gradients in the Elastomer Specimen

The physical characteristics of an elastomer are sometimes denoted in terms of a complex stiffness. Also since simulation of material behavior by mechanical viscoelastic models is generally performed in terms of complex stiffness or complex compliance, these quantities are defined below.

Complex Stiffness $K = K1 + iK2$

Complex Compliance $H = H1 - iH2$

Also, note the relationships

$H = 1/K$

$K1 = k_e$ the elastomer stiffness coefficient

and

$K2 = \omega c_e$ where ω is the frequency in radiand/sec.

With the above relations, the complex stiffness is also written as

$$K = k_e + i\,(\omega c_e).$$

From the computed k_e and c_e, the real and imaginary parts K1 and K2 may be determined and all the results are presented in terms of these parameters.

D. Compression Tests

The results of the compression experiments are shown in Figures 18 to 23. It is clearly seen that dependence of K1 or K2 on frequency is rather small under the thermal conditions ensured by the power monitoring system. Also, the dependence of the complex stiffness on preload is insignificant. The large scatter in Figures 22 and 23 is primarily due to the geometry of this particular sample. There are three pieces of elastomer between the plates in this case. It is known that in order to prevent any irregular motion of the resonant mass at least three support points are required. However, if only three supports are provided, then any misbehavior at any one of the supports will result in somewhat irregular motion. In fact, for this sample, substantial phase differences between the three output accelerometers were sometimes observed.

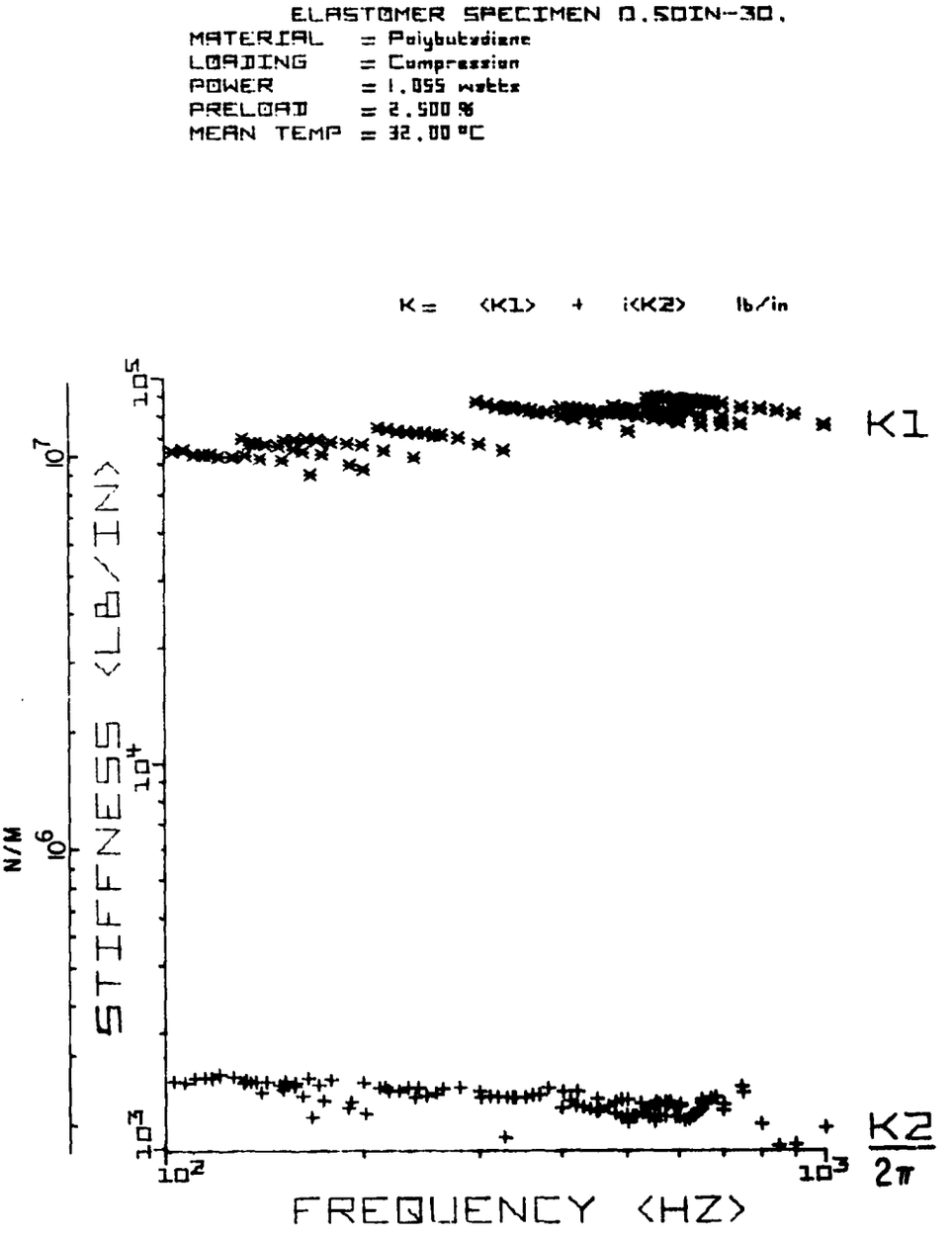

Fig. 18 Complex Stiffness of the Compression Sample With Thirty Specimens at 2-1/2 Percent Preload

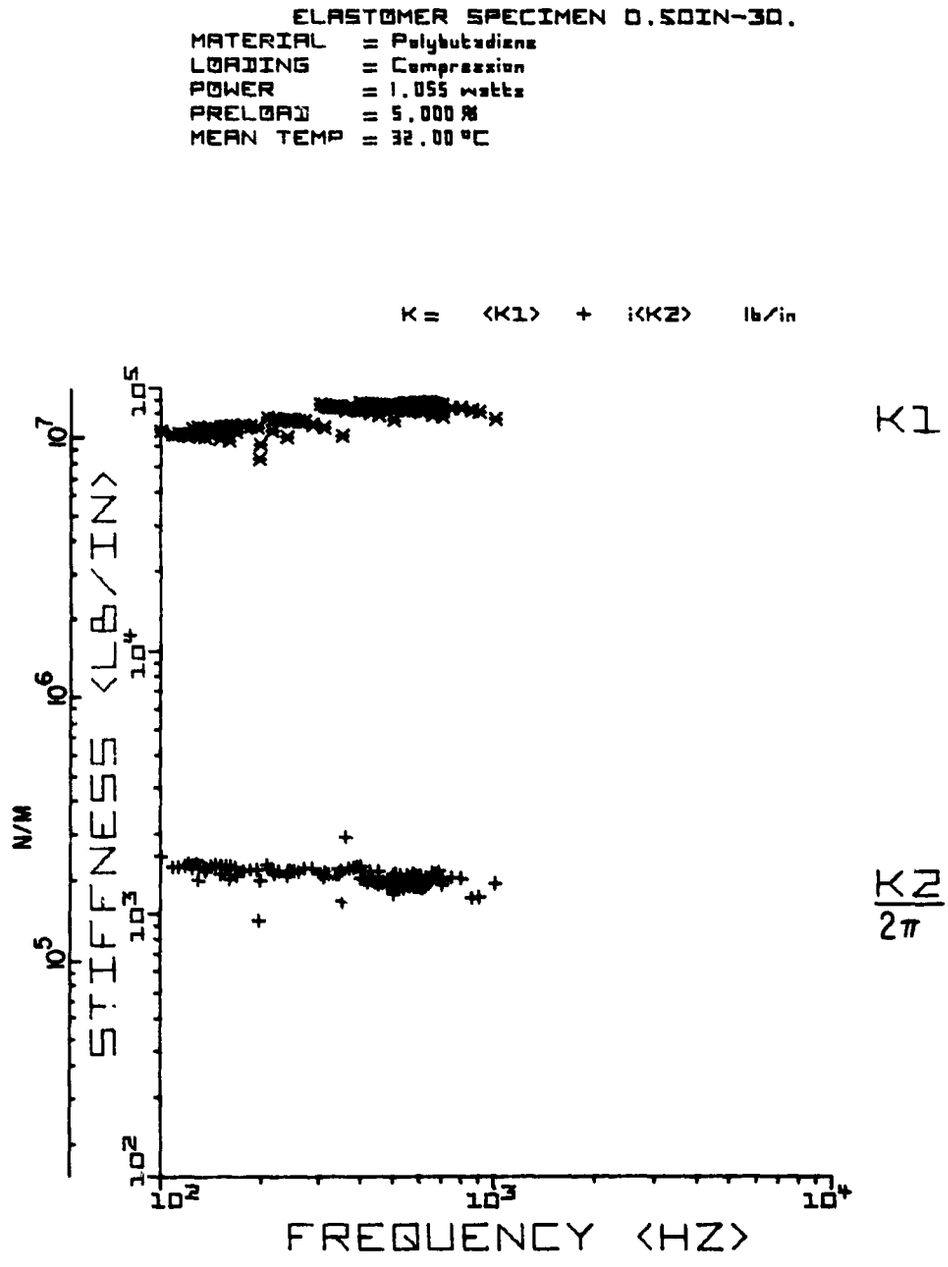

Fig. 19 Complex Stiffness of the Compression Sample With Thirty Specimens at Five Percent Preload

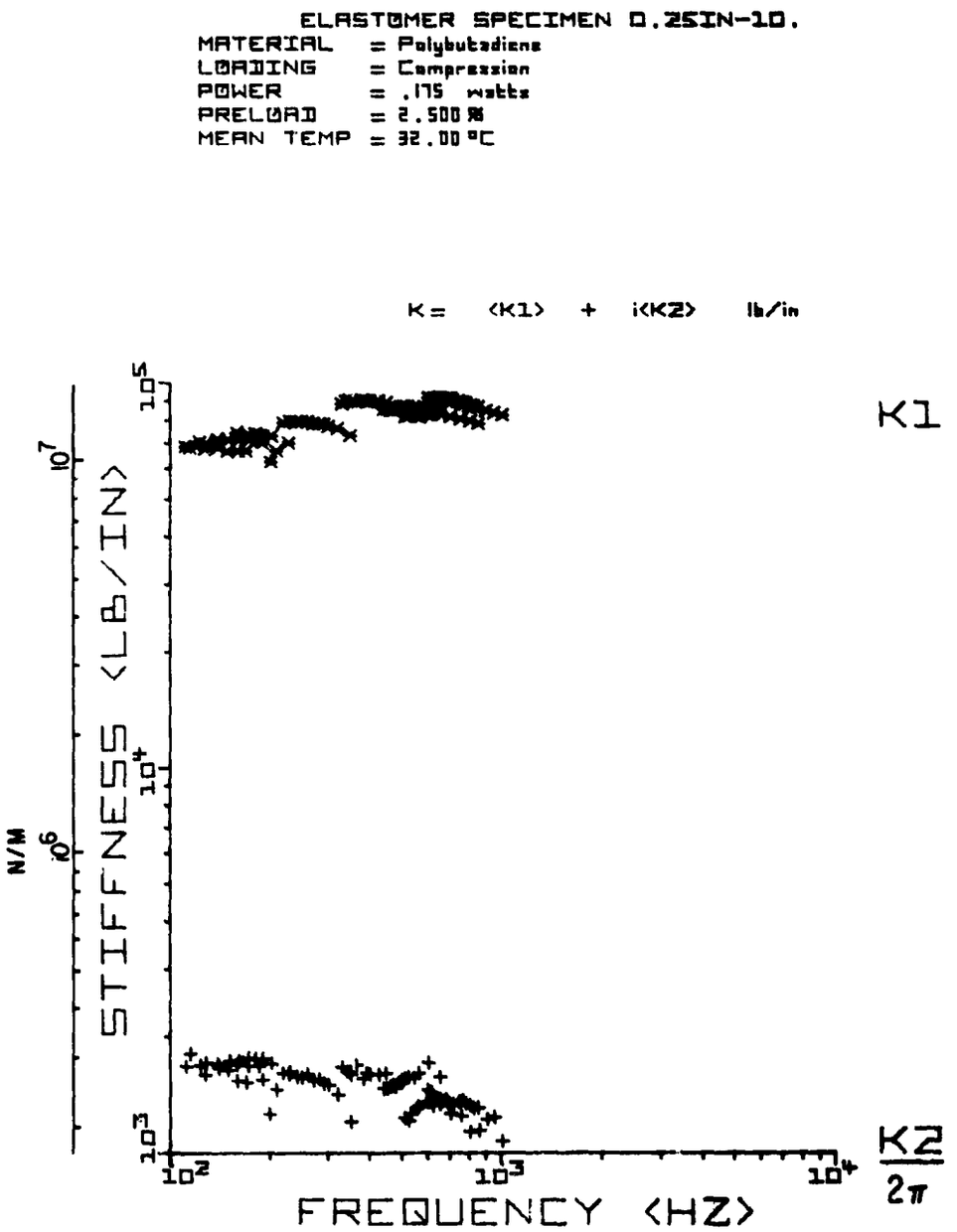

Fig. 20 Complex Stiffness of the Compression Sample With Ten Specimens at 2-1/2 Percent Preload

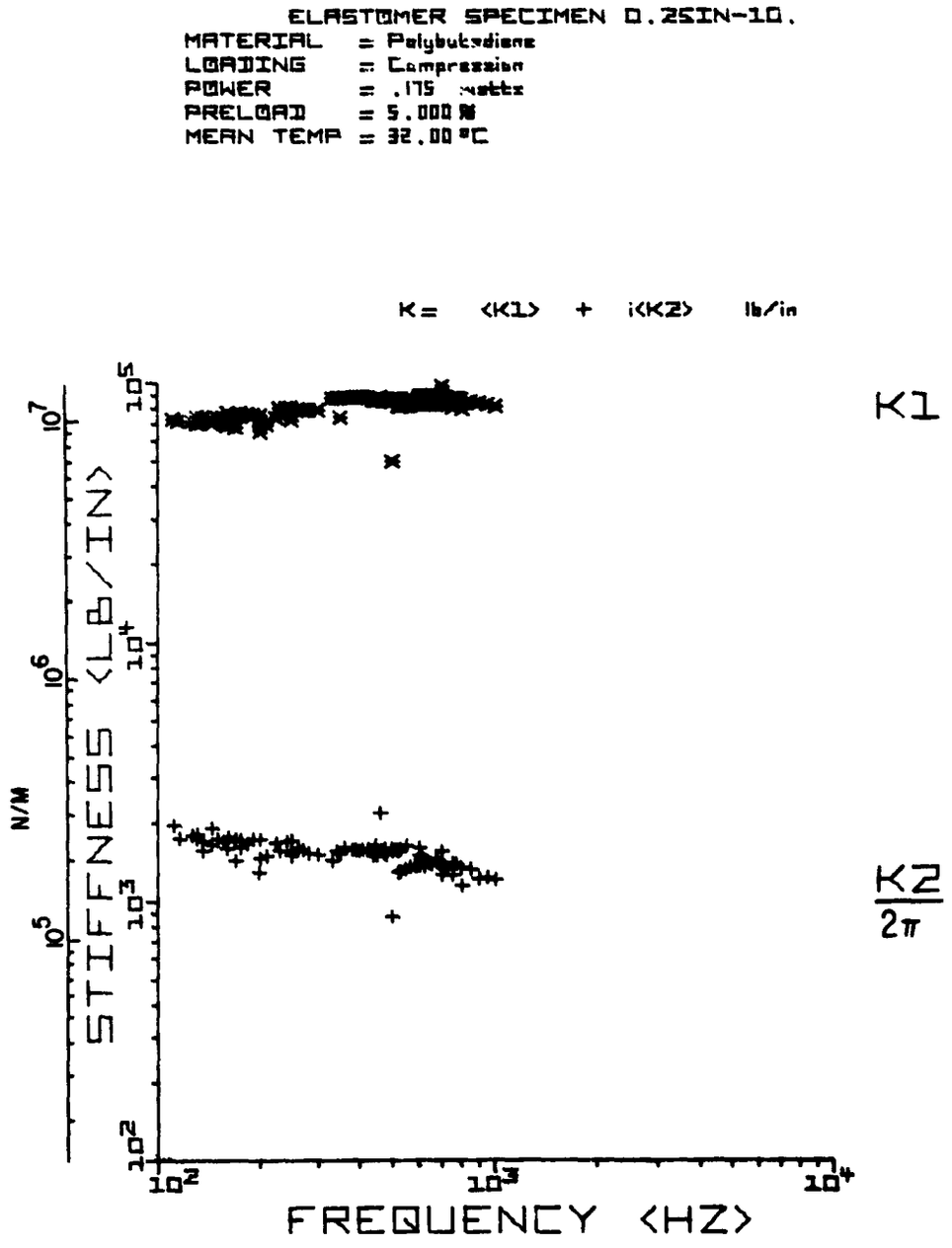

Fig. 21 Complex Stiffness of the Compression Sample With Ten Specimens at Five Percent Preload

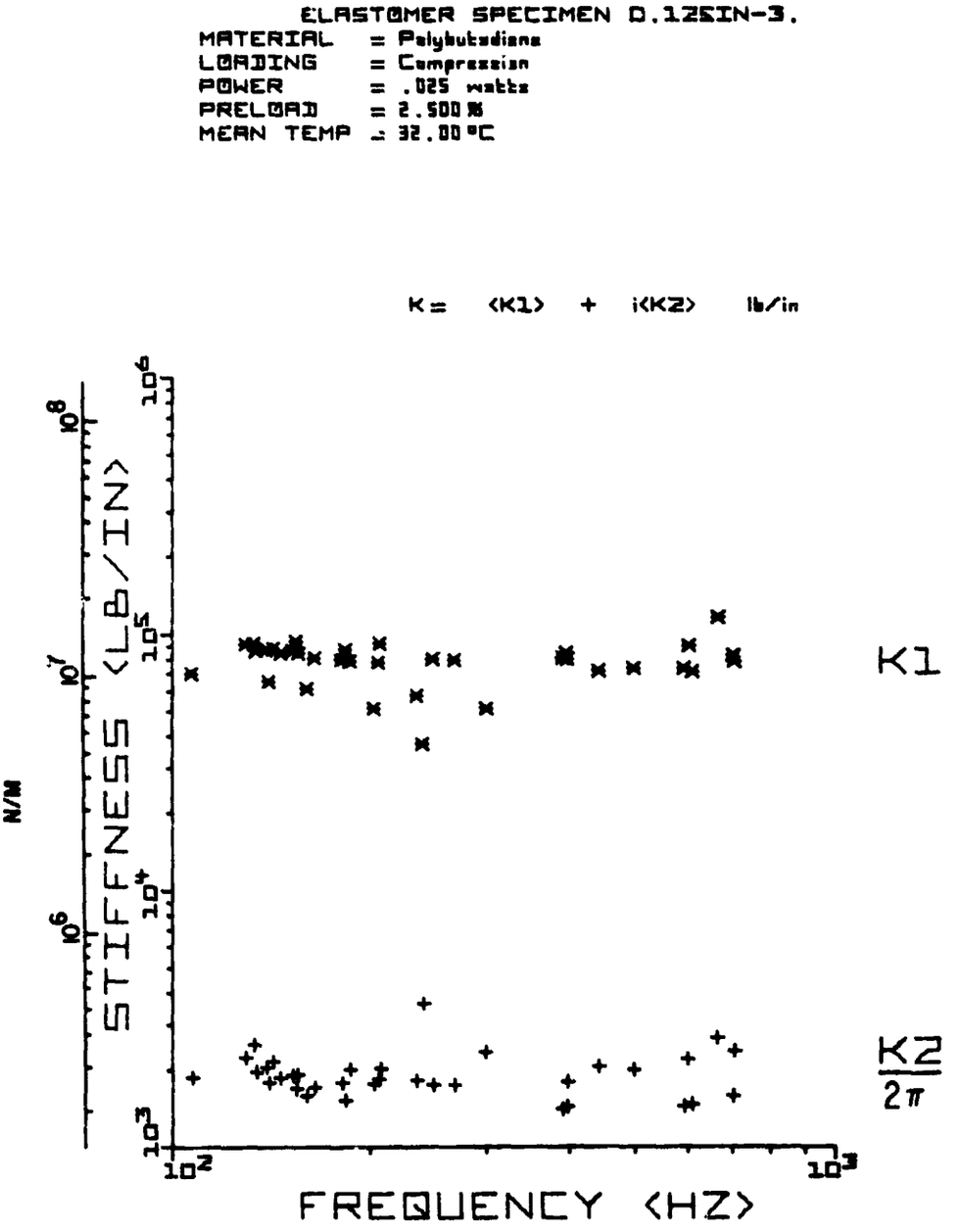

Fig. 22 Complex Stiffness of the Compression Sample With Three Specimens at 2-1/2 Percent Preload

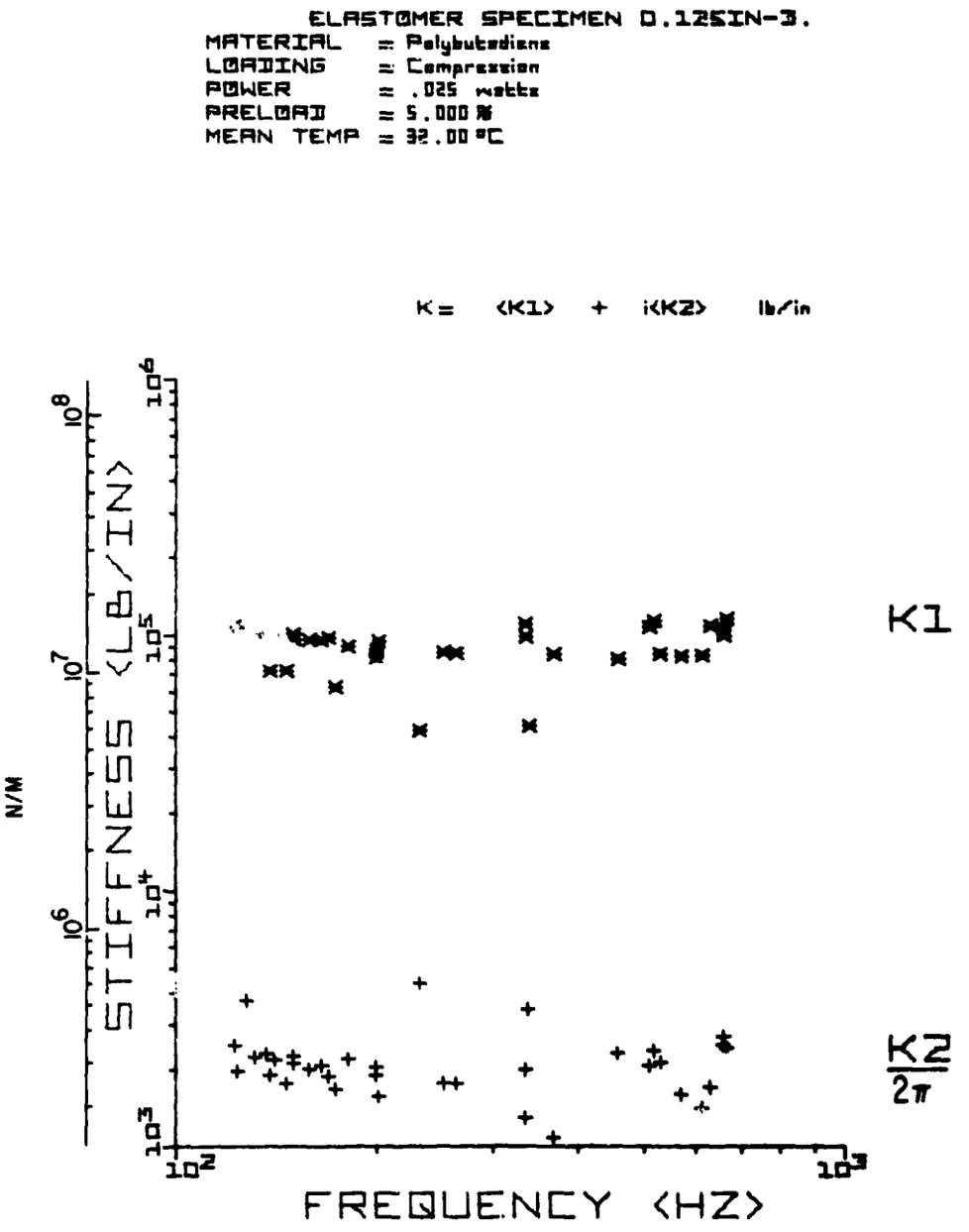

Fig. 23 Complex Stiffness of the Compression Sample With Three Specimens at Five Percent Preload

Close examination of the results of Figures 18 and 23 show the values for K1 to follow a number of distinguishable lines whose slopes differ from the overall trends. These lines respond to the different values of resonant mass, and it should be noted that each change in mass requires a reassembly of the test rig and basically a new set-up. These observations indicating the values of K1 to be somewhat dependent on the resonant mass, primarily imply that the inferred values of K1 to a certain extent are dependent of the natural frequency of the test rig. This dependence is less pronounced for K2. Although these observations are not completely understood at this time, it may be mentioned that, in general, the sensitivity of a resonant mass method to residual errors in the test procedure can be expected to vary with $(\frac{\omega}{\omega_n})$.

The variation of relative amplitude of deformation in the elastomer as a function of frequency (when the dissipation in the elastomer plus the lower cylinder is held constant) was found to be quite independent of preload. A typical variation of amplitude as a function of frequency is shown in Figure 24. The decrease in amplitude with increase in frequency indicates that the power dissipated in the elastomer also decreases with increases in frequency since K2 or $c_e\omega$ is fairly constant. It should, however, be noted that the computations of K1 and K2 are based on the assumption that the air cylinder damping coefficients are constant.

E. Shear Tests

Complex stiffness data for the shear experiments for the various specimens at different preloads are summarized in Figures 25 to 33. In general, the frequenc dependence is again small and also the effects of preloads appear to be insignificant. However, when compared with the compression data, it is seen that both the real and imaginary parts of the complex stiffness are somewhat higher in the case of shear tests.

Again, due to the power constraints, the relative amplitude variation as a function of frequency is nearly identical for all the specimens. Typical results are shown in Figure 24.

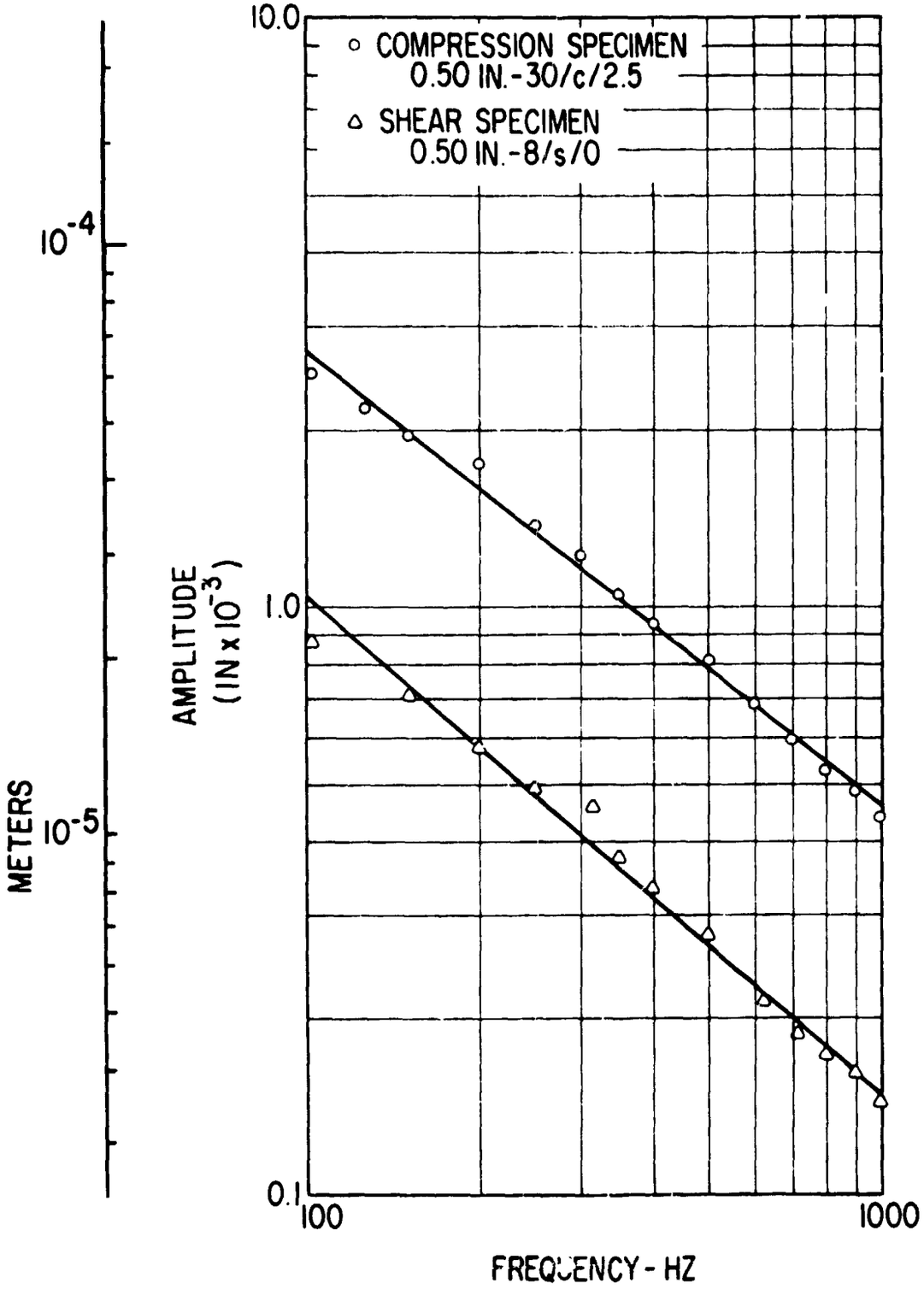

Fig. 24 Variation of Relative Deformation Amplitude in the Compression and Shear Elastomer Sample

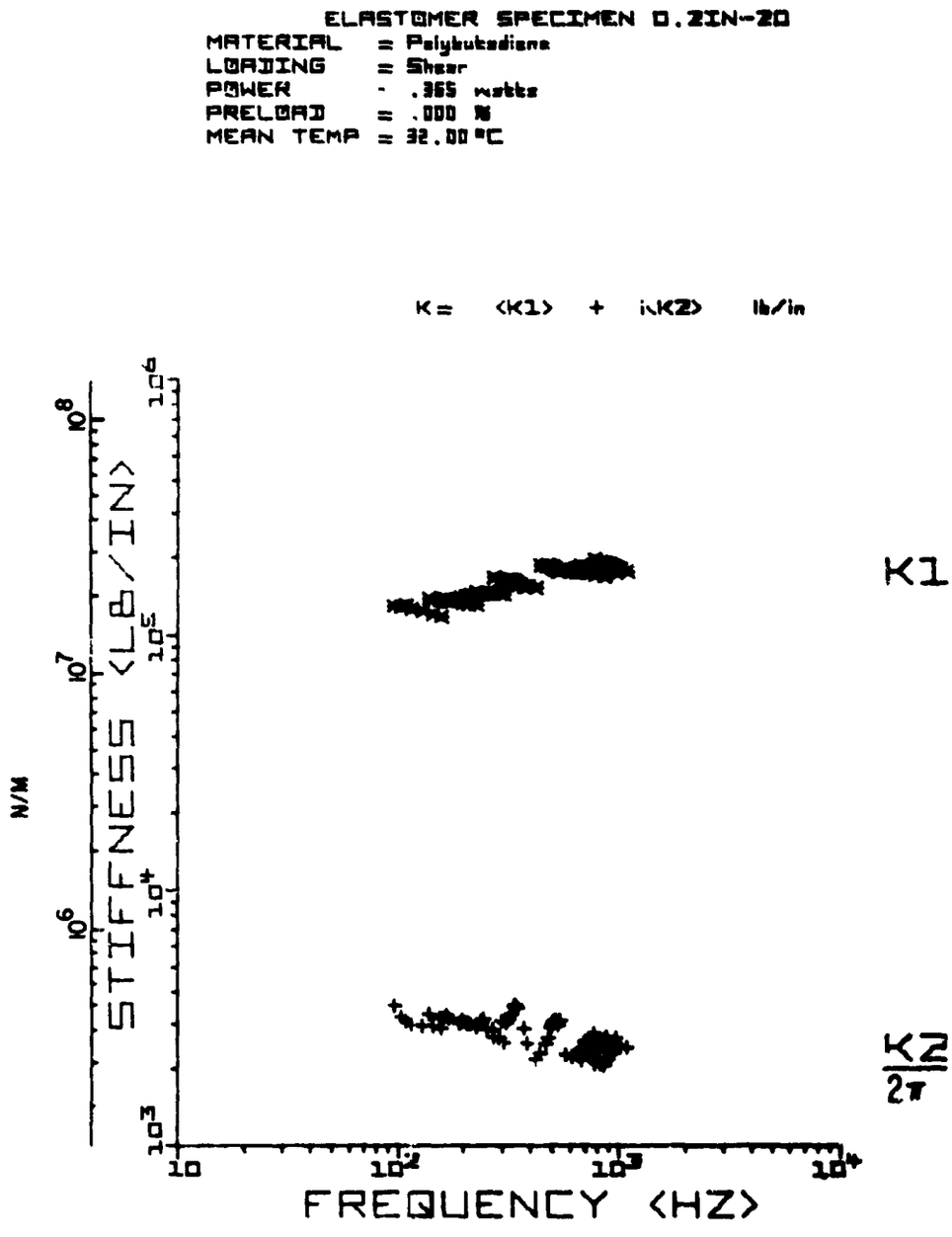

Fig. 25 Complex Stiffness of the Shear Sample With Twenty Specimens at no Preload

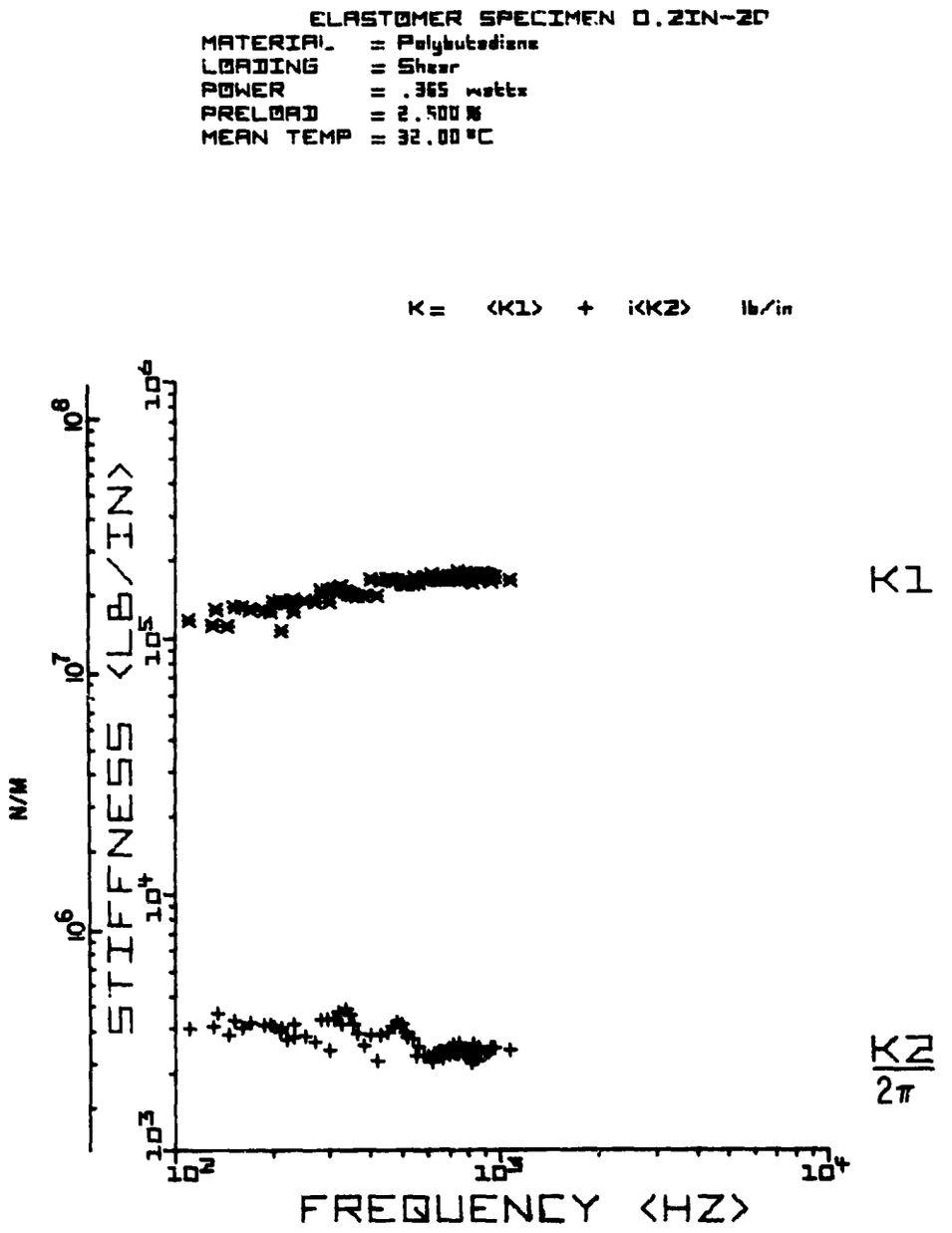

Fig. 26 Complex Stiffness of the Shear Sample With Twenty Specimens at 2-1/2 Percent Preload

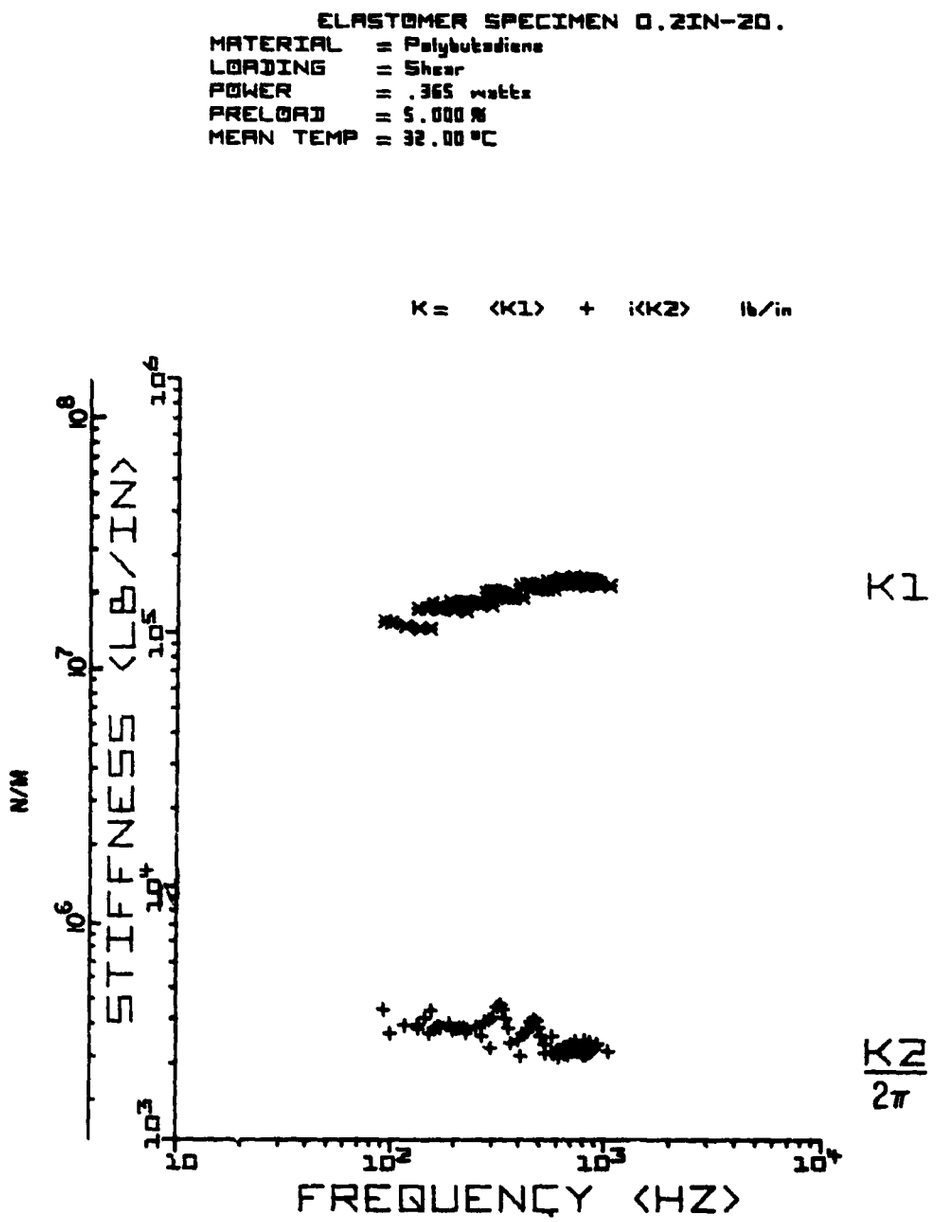

Fig. 27 Complex Stiffness of the Shear Sample With Twenty Specimens at Five Percent Preload

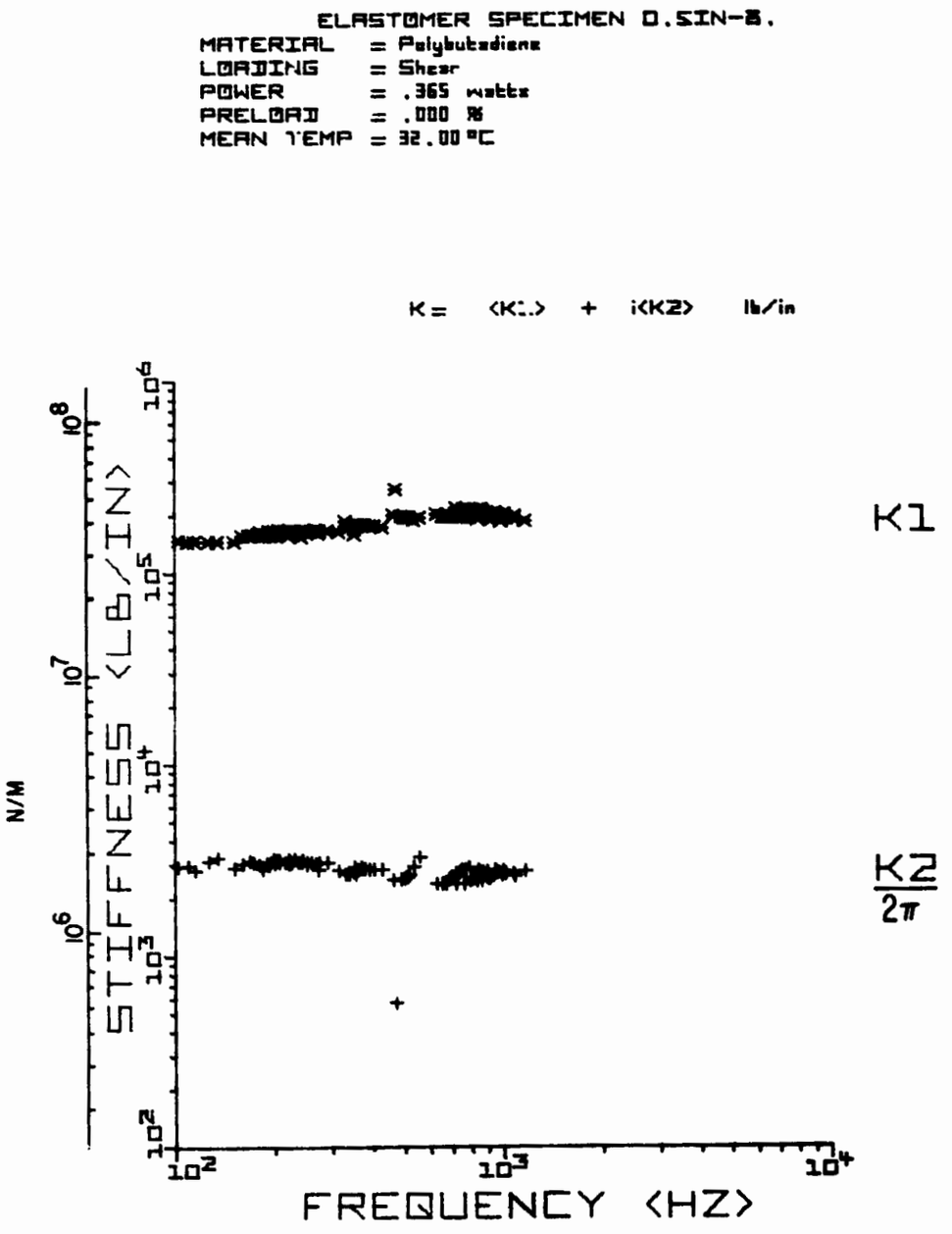

Fig. 28 Complex Stiffness of the Shear Sample With Eight Specimens at no Preload

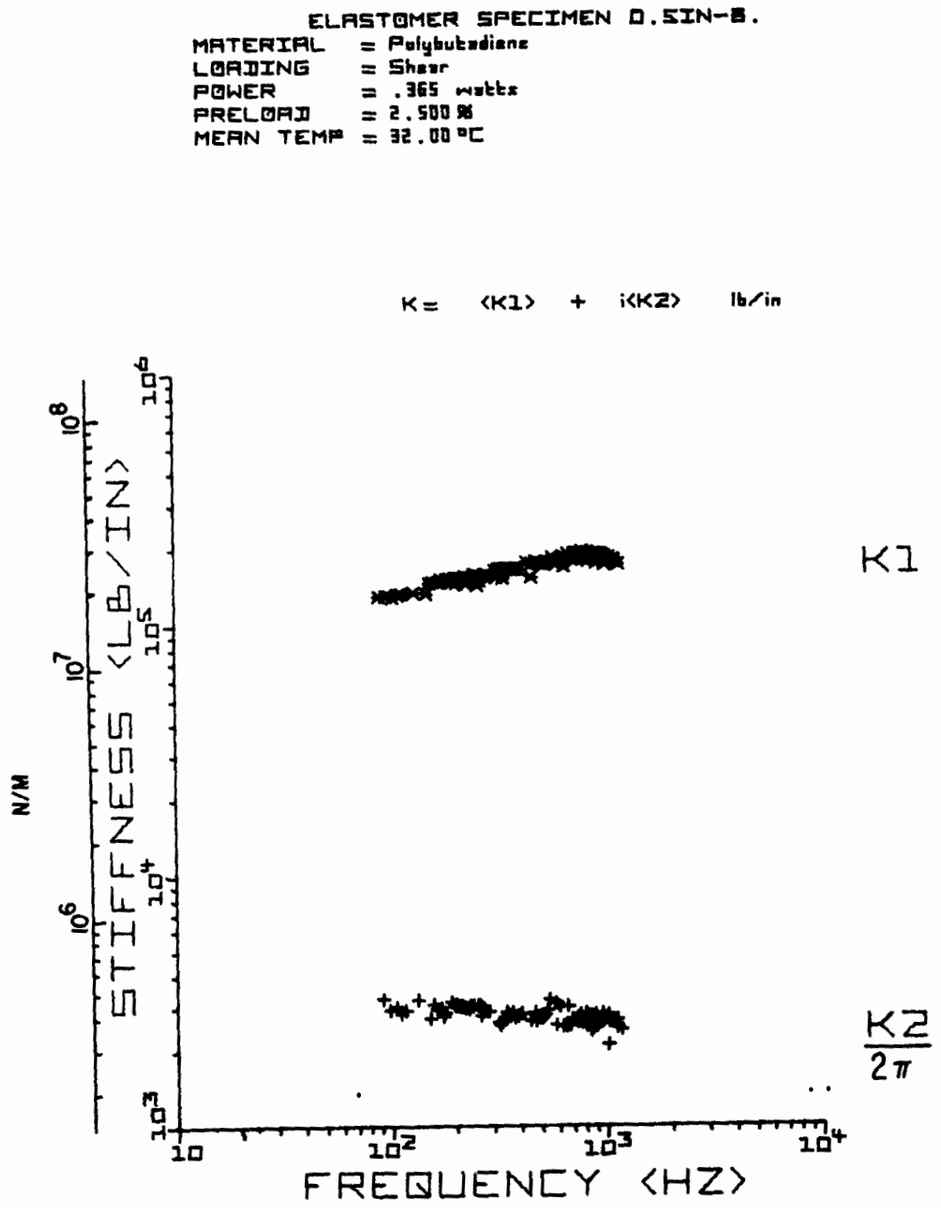

Fig. 29 Complex Stiffness of the Shear Sample With ght Specimens at 2-1/2 Percent Preload

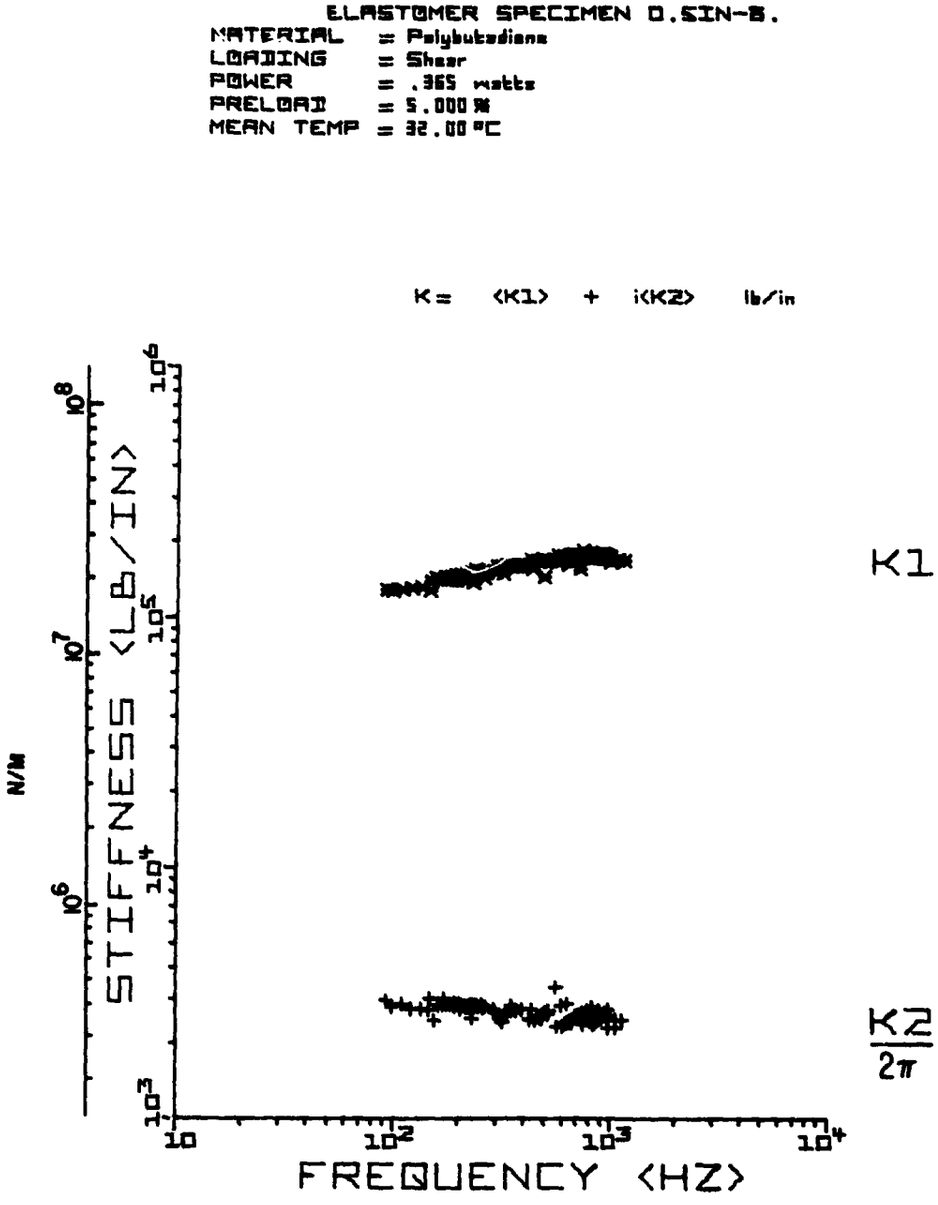

Fig. 30 Complex Stiffness of the Shear Sample With Eight Specimens at Five Percent Preload

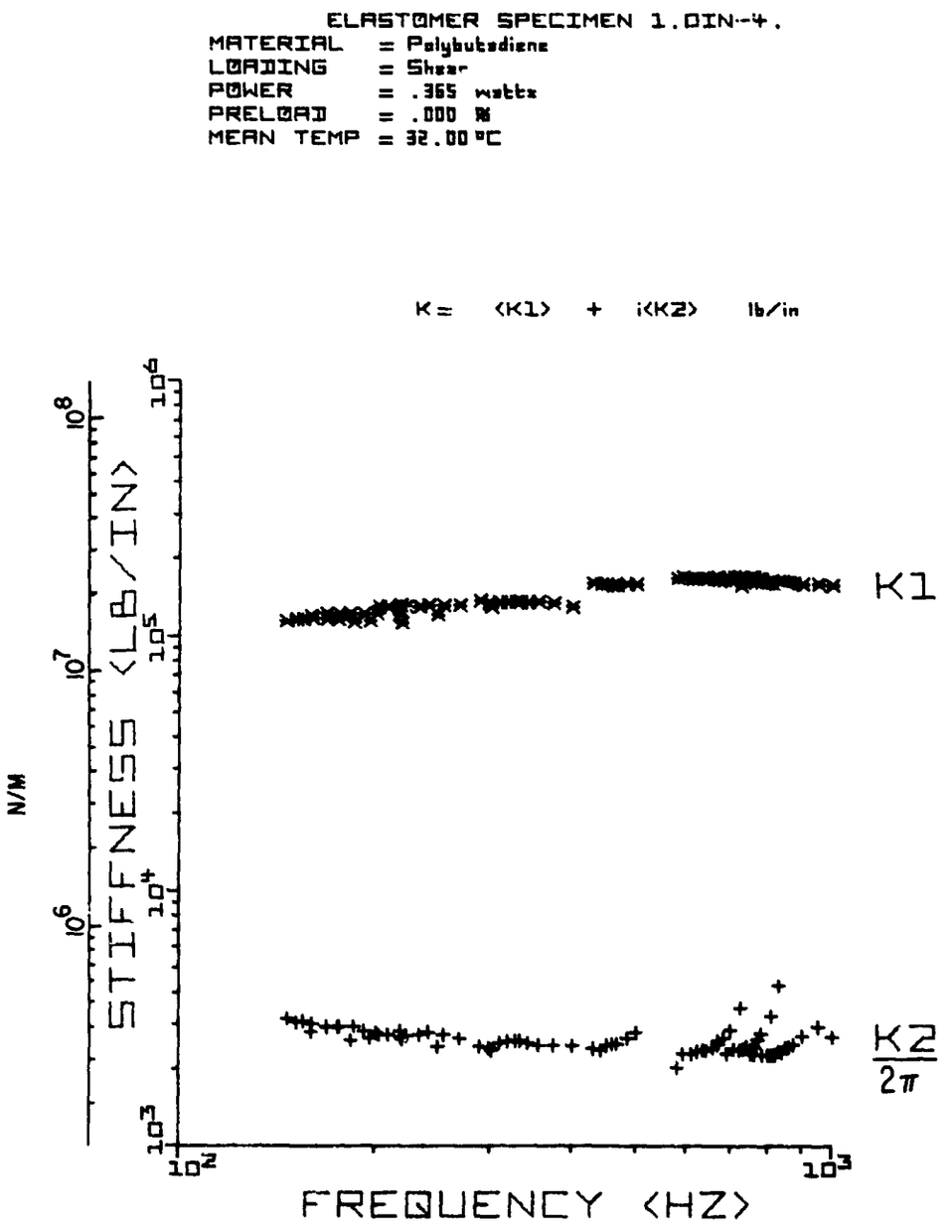

Fig. 31 Complex Stiffness of the Shear Sample With Four Specimens at no Preload

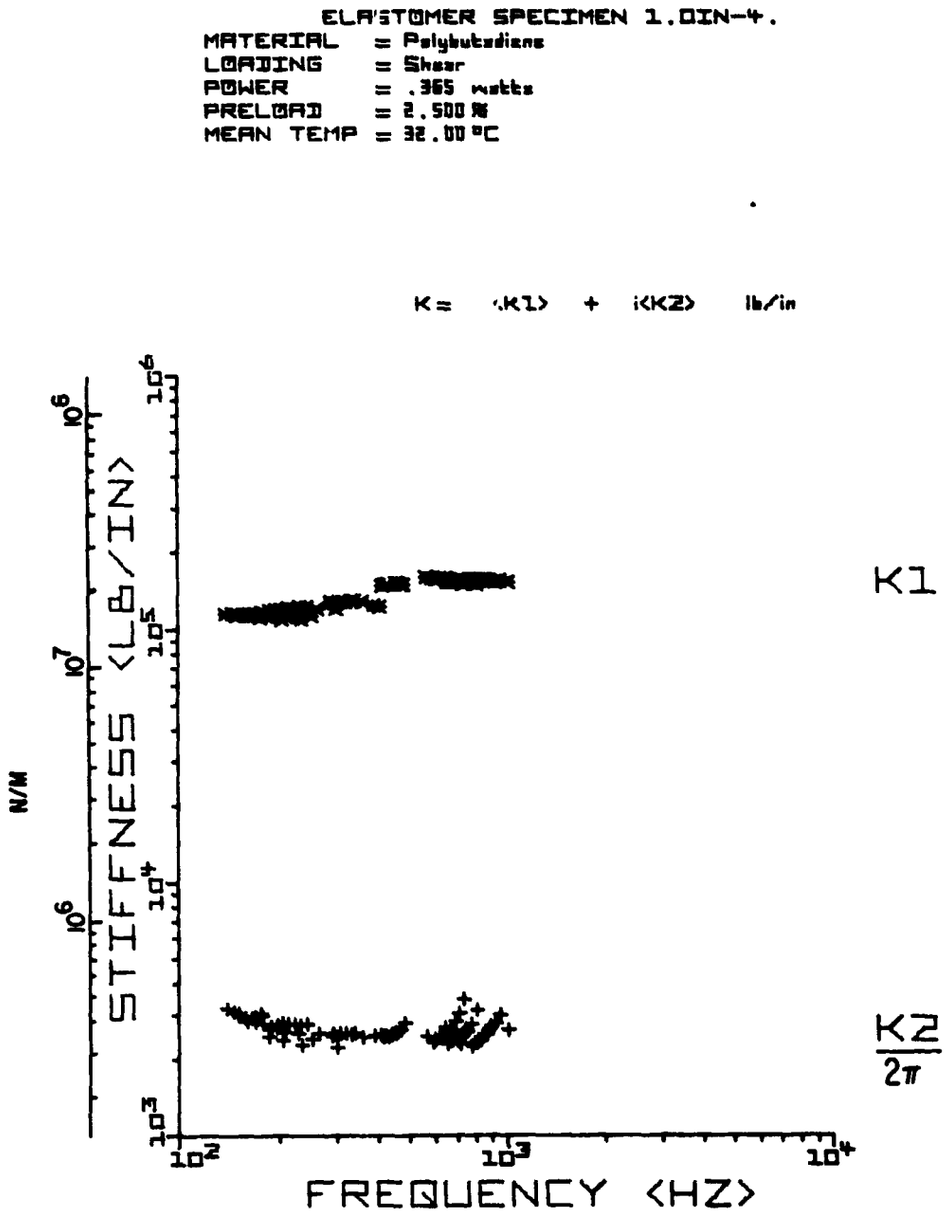

Fig. 32 Complex Stiffness of the Shear Sample With Four Specimens at 2-1/2 Percent Preload

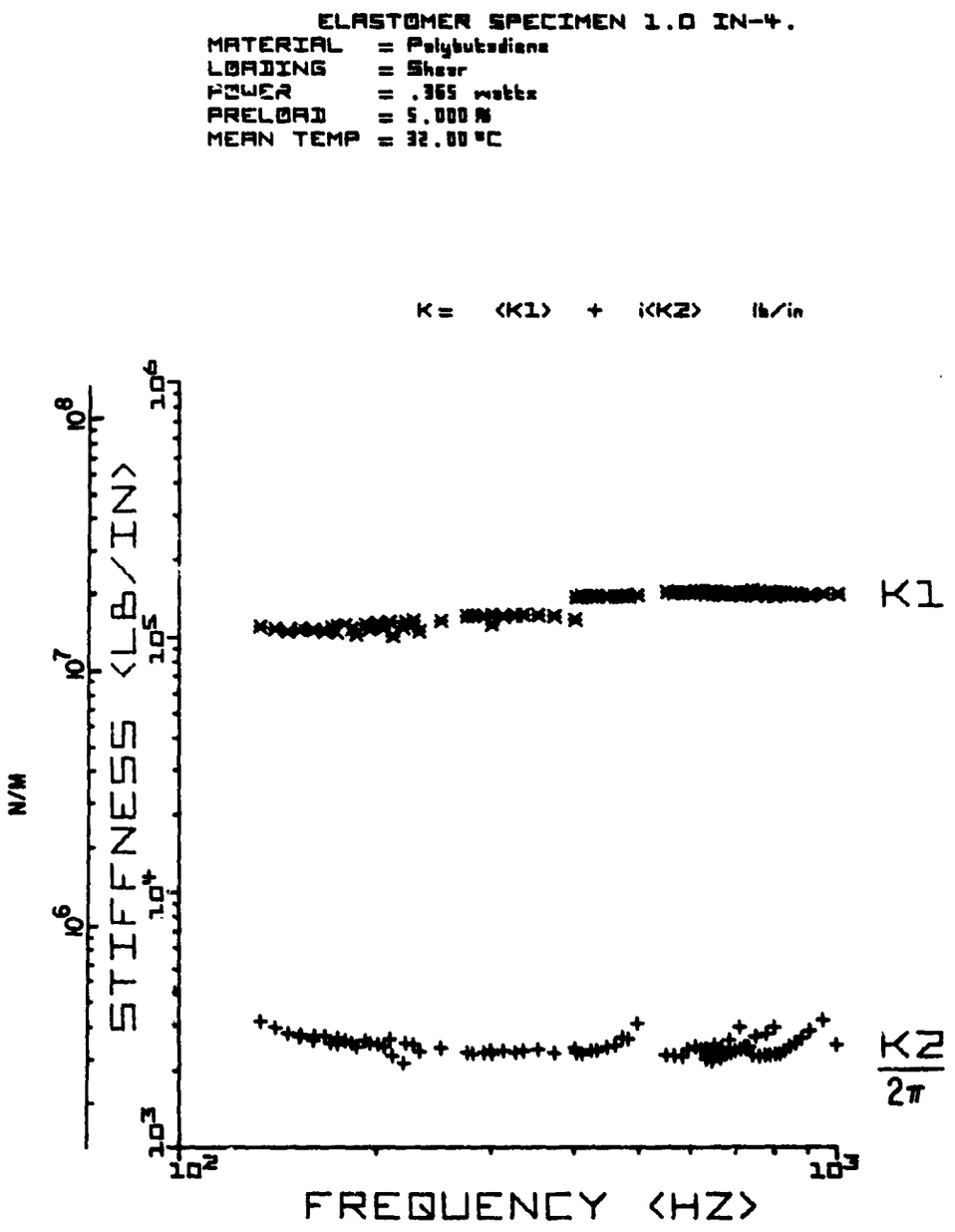

Fig. 33 Complex Stiffness of the Shear Sample With Four Specimens at Five Percent Preload

F. Summary and Correlation of Test Results

Within the experimental range of frequencies the complex stiffness shows a fairly mild frequency dependence for all compression and shear experiments. Thus, for the purpose of estimating specimen stiffness, single values of the complex stiffness may be stated for the entire frequency range without any appreciable errors. The second and fifth columns in Table 1 give the mean values over the frequency range of the real and imaginary stiffness components for each sample under each preload condition. The similarity of these mean values at different preloads indicates insensitivity to preload. The similarity in stiffness among elastomer samples which have different shape factors, but have been designed for similar stiffness (see design details in Appendix A), is also fairly similar.

The weak frequency dependence of the data may be summarized in terms of the coefficients of a power law correlation function of the form

$$Y = A\,\omega^{B}$$

where Y is one of the variables of interest (K1, K2, or amplitude) or

$$\ln\left(\frac{Y}{A}\right) = B \ln \omega.$$

Thus the data falls on a straight line on log-log paper. The coefficients A and B for each data set are computed by conventional least squares regression analysis and summarized in the third, fourth, sixth, and seventh columns of Table 1. These correlation terms may be used to determine the relaxation modulus of the material at constant temperature. Deformation amplitudes are also summarized in Table 1, both in terms of mean values over the frequency range in terms of the coefficients of the same power law correlation functions. As a demonstration, the power loss correlation to the 1.27 cm (0.5 in.) high compression sample with 2.5 per cent preload is superimposed on the experimental data in Figure 34.

A powerful technique for the correlation of elastomer data with marked frequency dependence is to fit mechanical viscoelastic models. For the present data, with its weak dependence on frequency, such techniques may not be employed very efficiently. However, as a demonstration of the approach, the behavior of the

TABLE 1

SUMMARY OF ELASTOMER TEST DATA

MATERIAL = Polybutadiene
TEMPERATURE = 32 deg-C

COMPLEX STIFFNESS K = K1 + iK2 lb/in
CORRELATION FORM Y = A*OMEGA**B

SPECIMEN DETAILS	K1 MEAN lb/in	K1 A	K1 B	K2 MEAN lb/in	K2 A	K2 B	AMPLITUDE MEAN in	AMPLITUDE A	AMPLITUDE B
0.50IN-30/C/2.5	7.541E+04	2.224E+04	1.589E-01	8.347E+03	1.873E+04	-1.051E-01	1.055E-03	3.854E-01	-7.677E-01
0.50IN-30/C/5.0	7.809E+04	2.545E+04	1.458E-01	8.657E+03	1.507E+04	-7.212E-02	1.042E-03	3.401E-01	-7.529E-01
0.25IN-10/C/2.5	8.042E+04	2.871E+04	1.325E-01	9.266E+03	2.809E+04	-1.427E-01	3.806E-04	2.040E-01	-8.082E-01
0.25IN-10/C/5.0	8.026E+04	3.577E+04	1.044E-01	9.447E+03	2.753E+04	-1.382E-01	3.924E-04	1.764E-01	-7.889E-01
0.125IN-3/C/2.5	7.662E+04	7.312E+04	6.368E-03	1.190E+04	1.378E+04	-2.004E-02	2.501E-04	2.407E-02	-6.216E-01
0.125IN-3/C/5.0	8.892E+04	7.007E+04	3.227E-02	1.295E+04	1.854E+04	-4.859E-02	2.250E-04	3.547E-02	-6.854E-01
0.5IN-8 /S/0.	1.708E+05	5.330E+04	1.548E-01	1.720E+04	3.457E+04	-8.886E-02	3.186E-04	2.478E-01	-8.473E-01
0.5IN-8 /S/2.5	1.666E+05	5.003E+04	1.530E-01	1.737E+04	3.138E+04	-7.521E-02	3.498E-04	4.985E-01	-9.232E-01
0.5IN-8 /S/5.0	1.598E+05	5.361E+04	1.391E-01	1.653E+04	2.678E+04	-6.142E-02	3.462E-04	2.162E-01	-8.198E-01
1.0IN-4 /S/0.	1.453E+05	2.569E+04	2.199E-01	1.624E+04	2.800E+04	-6.912E-02	3.497E-04	2.844E-01	-8.503E-01
1.0IN-4 /S/2.5	1.351E+05	2.550E+04	2.135E-01	1.631E+04	2.388E+04	-4.882E-02	3.799E-04	2.502E-01	-8.309E-01
1.0 IN-4 /S/5.0	1.307E+05	2.263E+04	2.238E-01	1.563E+04	1.923E+04	-2.647E-02	3.820E-04	2.635E-01	-8.339E-01
0.2IN-20 /S/0.	1.625E+05	3.708E+04	1.881E-01	1.689E+04	5.700E+04	-1.548E-01	3.395E-04	2.168E-01	-8.220E-01
0.2IN-20 /S/2.5	1.549E+05	3.336E+04	1.936E-01	1.681E+04	5.867E+04	-1.576E-01	3.398E-04	2.630E-01	-8.386E-01
0.2IN-20 /S/5.0	1.452E+05	3.689E+04	1.743E-01	1.600E+04	4.833E+04	-1.406E-01	3.683E-04	2.240E-01	-8.156E-01

COMPLEX STIFFNESS K = K1 + iK2 New/m
CORRELATION FORM Y = A*OMEGA**B

SPECIMEN DETAILS	K1 MEAN New/m	K1 A	K1 B	K2 MEAN New/m	K2 A	K2 B	AMPLITUDE MEAN m	AMPLITUDE A	AMPLITUDE B
0.50IN-30/C/2.5	1.321E+07	3.894E+06	1.589E-01	1.462E+06	3.280E+06	-1.051E-01	2.679E-05	9.790E-03	-7.677E-01
0.50IN-30/C/5.0	1.368E+07	4.457E+06	1.458E-01	1.516E+06	2.640E+06	-7.212E-02	2.646E-05	8.639E-03	-7.529E-01
0.25IN-10/C/2.5	1.408E+07	5.027E+06	1.325E-01	1.623E+06	4.920E+06	-1.427E-01	9.668E-06	5.180E-03	-8.082E-01
0.25IN-10/C/5.0	1.406E+07	6.264E+06	1.044E-01	1.654E+06	4.822E+06	-1.382E-01	9.968E-06	4.480E-03	-7.889E-01
0.125IN-3/C/2.5	1.342E+07	1.281E+07	6.370E-03	2.084E+06	2.414E+06	-2.004E-02	6.354E-06	6.114E-04	-6.216E-01
0.125IN-3/C/5.0	1.557E+07	1.227E+07	3.227E-02	2.268E+06	3.247E+06	-4.859E-02	5.715E-06	9.010E-04	-6.854E-01
0.5IN-8 /S/0.	3.149E+07	9.335E+06	1.548E-01	3.012E+06	6.054E+06	-8.886E-02	8.092E-06	6.294E-03	-8.473E-01
0.5IN-8 /S/2.5	2.918E+07	8.762E+06	1.530E-01	3.042E+06	5.497E+06	-7.521E-02	8.885E-06	1.266E-02	-9.232E-01
0.5IN-8 /S/5.0	2.799E+07	9.389E+06	1.391E-01	2.895E+06	4.689E+06	-6.141E-02	8.794E-06	5.491E-03	-8.198E-01
1.0IN-4 /S/0.	2.545E+07	4.499E+06	2.199E-01	2.844E+06	4.903E+06	-6.912E-02	8.881E-06	7.223E-03	-8.503E-01
1.0IN-4 /S/2.5	2.366E+07	4.465E+06	2.135E-01	2.857E+06	4.183E+06	-4.883E-02	9.648E-06	6.356E-03	-8.309E-01
1.0 IN-4 /S/5.0	2.289E+07	3.963E+06	2.238E-01	2.737E+06	3.369E+06	-2.647E-02	9.703E-06	6.692E-03	-8.339E-01
0.2IN-20 /S/0.	2.846E+07	6.494E+06	1.881E-01	2.959E+06	9.984E+06	-1.548E-01	8.624E-06	5.506E-03	-8.220E-01
0.2IN-20 /S/2.5	2.713E+07	5.843E+06	1.936E-01	2.944E+06	1.028E+07	-1.576E-01	8.631E-06	6.680E-03	-8.386E-01
0.2IN-20 /S/5.0	2.542E+07	6.461E+06	1.743E-01	2.803E+06	8.464E+06	-1.406E-01	9.355E-06	5.691E-03	-8.156E-01

N.B. Frequency OMEGA in the correlation function is in rad/sec.

A sample consists of several specimens of elastomer arranged in a prescribed configuration.

"Specimen details" code given in the table is derived as follows:

(1) Compression Sample: (Specimen thickness) IN - No. of Specimens/C/ (% Preload).
The diameter of all compression specimens is 1/2 in.

(2) Shear Sample: (Specimen length) IN - No. of Specimens/S/ (% Preload)
The specimen thickness and width normal to direction of deformation for all shear specimens are respectively 1/8 in and 1.92 in.

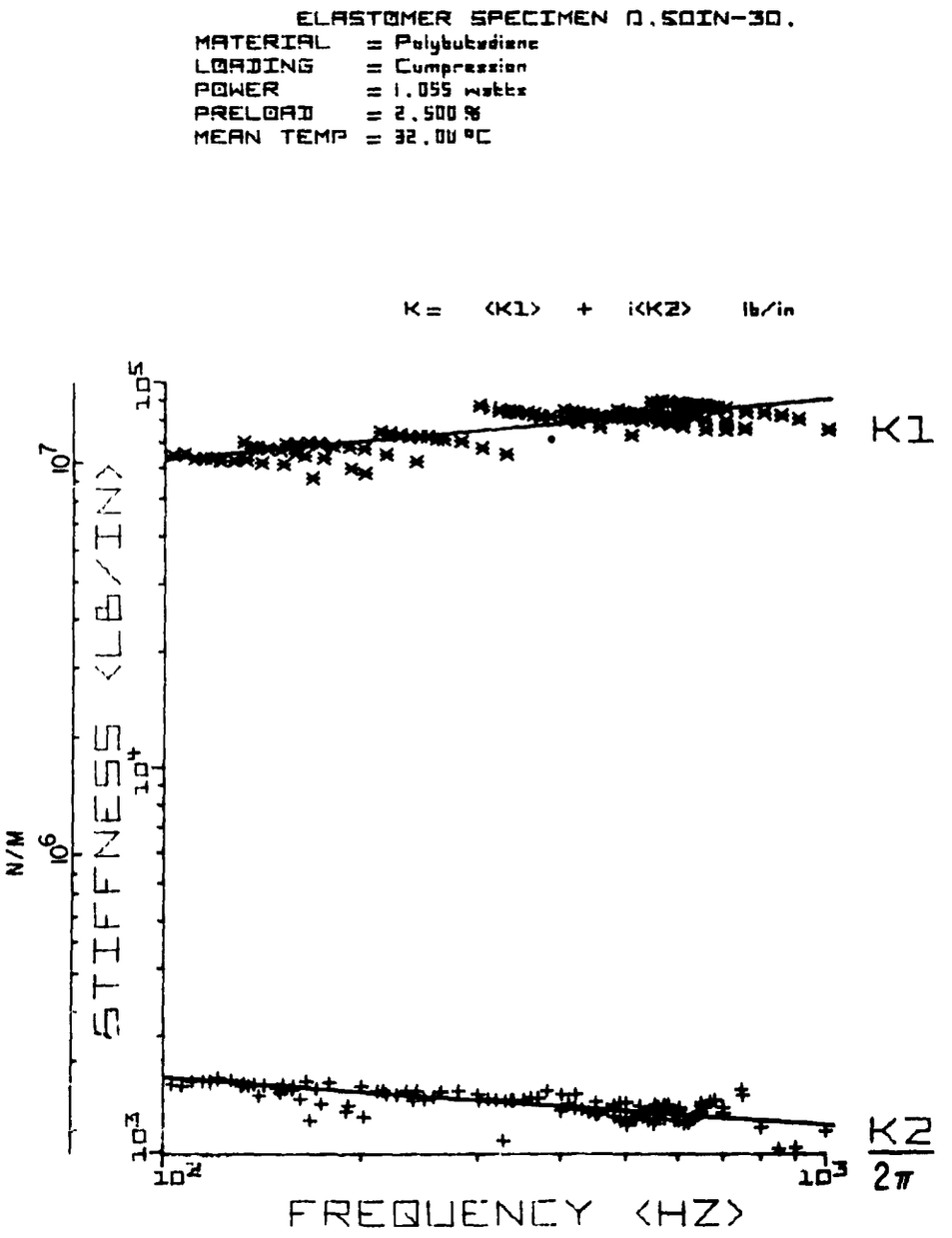

Fig. 34 Typical Power Law Correlation

data for the compression sample having 30 cylindrical elastomer specimens with 1.27 cm (0.5 in.) diameter and 1.27 cm (0.5 in.) thick was correlated with a double Voigt model. The least squares technique described in Appendix D was used to determine the various coefficients of the model. Since the selected model is of the series type, the analysis is best performed in terms of complex compliances. The results are shown in Figure 35. It is seen that most of the stiffness is determined by the static spring, and that the stiffness and damping behavior of the model follows reasonably closely the mean level of the measured stiffness and damping values. Within this order of agreement between experimental data and model predictions, a large number of different types of models may be shown to fit the data. However, the use of mean values, or the simple correlation functions, is adequate in the present case.

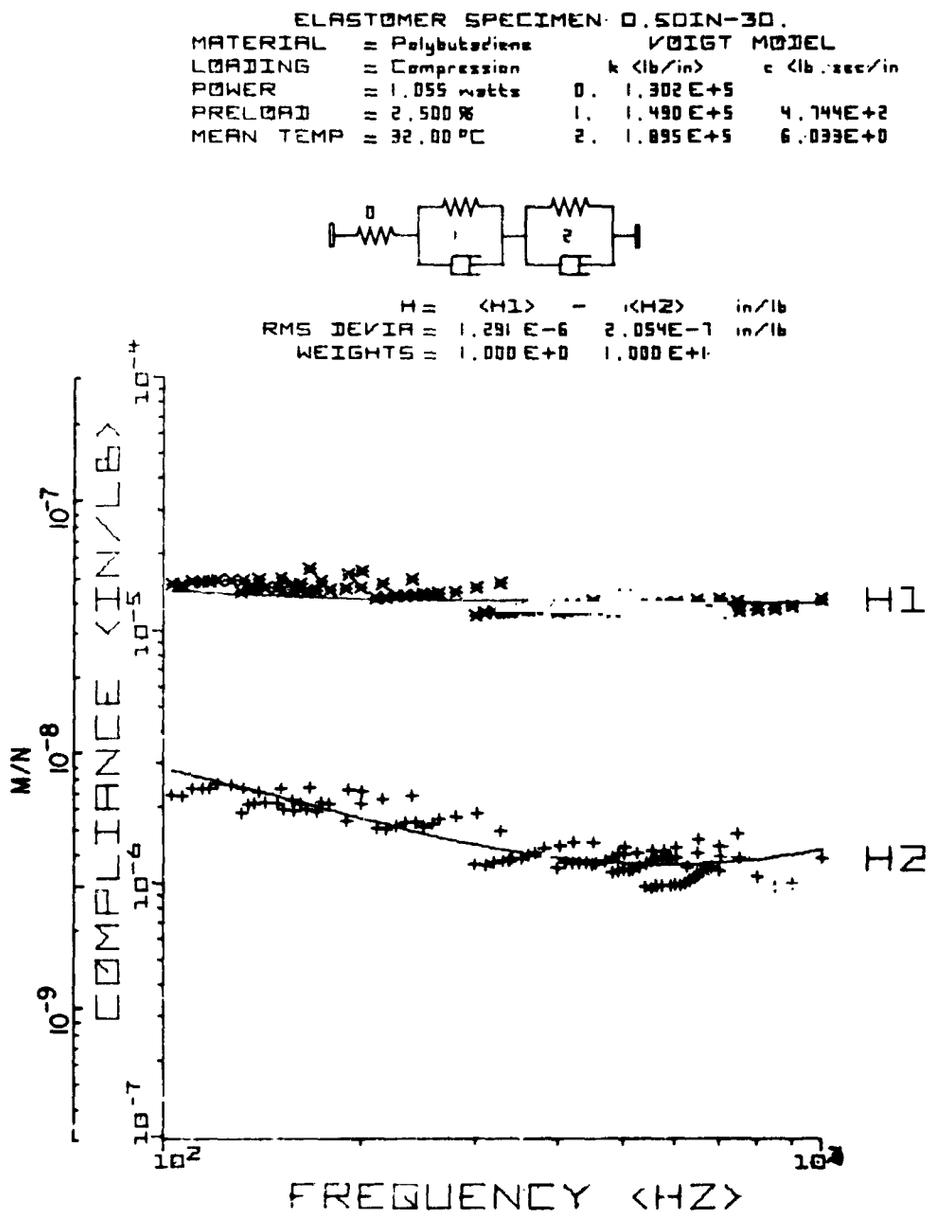

Fig. 35 Typical Correlation of Experimental Data With a Double Voigt Model

V. DISCUSSION

Examination of the experimental data indicates that, if the thermal state of the elastomer is held constant, the complex stiffness of the material is relatively insensitive to the variation of frequency. It is expected that, if K2 or $c_e\omega$ is a constant, then for constant power dissipation in the elastomer, the relative amplitude must also be frequency independent. However, in all the experiments, the power measurement was primarily used to establish an upper bound on the temperature gradient in the elastomer and, in fact, the measured power is a sum of elastomer dissipation and the dissipation in the lower cylinder. It may be shown [8] that, if the damping coefficient of the cylinder is a constant, and if the total work done per cycle is when the relative amplitude is x_r, then

$$\pi\, c_\ell \omega x_r^2 + \pi c_e\, \omega x_r^2 = W$$

The above equation may be rearranged as

$$x_r^2 = \frac{W/\pi}{K2 + c_\ell \omega} = \frac{2x\ \text{power}}{\omega(K2 + C_\ell \omega)}$$

Since the imaginary part of the complex stiffness $K2 = c_e\omega$ was found to be fairly insensitive to the frequency, the amplitude will decrease as a function of frequency at constant power, as found in all the experiments.

The uncertainties in the computed elastomer properties will be generally small when the nominal stiffness and damping values of the test samples are substantially larger than those of the various elements of the test rig, as shown by Equations (B5) and Table B1. A comparison of the elastomer coefficients shown in Table 1 with those of the test rig components clearly shows that the stiffness of any of the test rig elements is indeed small compared to the elastomer stiffness and, therefore, any errors will not significantly affect the computed stiffness of the elastomer. In case of the damping coefficient, however, Equations (B5) need further discussion. If the proper values of c_1 and c_2 from Table B1 are substituted in the second of the Equations (B5), the elastomer damping efficient may be written as

$$\frac{c_\ell + c_e}{m\omega} = \frac{\frac{c_u}{m\omega}\ \alpha\ (\cos\phi - \alpha) + \alpha \sin\phi \left(1 - \frac{k_2}{m\omega^2}\right)}{\alpha^2 - 2\alpha \cos\phi + 1}$$

Since the experimental data was collected at conditions close to resonance where transmissibility $\alpha >> 1$, and the residual stiffnesses are small compared to the elastomer stiffness, the above equation may be approximated as

$$\frac{c_\ell + c_e}{m\omega} \approx \frac{\sin\phi}{\alpha} - \frac{c_u}{m\omega}$$

or

$$c_e \approx \frac{m\omega \sin}{\alpha} - (c_\ell + c_u)$$

Thus, an error in the estimation of c_ℓ and c_u will have an additive error in c_e or a linear frequency dependent error in K2.

It is now clear that,if the nominal value of elastomer damping is substantially large in comparison with the sum of the cylinder damping coefficients, $(c_\ell + c_u)$, then any small uncertainties in the estimation of $c_\ell + c_u$ will not appreciably effect the elastomer damping coefficients c_e. If the results summarized in Table 1 are reexamined, it is seen that $K2 = c_e\omega$ is fairly insensitive to frequency. The elastomer damping, therefore, decreases as a function of frequency and the greatest significance of errors in cylinder damping are to be expected at the highest frequencies. The lowest values of K2 for the compression and shear samples from Table 1 are 1.462×10^6 N/m (8.347×10^3 lb/in.) and 2.737×10^6 N/m (1.563×10^4 lb/in.) respectively. At a frequency of 1000 Hz these values result in elastomer damping coefficients, c_e, of about 2.33×10^2 N-sec/m and 4.36×10^2 N-sec/m (1.33 and 2.49 lb-sec/in) respectively for the compression and shear samples. The total residual damping $(c_\ell + c_u)$ is about 1.05×10^2 N-sec/m (0.6 lb-sec/in.). Thus, uncertainties in the estimated residual damping may become significant in the extreme high frequency region. Under such conditions, methods both to reduce and more accurately determine these residual damping coefficients should be considered in relation to future test rig modifications.

The effects of preloads, if any, on the dynamic response of the elastomer are not clearly noticeable within the present data. Of course the maximum nominal strain due to the preload was no more than 5 percent. At least for the compression tests it might be expected that an increase in preload results in increased stiffness. This is indeed observed to some degree as shown in Table 1, however, the present data does not warrant such a general conclusion. In fact, for the shear samples a reversed effect is consistently observed.

Since vibration amplitude was not varied as an independent parameter, no conclusions can be drawn as to the influence of amplitude. It is, however, a premise of this work that, as long as the temperature of the elastomer remains constant, the influence of amplitude will be small. In other words dynamic characteristics measured under conditions which both limit the temperature rise and control the environmental temperature should be the same whether the amplitude is constant or the power dissipated is constant. Further investigation of the influence of amplitude will be necessary to consolidate this point.

Relations between the complex stiffness and some basic physical properties such as relaxation modulus could be mathematically expressed [9] in terms of Fourier relations. However, a much more rigorous analysis of the experimental data will be required in order to obtain the correlation functions describing the complex stiffness in the entire frequency range of zero to infinity. This clearly warrants more experiments and data analysis. It is anticipated that future investigations will accomplish this objective.

As described in Appendix A, the test samples were designed with the primary objective of investigating the elastomer behavior in the frequency range of 100 to 1000 Hz with varying shape factors. This objective has clearly been achieved in the present investigation. Furthermore, the results summarized in Table 1 show that variations in the dynamic stiffness within the three compression or the three shear samples are small. However, the dynamic stiffness of the shear samples is about twice that of the compression samples. If the static stiffness ratio of shear to compression samples is computed

from the simple relations given in Appendix A, it is found that this ratio varies from 1.8 to 2.27. Thus, the observed difference in dynamic stiffness of the shear and compression samples is primarily due to the differences in the static stiffness for the selected geometrical configurations. The absolute values of the dynamic stiffness, as might be expected, are substantially larger than those of the static stiffness (as defined in Appendix A). This is in agreement with most of the published investigations, e.g., Meyer and Sommer [5] or Cardillo [4]. Although no general conclusion with regard to the influence of shape factors on the dynamic properties of an elastomer sample may be presently justified, it is very likely that shape factors influence the static stiffness as described in Appendix A. In other words, samples with varying shape factors but similar static stiffness will have closely identical dynamic stiffness at any frequency, as demonstrated in this investigation.

VI. CONCLUSIONS

A BTR elastomer (polybutadiene) has been tested under shear and compressive loading, at $32^{o}C$, for constant power dissipation, over the frequency range 100 to 1000 Hz. Displacement amplitudes covered 2.54×10^{-6} to 7.6×10^{-5} m (strains of 0.0008 to 0.024). From the test results, for these conditions, the following conclusions may be drawn.

1. The procedure for monitoring and controlling power dissipation and environmental temperature was successful in allowing measurement of sample properties at a temperature constant with $\pm 1^{o}C$.
2. The dynamic properties in terms of complex stiffness are only weakly influenced by frequency.
3. A simple power law relationship may be used to represent the measured frequency dependence.
4. The dynamic properties in terms of complex stiffness are not significantly influenced by preload.
5. The use of published shape factors to design different shaped elastomer samples for equal stiffness resulted in samples whose dynamic stiffness and damping values were similar.

VII. RECOMMENDATIONS FOR FUTURE RESEARCH

On the basis of the work reported and the overall objectives of the Elastomer Technology Program, the following recommendations for future investigations are made.

1. Utilize the reported stiffness and damping properties for elastomer specimens of particular geometry to determine generally applicable material properties.
2. Apply these material properties in the prediction of stiffness and damping properties of the same material, but with different geometries.
3. In particular, predict the stiffness and damping of a cylindrical cartridge (such as might be used to flexibly support a rolling element bearing).
4. Test a cylindrical cartridge to determine its dynamic stiffness and damping properties and compare these measurements with corresponding predictions.
5. Design a cylindrical cartridge damper for controlling vibration of a specific rotor-bearing system and test the performance of the cartridge in this application.
6. By further controlled-temperature tests on elastomer specimens, determine what influence temperature has on the material properties of the BTR elastomer tested in the presently reported investigation.
7. Develop a model for prediction of elastomer behavior which accounts for temperature dependence of material properties.
8. As identified in this report, uncertainties in the damping of the lower cylinder could be significant at the higher test frequencies. Reduction of this uncertainty should be factored into future rig modifications by such means as use of a metallic foil to replace the present rubber seals.

APPENDIX A

TEST SAMPLE DESIGN

The frequency range over which the elastomer samples are required to be tested was a dominating factor in the design of the samples since acceptable data cannot be collected at frequencies far from the resonance. This may be seen by examination of a typical response plot for a base-excitation system, as described in Appendix B. For frequencies greater than three times the natural frequency, the system transmissibility approaches 1.0 and, depending on the amount of damping in the system, the phase angle between the input and output displacements tends to 180 degrees. Based on these facts, it was decided that no data should be collected at frequencies higher than three times the natural frequency. Since from a practical standpoint the upper bound on the vibration frequency is on the order of 1000 Hz, it was decided that the test set-up should provide a resonance frequency of at least 350 Hz with the smallest mass, which was approximately 0.9 Kg (2 lb.) in the present investigation. These constraints provided a stiffness which the test sample must have in order to meet the experimental requirements. Both the compression and shear samples were designed based on this criterion.

1. Compression Sample

The compression sample is an ensemble of several cylindrical elastomer specimens, as described in Section III. The size and number of these specimens was determined by the above design criterion. If d is the diameter and "a" is the height of any cylindrical elastomer specimen (as shown in Figure A1), and if a compressive load is applied along the axis of the specimen, then the nominal compressive stress is given by Payne and Scott [10]

$$\sigma = G\left(\frac{1}{\lambda^2} - \lambda\right) S \qquad \text{(A1)}$$

where G = Shear modulus of the material

λ = Ratio of strained to unstrained length

S = Shape factor

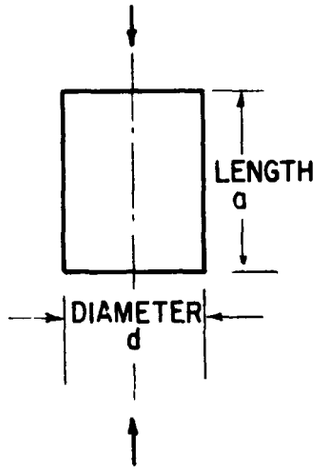

Fig. A1 Schematic of the Compression Specimen

The strain, ε, is simply $(1 - \lambda)$ and therefore Equation (A1) may also be written as

$$\sigma = G \left[(1 - \varepsilon)^{-2} - 1 + \varepsilon\right] S \tag{A2}$$

Since for most of the experiments in the present investigation the small strain assumption will be valid, Equation (A2) may be expanded in powers of ε, Hence

$$\sigma = GS[3\varepsilon + 3\varepsilon^2 + 4\varepsilon^3 + \ldots] \tag{A3}$$

If higher order terms are neglected in the above equation, then

$$\sigma = 3GS\varepsilon \tag{A4}$$

It should be noted that Equation (A4) is basically Hooke's Law, since the Young's modulus for most rubbers, $E = 3G$.

The static stiffness of the elastomer sample is defined by load per unit deflection, i.e.,

$$k_{st} = \frac{\sigma An}{\varepsilon a} \tag{A5}$$

where A is the cross sectional area of each elastomer specimen and n is the number of specimens in the ensemble.

Combining (A4) and (A5) results in

$$k_s = \frac{3GSAn}{a} \tag{A6}$$

Equation (A6) gives the static stiffness. However, in dynamic testing the natural frequency of the system will be primarily determined by the dynamic stiffness. Meyer and Sommer [5] have produced test results comparing the static and dynamic stiffnesses of several Polybutadiene compositions. For a composition having a Shore A hardness of 71, it is shown that the dynamic stiffness is three times larger than the static stiffness. Since no

compositional details on the material used in this investigation are available except that it has a Shore A hardness of 70, the above findings is used to compute the dynamic stiffness, k,

$$k = 3k_{st} = \frac{9GSAn}{a} \tag{A7}$$

The natural frequency ω_n for a mass m is given by

$$\omega_n^2 = \frac{k}{m} = \frac{9GSAn}{a}$$

or

$$\frac{Sn}{a} = \frac{4}{9\pi} \frac{m\omega_n^2}{Gd^2} \tag{A8}$$

where the cross sectional area is represented in terms of the diameter d.

The minimum mass for the present system is 0.9 Kg (2 lb) and the desired ω_n is 350 Hz. Also, as a practical value, 1.27 cm (0.5 in.) may be arbitrarily selected for the diameter. Substitution of these values in Equation (A8) results in

$$\frac{Sn}{a} = \frac{4}{9\pi} \frac{2(350 \times 2\pi)^2}{G \times 0.25 \times 386}$$

or

$$\frac{Sn}{a} = \frac{1.415 \times 10^4}{G} \tag{A9}$$

Note that the shear modulus G is in lb/in^2 and the height of the specimen "a" is in inches in Equation (A9).

It is now only necessary to estimate the shear modulus and determine the shape factor S. Gent [11] has shown an approximate inter-relationship between Shore A hardness, s, and the Young's modulus of elasticity, E. Assuming G = E/3 this relationship is given by

$$G = \frac{14.22\ (56 + 7.66s)}{3 \times 2.67 \times\ 0.0515 \times (254 - 2.54s)} \times 6.894 \times 10^3\ N/m^2 \qquad (A10)$$

Equation (A10) is plotted in Figure A2, taken from Gent. Using thie relationship, the shear modulus for a 70 durometer or Shore A hardness is estimated as 1.86×10^6 N/m^2 (270 lb/in^2). Substitution of this in Equation (A9) gives

$$\frac{Sn}{a} = 52.5 \qquad (A11)$$

The shape factor, S, is defined by Payne and Scott [10] by a function

$$S = 1 + B\left(\frac{d}{a}\right)^2$$

where B is a constant which depends on the shear modulus. For G = 1.86×10^6N/m^2 (270 lb/in^2), B is estimated as 0.063. Thus,

$$S = 1 + 0.063\left(\frac{d}{a}\right)^2$$

With the objective of studying the effects of shape factor on the dynamic properties, three different thicknesses of 12.7, 6.35, and 3.675 mm (0.5, 0.25, and 0.125 in.) were selected to give shape factors of approximately 1, 1.25 and 2. For these thicknesses and the shape factors, the number of specimens required in each ensemble were determined to be respectively 25, 10, and 3 for the three samples. For the first sample, the number n was in fact changed to 30 primarily because of pratical reasons for geometrical symmetry of the sample. In any case this will increase the natural frequency and is, therefore, perfectly acceptable.

2. Shear Sample

The design of the shear samples is somewhat simpler than that of the compression samples since no shape factors are associated with shear deformation. However, as shown in Figure A3, when a piece of rubber is shear-strained in a conventional manner both shear and bending occur. It has been shown [10] that the applied shear force, F, results in a deflection, δ, given by the expression

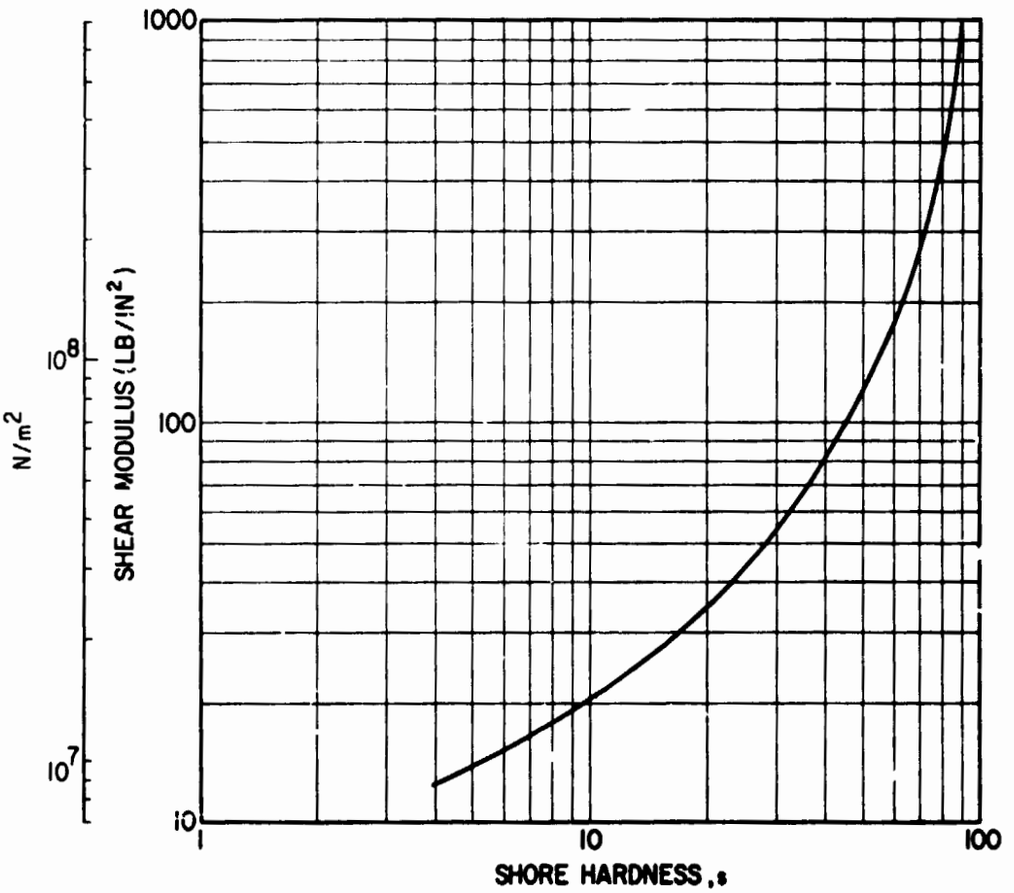

Fig. A2 Relationship Between Shore Hardness and Shear Modulus

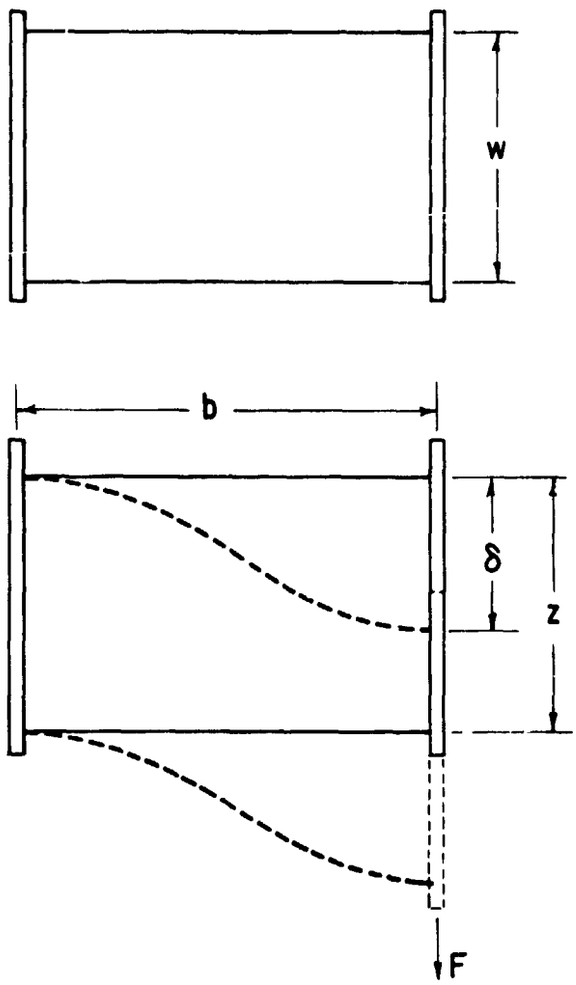

Fig. A3 Schematic of the Shear Specimen

$$\delta = \frac{Fb}{GA}\left[1 + \frac{b^2}{36\rho^2}\right] \tag{A13}$$

where b is the specimen thickness as shown in Figure A3, G is the shear modulus, ρ is the radius of gyration of the cross section about the neutral axis of bending and A is the cross sectional area. The bending effect is indicated by the second term in the brackets.

For the rectangular sample shown in Figure A3, $A = wz$ and $\rho^2 = z^2/12$. By substituting these quantities in Equation (A13), the sample static stiffness in shear is expressed as

$$k_{st} = \frac{F}{\delta} = \frac{Gwz}{b\left[1 + \frac{b^2}{36\rho^2}\right]} \tag{A14}$$

Bending will be negligible when $b^2/36\rho^2 << 1$, and for this simple case

$$k_{st} = \frac{Gwz}{b} \tag{A15}$$

As in the case of the compression specimens, assuming that the dynamic stiffness, k, is three times the static stiffness, the sesonant frequency ω_n for a mass m and a sample consisting of n identical specimens in parallel is given by

$$\omega_n^2 = \frac{k}{m} = \frac{3Gwzn}{mb} \tag{A16}$$

or

$$\frac{wzn}{b} = \frac{m\omega_n^2}{3G}$$

Now if a resonant frequency of 350 Hz is desired for the minimum possible mass of 0.9 Kg (2 lbs), Equation (A16) gives

$$\frac{wzn}{b} = \frac{2 \times (350 \times 2\pi)^2}{3 \times 386 \times 270} = 31 \tag{A17}$$

If the actual value of wzn/b is greater than 31, then the resonant frequency will be somewhat greater than 350 Hz (as given by Equation A16). Such a design will be perfectly acceptable as long as the lowest desired resonant frequency is attainable with the maximum available mass. With these design guidelines, it was decided that a satisfactory shear sample may consist of four elastomer specimens with the following dimensions

Sample No. 1: n = 4; w = 5.08 cm(2 in.); z = 2.54 cm(1.0 in.)

It may be noted that the above configuration gives wzn/b = 64 and therefore the resonant frequency corresponding to the mass of 2 lb will be 350 64/31 or 502 Hz. If the lowest desired frequency is 100 Hz, then the required mass will be approximately 51 lb, which is well within the experimental limitations on maximum mass. Also, bending effects have been neglected in the above design, which is quite justifiable since the bending term $(b^2/36\rho^2)$ in this case is 0.0052, which is indeed quite small compared to unity.

In order to allow for some bending effects within the experimental limitations, two additional configurations were selected such that (wzn/b) is held constant for all three samples to meet the stiffness requirements. The selected configurations are

Sample No. 2: n = 8; w = 5.08 cm (2.0 in.); b = 0.318 cm (0.125 in.)
z = 1.27 cm (0.5 in.)
Sample No. 3; n = 20; w = 5.08 cm(2.0 in.); b = 0.318 cm (0.125 in.)
z = 0.508 cm (0.2 in.)

The magnitude of the bending term $(b^2/36\rho^2)$ is estimated to be 0.0208 and 0.13 for Samples No. 2 and No. 3, respectively. Thus the shear specimens have some variation in the possible bending effects.

APPENDIX B

DYNAMIC CHARACTERISTICS OF TEST RIG COMPONENTS

A. Guide Bearings

The two guide bearings, consisting of spoke assemblies, are identical with regard to their geometry and dynamic response. Therefore, the experiment discussed below applies to both spoke assemblies.

Since the only mode of dissipation in the spoke assemblies is internal friction in the metal and at the joints, the associated damping will be negligibly small. It was found that within the desired precision on the test rig response, the damping of the spokes may be neglected. In order to measure the stiffness a simple experiment was performed. The outside ring of the spoke assembly was clamped on the shaker table, as shown schematically in Figure B1. The natural frequency of the system was measured, and knowing the mass of the hub* (see Section III), the stiffness of the spokes was computed in a straight forward manner. The reduced dynamic model and the system characteristics are also outlined in Figure B1. It was found that the stiffness of each spoke assembly, k_s, is 3.67×10^4 N/m (210 lb/in).

B. Mechanical Spring

Any damping in the mechanical spring is once again negligible. However, due to the size of the spring (see Figure 16), its equivalent mass must be determined experimentally. The spring was clamped on the shaker table and the natural frequency ω_m of the system was measures. The dynamic model, in this case, will be similar to the one shown in Figure B1. In the second experiment, a small mass, Δ_m was attached to the top of the spring and the natural frequency ω_m' was again measured. From these measurements, the computation of equivalent spring mass, m_m, and the stiffness, k_m is straightforward.

$$\omega_m = \sqrt{\frac{k_m}{m_m}} \quad \text{and} \quad \omega_m' = \sqrt{\frac{k_m}{m_m + \Delta m}}$$

*The equivalent mass of the spokes is negligible compared to the mass of the hub.

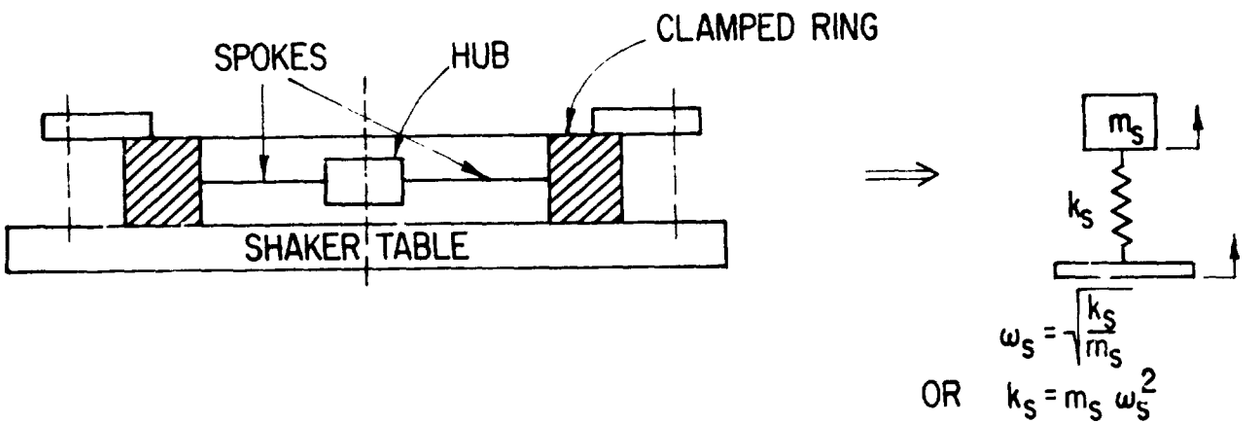

Fig. B1 Dynamic Model of the Guide Bearing

Thus

$$m_m = \frac{\Delta m}{\left(\frac{\omega_m}{\omega'_m}\right)^2 - 1} \qquad \text{and} \qquad k_m = \omega_m^2 m_m = \frac{\Delta m\ \omega_m^2}{\left(\frac{\omega_m}{\omega'_m}\right)^2 - 1} \tag{B1}$$

It was found that the equivalent mass m_m = 0.877 kg (1.93 lbs) and the corresponding stiffness $k_m = 2.96 \times 10^5$ N/m (1695 lb/in).

C. Lower Cylinder with Free Piston

It is possible to mount the lower cylinder with the mechanical spring directly on the shaker table and obtain a base excitation system, shown schematically in Figure B2. The analysis for such a system is quite simple [12], and if the output motion is measured as a function of the input table excitation, the stiffness and damping of the cylinder can be calculated. It is assumed that the stiffness of the cylinder is a function of the air pressure only.

The analysis for the base excitation system of Figure B2 is outlined in Appendix C, and it is shown that if the system transmissibility, α (defined by the ratio of output to input amplitude) and the phase angle ϕ between the output and input are measured, the values stiffness k_1 and c_1 may be computed. Within the scope of the present investigation, it is conservatively assumed that k_1 and c_1 are frequency independent, as discussed in the Discussion section. Under this assumption, it is shown in Appendix C that only the measurements of α and the frequency at resonance are necessary in order to determine k_1 and c_1. In fact, the phase angle ϕ could be computed by knowing k_1 and c_1 from the measurement of α at resonance, and the resonant frequency. Thus, the resonant frequency and values of α were measured as a function of the air pressure in the cylinder. The phase angle ϕ at resonance was also measured for the purpose of comparing it with the computed value. The amplitudes were low enough such that fluctuations of pressure in the cylinder were less than 1% under the adiabatic assumption for the highest amplitudes imposed.

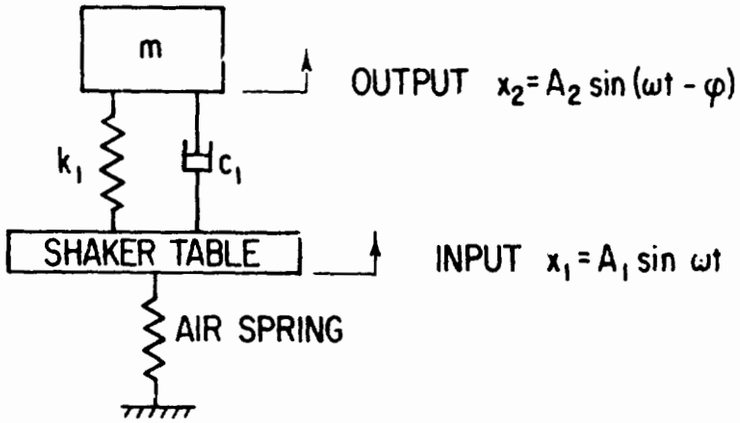

$m = m_{p\ell} + m_m + m_{acc}$ = 3.39 LB 1.54 Kg

$k_1 = k_\ell + k_m$

$c_1 = c_\ell$

Fig. B2 Dynamic Model of the Lower Cylinder Mounted on the Shaker Table with the Mechanical Spring

With the above measurements and the analysis described in Appendix C, k_1, c_1 and ψ were computed, and finally, using the relations shown in Figure B2, k_ℓ and c_ℓ were determined. The results are shown as a function of air pressure in the cylinder in Figure B3. The computed and measured phase angles at resonance are also compared in this plot, where the solid curve represents the computed results and the experimental data is shown by the discrete points. It is seen that within the precision limits of phase angle measurement the agreement is fairly good. The cylinder stiffness is very well approximated by a linear function of pressure and the variation in the damping is rather small. However, it should be noted that the motion of the piston is free in this experiment while it is constrained in the assembled test rig. Such a constraint may influence the cylinder characteristics, since it certainly influences alignment of the seals.

In order to put some constraint on the piston motion, the lower guide bearing was clamped to the piston and the experiment was repeated. The analysis of this setup, and of a similar setup for the upper cylinder, are special cases of the general response of the test rig and hence this response is formulated before discussing the above two special cases.

b. Generalized Test Rig Response

The dynamic model of the test rig shown in Figure 15 is reducible to the form shown in Figure B4 by combining the various elements appearing in parallel. Now the equation of motion of the resonant mass will be independent of the shaker air spring and it may be written as

$$m\ddot{x}_2 + c_1(\dot{x}_2-\dot{x}_1) + c_2\dot{x}_2 + k_1(x_2-x_1) + k_2x_2 = 0 \qquad \text{(B2)}$$

It is found experimentally that all motions are sinusoidal and hence solution of the above equation of motion becomes straightforward

$$\begin{aligned} x_1 &= A_1 \sin \omega t \\ x_2 &= A_2 \sin (\omega t - \phi) \end{aligned} \qquad \text{(B3)}$$

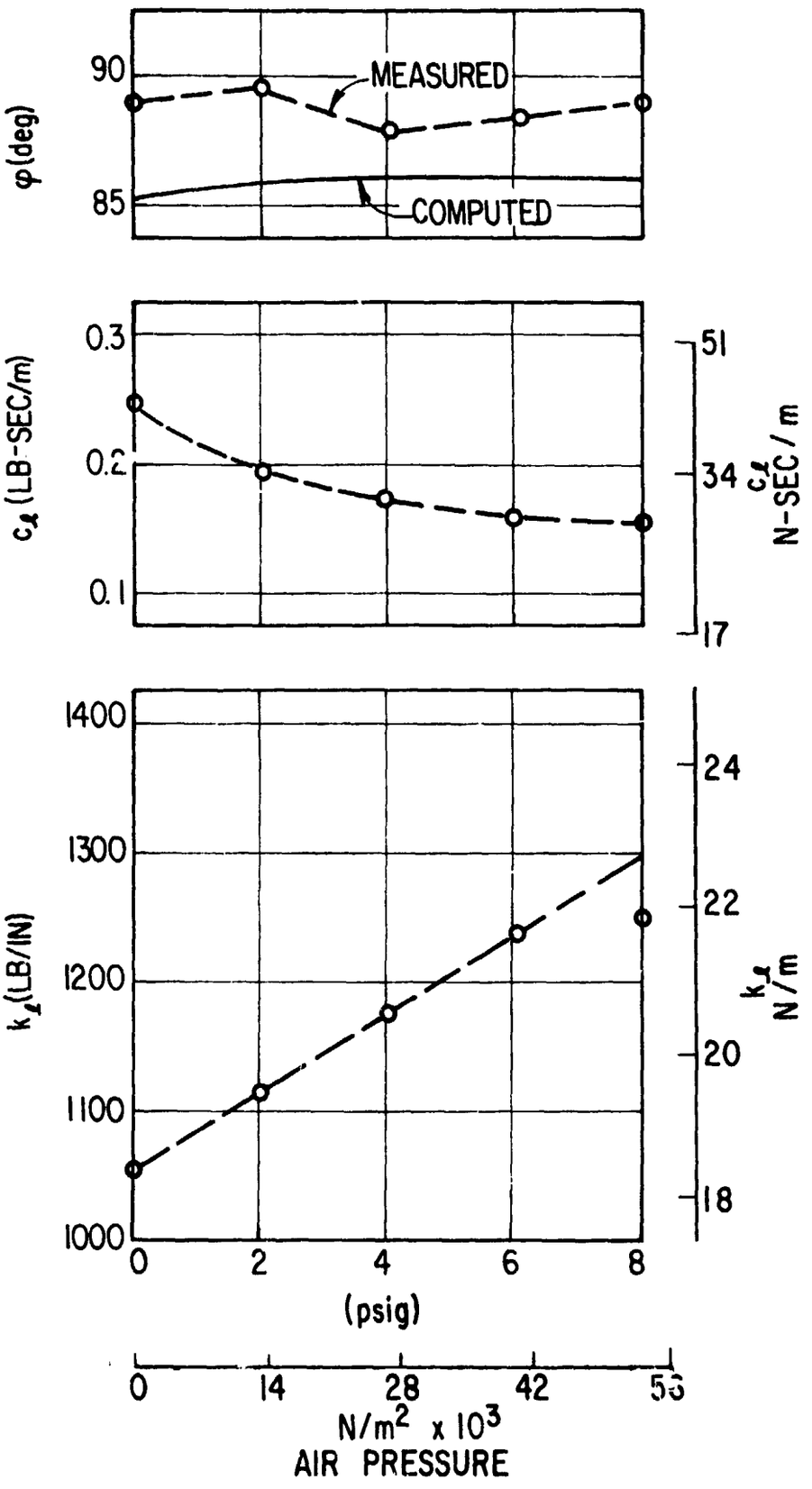

Fig. B3 Response of the Lower Air Cylinder

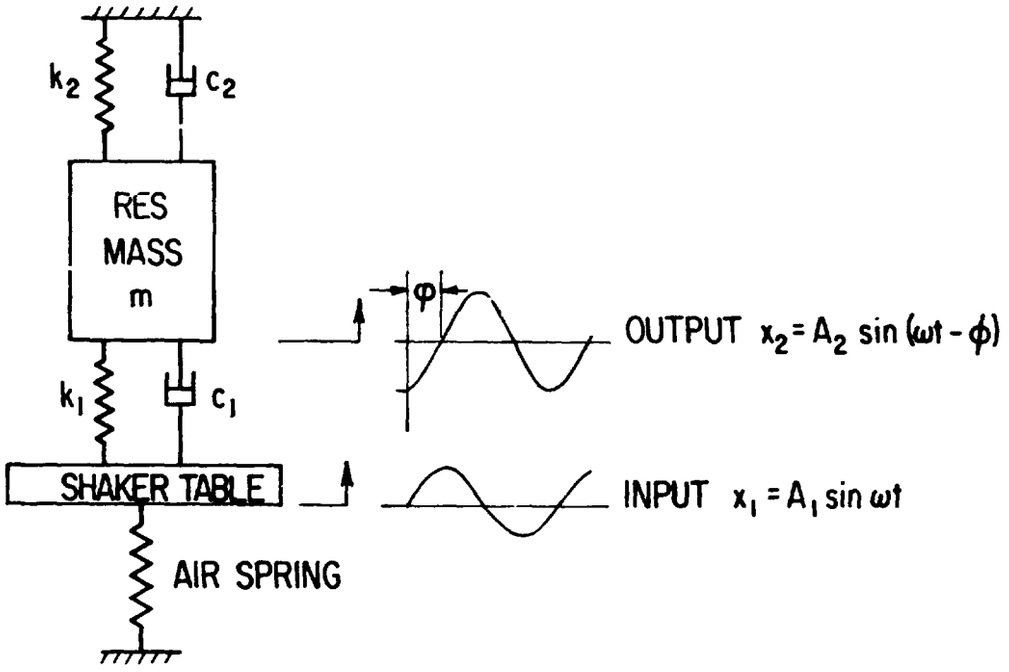

Fig. B4 Reduced Model of the Test Rig

Combining Equations (B2) and (B3) and separating the coefficients of sin ωt and cos ωt terms gives

$$\frac{c_1}{m\omega}\sin\varphi + \frac{c_2}{m\omega}\sin\varphi + \frac{k_1}{m\omega^2}\left(\cos\varphi - \frac{1}{\alpha}\right) + \frac{k_2}{m\omega^2}\cos\varphi - \cos\varphi = 0$$

and (B4)

$$\frac{c_1}{m\omega}\left(\cos\varphi - \frac{1}{\alpha}\right) + \frac{c_2}{m\omega}\cos\varphi - \frac{k_1}{m\omega^2}\sin\varphi - \frac{k_2}{m\omega^2}\sin\varphi + \sin\varphi = 0$$

where

$$\alpha = A_2/A_1.$$

Equations (B4) form the two algebraic equations which may be solved for any two unknowns. For the purpose of reducing the elastomer data, the unknowns will be k_1 and c_1 while in the experiments with the upper cylinder and the mechanical spring assembly, the unknowns are k_2 and c_2. Also for calculating the test rig response the solutions are required for α and φ. Equations (B4) are, therefore, rearranged in three different forms.

$$\frac{k_1}{m\omega^2} = \frac{\frac{k_2}{m\omega^2}\alpha(\cos\varphi - \alpha) + \frac{c_2}{m\omega}\alpha\sin\varphi - \alpha\cos\varphi + \alpha^2}{\alpha^2 - 2\alpha\cos\varphi + 1}$$

$$\frac{c_1}{m\omega} = \frac{\frac{c_2}{m\omega}\alpha(\cos\varphi - \alpha) + \alpha\sin\varphi\left(1 - \frac{k_2}{m\omega^2}\right)}{\alpha^2 - 2\alpha\cos\varphi + 1} \qquad \text{(B5)}$$

$$\frac{k_2}{m\omega^2} = 1 + \frac{k_1}{m\omega^2}\left(\frac{\cos\varphi}{\alpha} - 1\right) - \frac{c_1}{m\omega}\frac{\sin\varphi}{\alpha}$$

$$\frac{c_2}{m\omega} = \frac{k_1}{m\omega^2}\frac{\sin\varphi}{\alpha} - \frac{c_1}{m\omega}\left(1 - \frac{\cos\varphi}{\alpha}\right) \qquad \text{(B6)}$$

and

$$\alpha^2 = \frac{\left(\frac{k_1}{m\omega^2}\right)^2 + \left(\frac{c_1}{m\omega}\right)^2}{\left(1 - \frac{k_1 + k_2}{m\omega^2}\right)^2 + \left(\frac{c_1 + c_2}{m\omega}\right)^2} \tag{B7}$$

$$\tan\varphi = \frac{\frac{c_1}{m\omega}\left(1 - \frac{k_1 + k_2}{m\omega^2}\right) + \frac{k_1}{m\omega^2}\left(\frac{c_1 + c_2}{m\omega}\right)}{\frac{c_1}{m\omega}\left(\frac{c_1 + c_2}{m\omega}\right) - \frac{k_1}{m\omega^2}\left(1 - \frac{k_1 + k_2}{m\omega^2}\right)}$$

The expressions of k_1, c_1, k_2, and c_2 in terms of the various coefficients shown in Figure 15 are summarized in Table B1 for the different test setups.

It is clear that the experiment with the lower cylinder assembled with the guide bearing and the mechanical spring, is a special case of the above formulation. Likewise, the experiment with upper piston connected directly to the mechanical springs and the guide bearings forms another special case. Since, in the case of both of these experiments, the stiffness and damping coefficients are assumed to be frequency independent, the formulation could be expressed in terms of the resonance conditions. This will be very similar to the analysis presented for the base excitation system in Appendix C.

The system transmissibility α is written in terms of the nondimensional quantities.

$$\bar{\Omega} = \frac{\omega}{\omega_n}\ ;\quad u_1 = \frac{k_1}{m\omega_n^2}\ ;\quad u_2 = \frac{k_2}{m\omega_n^2}\ ;\quad v_1 = \frac{c_1}{m\omega}\ ;\quad v_2 = \frac{c_2}{m\omega}\ ;\quad \omega_n = \sqrt{\frac{k_m}{m}}$$

$$\alpha^2 = \frac{u_1^2 + \bar{\Omega}^2 v_1^2}{\bar{\Omega}^4 + \bar{\Omega}^2 (v_i \quad v_2)^2 - 2(u_1 + u_2) \quad + \quad (u_1 + u_2)^2} \tag{B8}$$

TABLE B1

REDUCED STIFFNESS AND DAMPING COEFFICIENTS

Test Setup	k_1	c_1	k_2	c_2
Mechanical Spring with All System Components	$k_\ell + k_m$	c_ℓ	$k_u + 2k_s$	c_u
Elastomer Specimen with All System Components	$k_\ell + k_e$	$c_\ell + c_e$	$k_u + 2k_s$	c_u
Mechanical Spring with Lower Cylinder and Guide Bearing	$k_m + k_\ell$	c_ℓ	k_s	0.
Mechanical Spring with All System Components Except the Lower Cylinder	k_m	0.	$k_u + 2k_s$	c_u

Since at resonance α is a maximum, the second required equation is obtained by differentiating Equation (B8) with respect to $\bar{\Omega}$.

$$\frac{\partial \alpha^2}{\partial \bar{\Omega}} = 0$$

or

$$v_1^2 \bar{\Omega}^4 + 2 u_1^2 \bar{\Omega}^2 + u_1^2 (v_1 + v_2)^2 - 2(u_1 + u_2) - v_1^2 (u_1 + u_2)^2 = 0 \quad \text{(B9)}$$

Equations (B8) and (B9) are solved for either u_1 and v_1 or u_2 and v_2. Once these solutions are obtained, the phase angle at resonance is obtained by the second of Equations (B7). It is clear that the set of algebraic equations are nonlinear and, therefore, the conventional Newton-Raphson iteration method is used to obtain a final solution. The two equations are expressed in the following functional forms

$$f_1 = u_1^2 + \bar{\Omega}^2 v_1^2 - \alpha^2 \left[\bar{\Omega}^4 + \bar{\Omega}^2 \left\langle (v_1+v_2)^2 - 2 (u_1+u_2) \right\rangle + (u_1+u_2)^2\right] \quad \text{(B10)}$$

$$f_2 = v_1^2 \bar{\Omega}^4 + 2 u_1^2 \bar{\Omega}^2 + u_1^2 \left\langle (v_1+v_2)^2 - 2 (u_1+u_2) \right\rangle - v_1^2 (u_1+u_2)^2$$

Note that, when Equations (B8) and (B9) are satisfied, $f_1 = f_2 = 0$.

The recurrence formulae for the computation of u_1, v_1 or u_2, u_2 are given as

$$\left.\begin{aligned} u_{i_{k+1}} &= u_{i_k} + \Delta u_{i_k} \\ v_{i_{k+1}} &= v_{i_k} + \Delta v_{i_k} \end{aligned}\right\} \qquad i = 1,2 \quad \text{(B11)}$$

where

$$\begin{bmatrix} \dfrac{\partial f_1}{\partial u_{i_k}} & \dfrac{\partial f_{1_k}}{\partial v_{i_k}} \\ \dfrac{\partial f_{2_k}}{\partial u_{i_k}} & \dfrac{\partial f_{2_k}}{\partial v_{i_k}} \end{bmatrix} \begin{Bmatrix} \Delta u_{i_k} \\ \Delta v_{i_k} \end{Bmatrix} = \begin{Bmatrix} - f_{1_k} \\ - f_{2_k} \end{Bmatrix} \qquad i = 1,2.$$

Once the above solutions are obtained, the phase angle at resonance is expressed as

$$\tan\varphi = \frac{\bar{\Omega}\,(u_2\,v_1 - u_1\,v_2) - \bar{\Omega}^3\,v_1}{\bar{\Omega}^2\,(u_1 - v_1^2 - v_1 v_2) - u_1\,(u_1 + u_2)} \tag{B12}$$

Thus, if the stiffness and damping coefficients are independent of frequency, it is only necessary to measure the system transmissibility and the frequency at resonance in order to compute the unknown coefficients. The special cases of the lower and upper cylinder with constrained piston motion may now be considered.

E. Lower Cylinder with Constrained Piston

Some constraint on the motion of the piston in the lower cylinder is provided by connecting it to the lower guide bearing. The dynamic model of this system is shown schematically in Figure B5. For a prescribed amplitude of table excitation, the frequency was varied until resonance was observed. The output motion of the resonant mass was then noted, and thus the transmissibility α and the frequency at resonance were determined as functions of the air pressure in the lower cylinder. The amplitudes were low enough that fluctuations in the air pressure were less than 1% assuming adiabatic expansion for the largest amplitudes impos[illegible]ations (B11) with i = 1, were solved for u_1 and v_1 and thus the cyl[illegible] tiffness and damping coefficients were determined.

The results are plotted as functions of pressu[illegible]igure B6. Although the stiffness again varies linearly as a function of pressure, the absolute values are somewhat higher than those obtained with the free piston motion in Figure B3. A possible reason for this effect is the change in cylinder volume between the two tests [12]. The linear relationship shown by the dashed curve was used in calculating the lower cylinder stiffness for the purpose of reducing the elastomer data.

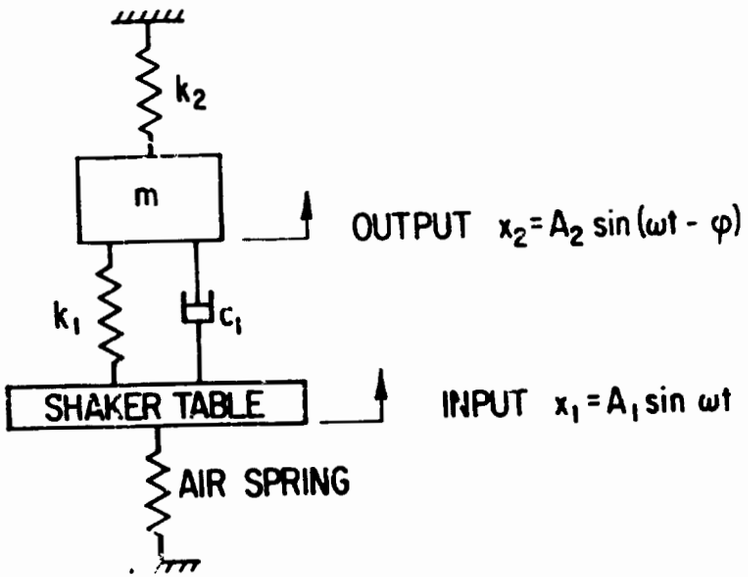

$m = m_{p_\ell} + m_m + m_{acc} + m_s + m_{sp} = 5.08\,LB\ 2.31\,Kg$

$k_2 = k_s$

$k_1 = k_\ell + k_m$

$c_1 = c_\ell$

Fig. B5 Dynamic System Model for Lower Cylinder Mounted with the Mechanical Spring when the Lower Piston is Constrained by the Lower Guide Bearing

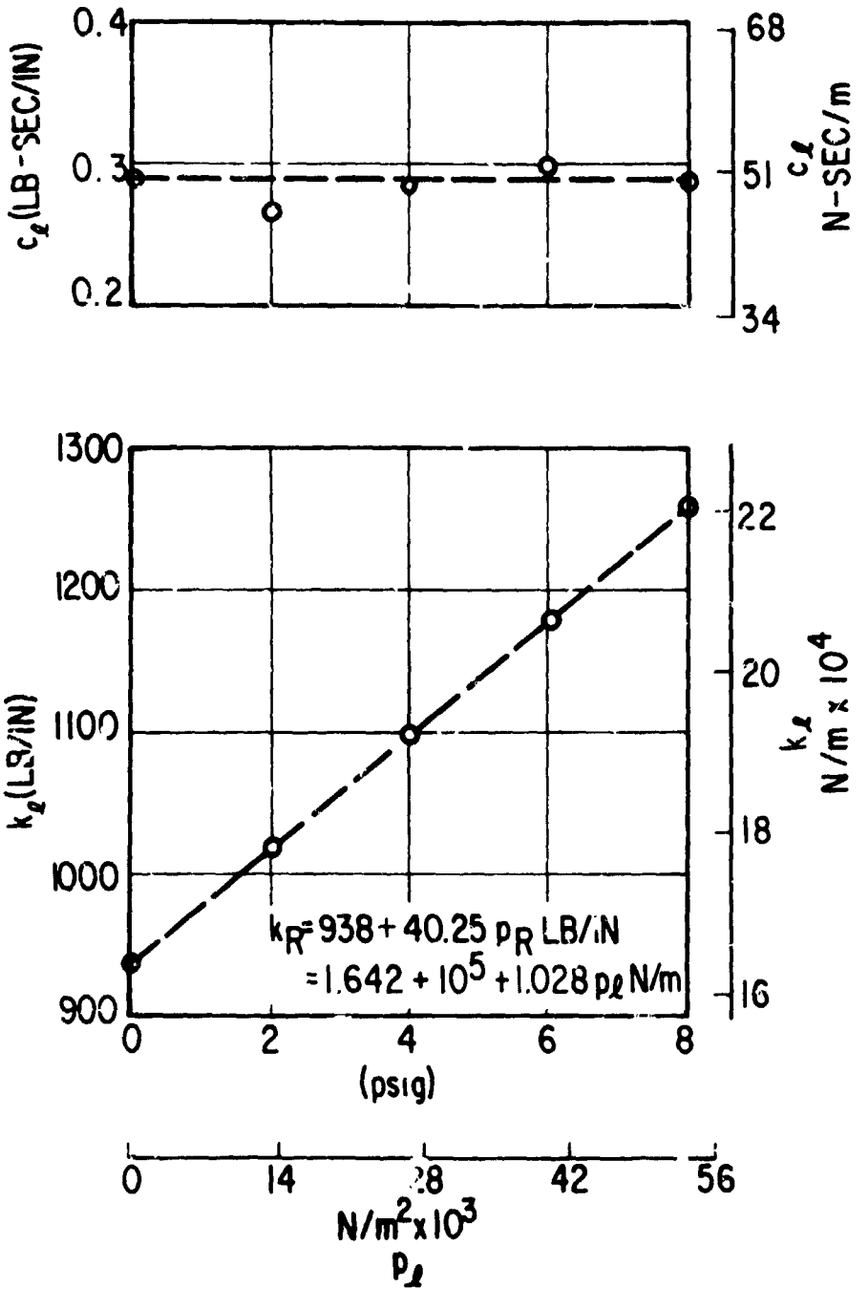

Fig. B6 Lower Cylinder Stiffness and Damping With Constrained Piston Motion

Variations in the damping coefficients are rather irregular, and assuming a constant value as shown by the dashed curve seems very reasonable. It should be noted that constraining the piston motion does increase the damping to an appreciable extent. For reducing the elastomer data, cylinder damping was therefore determined by performing a least-squares analysis of the response of the completely assembled test rig, except that the mechanical spring was used instead of the elastomer specimen. Details of this approach are discussed later in this Appendix.

The differences between the computed and measured phase angles are of the same general order as shown earlier in Figure B3.

F. Upper Cylinder with Constrained Piston

Similar to the lower cylinder, an experiment was set-up with the upper cylinder mounted in place. The piston was connected through both guide bearings directly to the meachanical spring mounted on the shaker table. Thus, the lower cylinder was eliminated in this test. A dynamic model of the system is shown schematically in Figure B7.

Since the range of pressure variation in the upper cylinder during the actual tests was much smaller than that for lower cylinder, the air pressure was varied only up to 2.76×10^4 N/m^2 (4 psig) in this experiment. The transmissibility α and the frequency at resonance were measured as functions of air pressure in the cylinder. Equations (B11) with i=2, were solved in this case for u_2 and v_2 and thus the cylinder stiffness and damping were determined as functions of the pressure.

The stiffness is again found to vary linearly with pressure as shown in Figure B8. The relationship shown by the dashed curve was used during reduction of data from the elastomer tests. It may be noted that the stiffness of the upper cylinder is somewhat less than that of the lower cylinder. An explanation of this difference lies in the fact that in the assembled configuration, the volume in the upper cylinder is greater than that in the lower one.

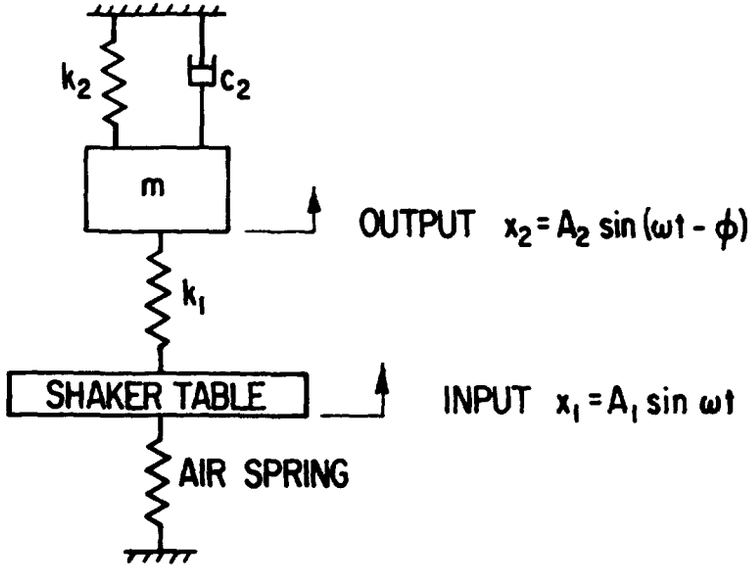

$m = m_{pu} + 2m_s + m_{acc} + m_r + m_m = 12.70$ LB

$k_1 = k_m$

$k_2 = k_u + 2k_s$

$c_2 = c_u$

Fig. B7 Dynamic Model of the Upper Cylinder Mounted With the Mechanical Spring When the Piston Motion is Constrained by Both Guide Bearings.

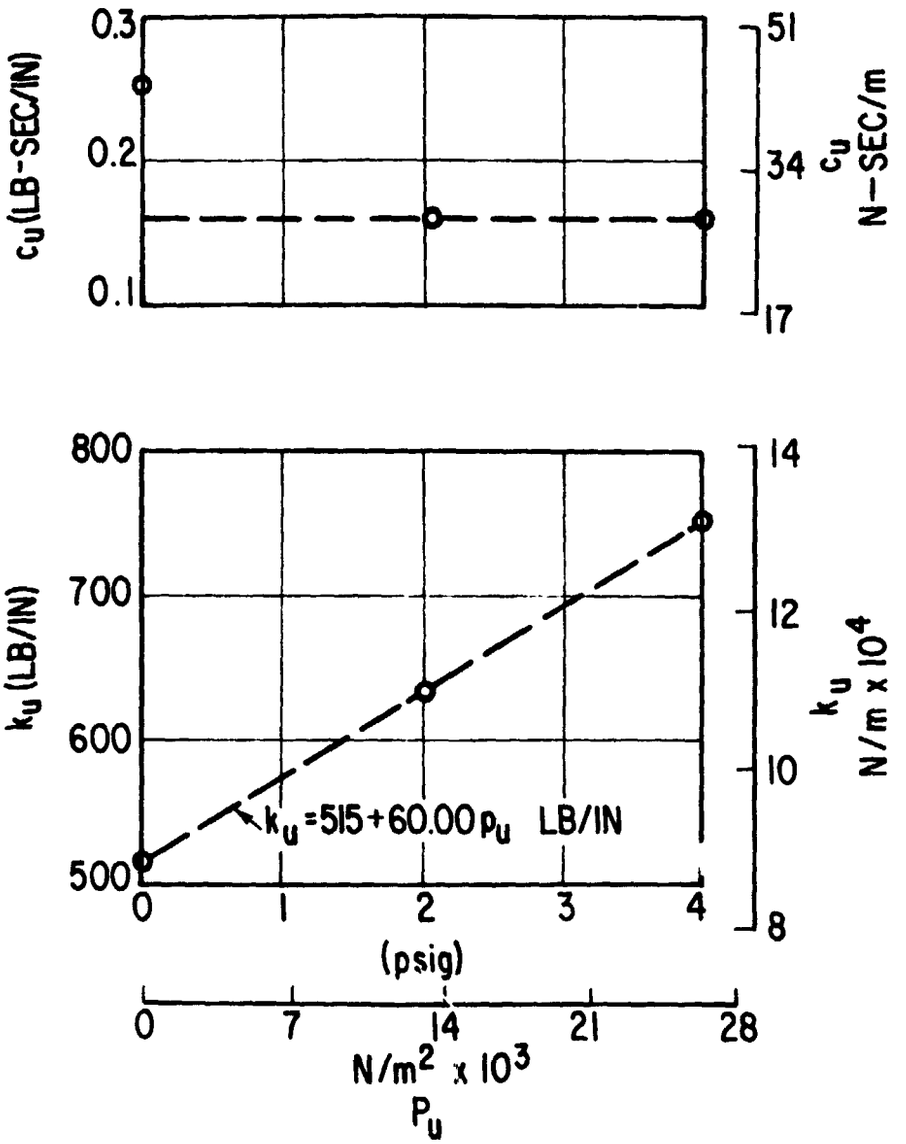

Fig. B8 Upper Cylinder Response With Constrained Piston Motion

The computed and measured phase angles in this experiment are in reasonable agreement and the order of deviations are the same as those shown earlier in Figure B3.

For any finite air pressure, the damping was again found to be fairly constant. However, the cylinder seems to provide significantly more damping at atmospheric pressure. After completing all the tests, the cylinders were disassembled to examine any differences between the mountings of the seals on the pistons. It was found that unlike the lower cylinder, the seal was not cemented to the entire area of the piston in the upper cylinder. This geometrical difference will affect the alignment of the seals and, hence, may explain some differences in the damping coefficients. In any case, the damping coefficients required for reducing the elastomer data were determined from the completely assembled test rig response as discussed below.

G. Test Rig Response with a Mechanical Spring

All components of the test rig were properly assembled in this experimental set-up except that the elastomer specimen was replaced by the mechanical spring. The only damping in the system so assembled is due to the seals in the upper and lower cylinders. Also, the geometrical configuration of the test rig was very close to the one used when obtaining the elastomer response data. Thus, the alignment of the seals was very close to actual conditions and the computation of the damping coefficients from the response measurement of this system becomes quite meaningful.

The dynamic model for the complete test rig was shown earlier in Figures 15 and B4. The reduced form shown in Figure B4 is directly applicable to the present configuration with the relations of the various system elements defined in Table B1. The value of the resonant mass, m, was determined by summing up all relevant masses and was found to be 6 Kg (13.39 lbs). Stiffnesses of the spoke assemblies, the mechanical spring and both the cylinders have already been established in the preceding experiments. Thus, from the measurement of the test rig response the damping coefficients for the upper and lower cylinders may be calculated.

The experimental procedure consisted of measuring the transmissibility α, the frequency, and the phase angle at resonance as functions of pressure in the cylinder. Pressure in the lower cylinder was varied from 0 to 8.27 x 10^4 N/m^2 (0 to 12 psig) at three different values 0, 1.33 x 10^4 and 2.76 x 10^4 N/m^2 (0, 2, and 4 psig) of pressure in the upper cylinder and thus, large data matrices were obtained to cover the entire range of operation of the test rig. Of the three measurements, α has probably the best accuracy. Frequency measurements are generally good to within 1 Hz but since most of the data obtained in this experiment lies in a very narrow band close to the natural frequency of the mechanical spring, small frequency errors can be significant. Keeping all these points in view, the damping coefficients were determined by a least-squares analysis of the transmissibility data. It is clear that the problem at hand is non-linear and some type of iterative or marching technique is required. The analysis used is briefly outlined below.

A data matrix for c_u and c_ℓ varying from 0 to 1 lb-sec/in was formed and for each combination, α at resonance is computed by Equations (B8) and (B9). Symbolically, let p_{u_i} and p_ℓ denote the pressures in the upper and lower cylinders where $1 \leq i \leq n_u$ and $1 \leq j \leq n_\ell$ as determined by the selected experimental data matrix. Also, let c_ℓ and c_u have the values c_{ℓ_k} and c_{u_h} respectively where $1 \leq k \leq n$ and also $1 \leq h \leq n$. If the measured transmissibility for pressures p_{u_i} and p_{ℓ_j} is α_{ij}, and the computed value under these conditions and with $c_\ell = c_{\ell_k}$ and $c_u = c_{u_h}$ be $\tilde{\alpha}_{ijkh}$, then the total squared deviation is obtained by proper summation:

$$L_{kh} = \sum_{i=1}^{n_u} \sum_{j=1}^{n_\ell} (\tilde{\alpha}_{ijkh} - \alpha_{ij})^2$$

The entire matrix for c_u and c_ℓ is scanned for the minimum squared deviation and the corresponding values of c_u and c_ℓ are taken to be the required values. It is true that the accuracies of c_u and c_ℓ are determined by the internal size used to divide the region of 0 to 1 in finite number of data points. Initially the interval size is taken as 0.1 and the required c_u and c_ℓ are determined and

then a new matrix with interval size 0.01 is set up around these computed values and the previously obtained solution is refined by adding an additional digit. The procedure could be repeated for obtaining any more significant digits if necessary.

Using the above scheme, the damping coefficients for the lower and upper cylinders were found to be respectively 102 and 2.45 N-sec/m (0.583 and 0.014 lb-sec/in). These values were used in determining the elastomer characteristics from the experimental data.

APPENDIX C

RESPONSE OF A BASE-EXCITATION SYSTEM

Since the stiffness and damping in the air cylinders have been assumed to be independent of frequency, at least within the scope of the present investigation, it is necessary to analyze the test rig response to determine these coefficients of damping and stiffness. In the absence of the upper cylinder the test rig is represented by a conventional base excitation system. The response of such a system is very well known [12] and this Appendix briefly outlines the analysis applicable to such a system.

The response of a simple base excitation system, as shown in Figure C1, is given in terms of transmissibility α, and the phase angle φ, defined by the equations given in Reference [9].

$$\alpha = \frac{A_2}{A_1} = \sqrt{\frac{1 + \left(2\zeta \frac{\omega}{\omega_n}\right)^2}{1 - \left(\frac{\omega}{\omega_n}\right)^2 + \left(2\zeta \frac{\omega}{\omega_n}\right)^2}}$$

and (C1)

$$\tan \varphi = \frac{2\zeta \left(\frac{\omega}{\omega_n}\right)^3}{1 - \left(\frac{\omega}{\omega_n}\right)^2 + \left(2\zeta \frac{\omega}{\omega_n}\right)^2}$$

where:

ω = excitation frequency (rad/sec)

$\omega_n = \sqrt{\frac{k}{m}}$, the natural frequency of the spring mass system (rad/sec)

k = spring stiffness (N/m)

m = resonant mass (N-sec^2/in.)

$\zeta = \frac{c}{c_c}$, damping ratio

c = system damping coefficient (N-sec/m)

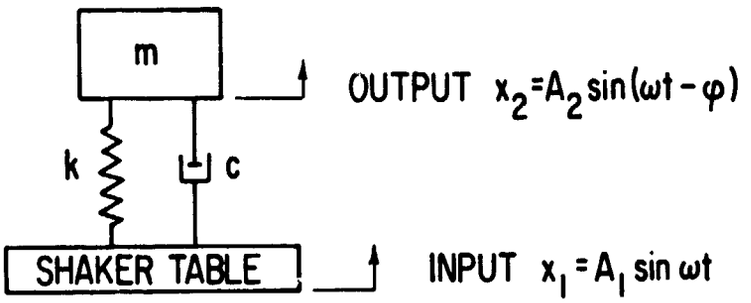

Fig. C1 Schematic of a Base Excitation System

c_c = $2m\omega_n$, critical damping coefficient (N-sec/m)

A_1 = input amplitude (m)

A_2 = output amplitude (m)

φ = phase angle (degree)

Thus, if the input and output amplitudes and the phase angle, φ, are measured, the system stiffness and damping may be computed from the above equations. For simplicity, Eq. (C1) may be rearranged for this computation.

$$\frac{k}{m\omega^2} = \frac{\alpha\,(\alpha - \cos\varphi)}{1 + \alpha\,(\alpha - 2\cos\varphi)}$$

and (C2)

$$\frac{c}{m\omega} = \frac{-\alpha \sin\varphi}{1 + \alpha\,(\alpha - 2\cos\varphi)}$$

Since the measurement of the phase angles may sometimes involve large errors, the values of k, and c, as computed by Equation (C2) may result in some error. However, the measurements of A_2 and A_1 or α and the frequency ω are relatively precise. Hence, if k and c are derived from the amplitude ratio α_{max} and the frequency Ω at resonance, then the errors in the computed k and c will be small compared to those determined by Equation (C2). Now if k and c are assumed to be independent of frequency, then the two equations required to compute k and c become:

$$\alpha_{max} = \sqrt{\frac{1 + \left(2\zeta\frac{\Omega}{\omega_n}\right)^2}{\left[1 - \left(\frac{\Omega}{\omega_n}\right)^2\right]^2 + \left(2\zeta\frac{\Omega}{\omega_n}\right)^2}}$$

and (C3)

$$\frac{d}{d\omega}\left[\sqrt{\frac{1 + \left(2\zeta\frac{\omega}{\omega_n}\right)^2}{\left[1 - \left(\frac{\omega}{\omega_n}\right)^2\right]^2 + \left(2\zeta\frac{\omega}{\omega_n}\right)^2}}\right] = 0, \text{ at } \omega = \Omega.$$

The preceding two equations are easily solved for $(\frac{\Omega}{\omega_n})$ and α_{max} as a function of ζ. The phase angle at resonance is then computed from the second of Equation (C1).

$$\left(\frac{\Omega}{\omega_n}\right)^2 = \frac{\sqrt{1 + 8\zeta^2} - 1}{4\zeta^2}$$

$$\alpha_{max}^2 = \frac{1}{4\zeta^2} - \frac{3\zeta^2}{4} - \frac{3\zeta^4}{4} + \frac{5}{4} \qquad \text{(C4)}$$

$$\theta = \frac{\pi}{2} - \varphi = \arctan\left[\zeta\left(3 + 5\zeta^2 + \frac{21}{2}\zeta^4\right)\right]$$

These solutions are readily plotted in Figure C2 with an additional notation:

$$\beta = 1 - \frac{\Omega}{\omega_n} . \qquad \text{(C5)}$$

The computations of k and c with the measured α_{max} and Ω are now straightforward from Figure C2. For example, for $\alpha = 2.5$, the following values are noted:

$$\zeta = 0.22 ; \quad \beta = 0.042 ; \quad \theta = 34^\circ$$

and from the definitions of ζ, β, and θ, it is found that $\varphi = 56^\circ$, $(\frac{\Omega}{\omega_n}) = 0.958$. For a mass equivalent to say 0.9 kg (2 lb), this gives $k = 7.66 \times 10^4$ N/m (437 lb/in.) and $c = 37.1$ N-sec/m (0.212 lb-sec/in.).

Once k, and c are determined, the system response is directly computed, using Equation (C1). This response may be compared with the one obtained experimentally to ascertain some confidence on the computed values of k and c.

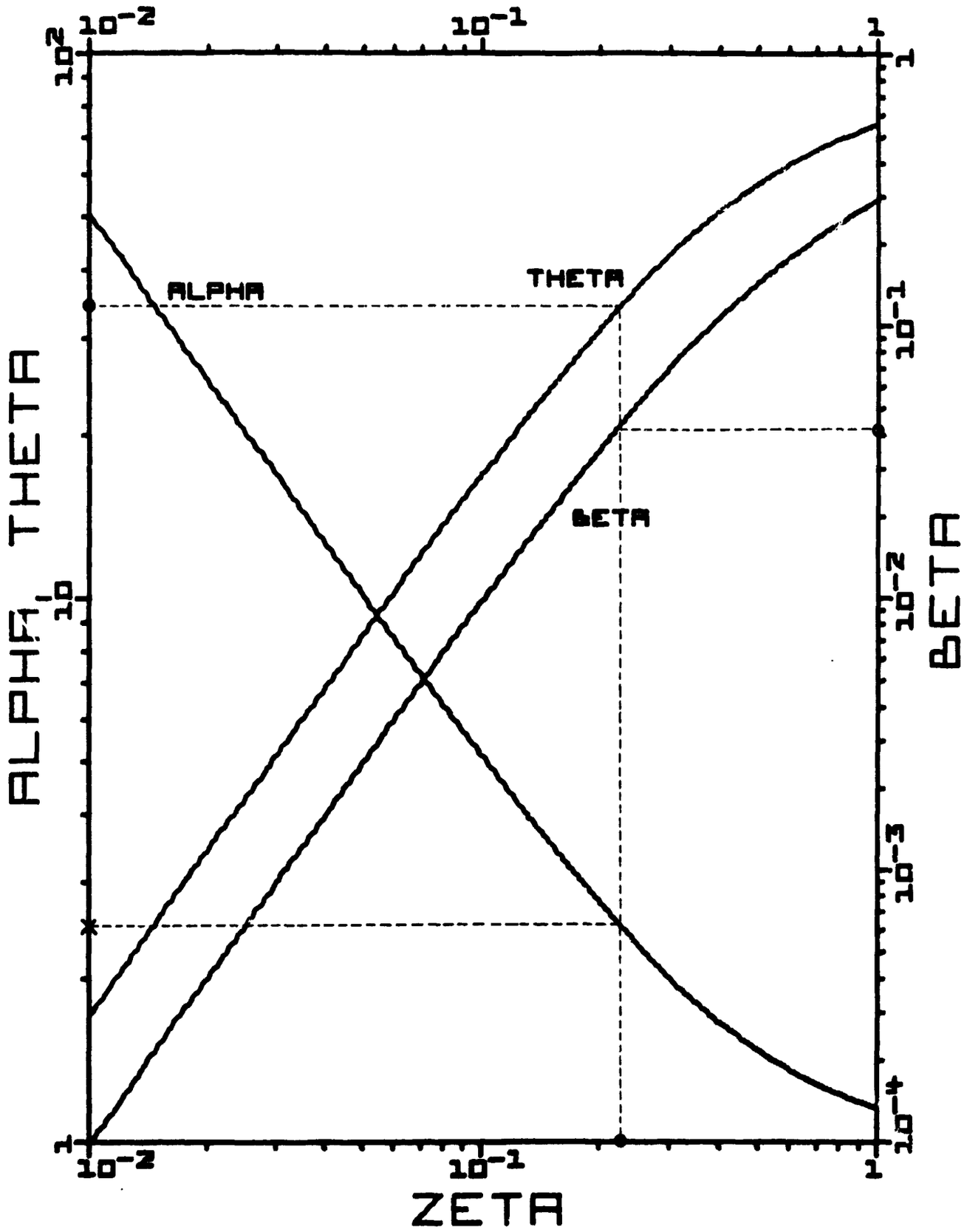

Fig. C2 Response of a Base Excitation System at Resonance

APPENDIX D

MECHANICAL MODEL ANALOGIES OF ELASTOMER DYNAMIC RESPONSE

During the course of this study, techniques for fitting equivalent mechanical models to elastomer stiffness and damping data were developed. This Appendix describes these techniques. Figure 35 of the report compares the prediction of one such model with the data to which the model was fitted.

Mechanical models simulating viscoelastic behavior of elastomers may be obtained by combining several springs and dashpots in a prescribed fashion. The simplest arrangements are when only one spring and one dashpot are connected either in series or in parallel as shown in Figure D1. The series arrangement is generally called a Maxwell element, while the parallel configuration is termed as a Voigt element. Sometimes the parallel arrangement is also referred to as a Kelvin element, since it was introduced by Kelvin before Voigt. In general, for a solid material, a Maxwell model may be defined by a combination of several Maxwell elements connected in parallel with a spring and a dashpot. Likewise, a general Voigt model may consist of several Voigt elements connected in series with a spring. These models are shown schematically in Figure ... Although several other combinations are possible, Lazan [13] has shown that a large number of arrangements are reducible to either a Maxwell or a Voigt type of model. The analysis for both these models is quite simple. In fact, if the Maxwell model is analyzed in terms of complex stiffness, the analysis will apply directly to the Voigt model when the stiffness function is replaced by compliance.

1. Maxwell Model

Since the force in a spring and the dashpot in a Maxwell element is the same, the model is best analyzed in terms of complex stiffness. Let the model consist of n Maxwell elements connected in parallel with a spring of stiffness k_o, and a dashpot with damping coefficient c_o. Also, let the jth element have a spring of stiffness k_j and a dashpot with a damping coefficient of c_j. For solid materials, k_o will be finite and will correspond to the static stiffness and c_o may be zero. A relaxation time $\tau_j = c_j/k_j$ is a measure of the time required for stress relaxation in the jth Maxwell element. A straightforward algebraic manipulation will show that the complex stiffness of the Maxwell model is described by the function [9]

MAXWELL
ELEMENT

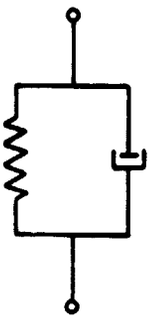

VOIGT
ELEMENT

Fig. D1 Basic Elements of Visco-Elastic Models

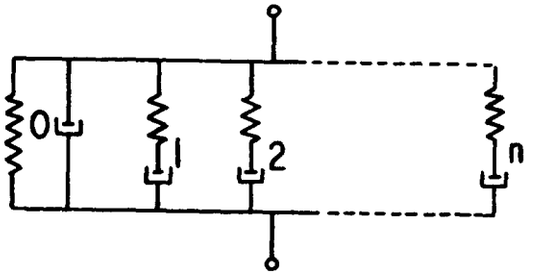

MAXWELL MODEL

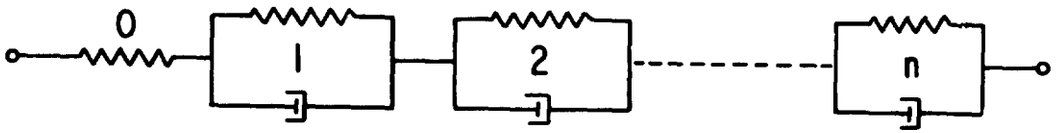

VOIGT MODEL

Fig. D2 Generalized Maxwell and Voigt Models

$$K(\omega) = \left\{ k_o + \sum_{j=1}^{n} \frac{k_j \omega^2 \tau_j^2}{(1 + \omega^2 \tau_j^2)} \right\} + i \left\{ c_o \omega + \sum_{j=1}^{n} \frac{k_j \omega \tau_j}{(1 + \omega^2 \tau_j^2)} \right\} \quad \text{(D1)}$$

For brevity, Equation (D1) is written as

$$K(\omega) = K1(\omega) + i\, K2(\omega) \quad \text{(D2)}$$

where

$$K1(\omega) = k_o + \sum_{j=1}^{n} \frac{k_j \omega^2 \tau_j^2}{1 + \omega^2 \tau_j^2}$$

and (D3)

$$K2(\omega) = c_o \omega + \sum_{j=1}^{n} \frac{k_j \omega \tau_j}{1 + \omega^2 \tau_j^2}$$

If K1 and K2 are determined experimentally as a function of frequency, then Equations (D3) may be used to compute the various model coefficients. A least-squares method may be used to accomplish this task. Let the experimental data be tabulated at frequencies ω_ν, $1 \le \nu \le m$, where m is the total number of data points and also for generality let the functions K1 and K2 be weighted by constants W1 and W2, then the sum of squared deviation (SSD) is defined as

$$SSD = W1 \sum_{\nu=1}^{m} \left[K1_\nu - k_o - \sum_{j=1}^{n} k_j f_j(\omega_\nu) \right]^2 \quad \text{(D4)}$$

$$+W2 \sum_{\nu=1}^{m} \left[K2_\nu - c_o \omega_\nu - \sum_{j=1}^{n} k_j h_j(\omega_\nu) \right]^2$$

where

$$f_j(\omega_\nu) = \frac{\omega_\nu^2 \tau_j^2}{1 + \omega_\nu^2 \tau_j^2} = \frac{1}{1 + \left(\frac{\Omega_j}{\omega_\nu}\right)^2}$$

$$h_j(\omega_\nu) = \frac{1}{1 + \omega_\nu^2 \tau_j^2} = \frac{1}{1 + \left(\frac{\omega_\nu}{\Omega_j}\right)^2}$$

and

$$\Omega_j = \frac{1}{\tau_j}$$

Equation (D4) may be differentiated with respect to all the model coefficients and derivatives set equal to zero for minimum SSD. These resulting equations are to be solved simultaneously for the required coefficients. It is clear that the coefficients k_j appear in a linear fashion but τ_j or Ω_j are nonlinear and are, therefore, determined by iterati. method.

For any set of values for Ω_j, $i \le j \le n$, the linear coefficients k_o, c_o, and k_j, $1 \le j \le n$ are determined by solving the "normal equations" for a conventional linear regression analysis [14].

Differentiation of Equation (D4) with respect to the nonlinear coefficient gives

$$\frac{\partial(SSD)}{\partial\Omega_i} = -2W1 \sum_{\nu=1}^{m} \left[K1_\nu - k_o - \sum_{j=1}^{n} k_j f_j(\omega_\nu) \right] k_i f_i'(\omega_\nu)$$
$$-2W2 \sum_{\nu=1}^{m} \left[K2_\nu - c_o \omega_\nu - \sum_{j=1}^{n} k_j h_j(\omega_\nu) \right] k_i h_i'(\omega_\nu) \qquad \text{(D5)}$$

where

$$f_i' = \frac{\partial f_i}{\partial \Omega_i} \quad \text{and} \quad h_i' = \frac{\partial h_i}{\partial \Omega_i} .$$

For minimum SSD, the derivatives given by the above equations must be zero. Thus, the n simultaneous equations for Ω_j, $1 \le j \le n$ become

$$L_i = - W1 \sum_{\nu=1}^{m} \left[K1_\nu - k_o - \sum_{j=1}^{n} k_j f_j (\omega_\nu) \right] k_i f_i' (\omega_\nu)$$

$$- W2 \sum_{\nu=1}^{m} \left[K2_\nu - c_o \omega_\nu - \sum_{j=1}^{n} k_j h_j (\omega_\nu) \right] k_i h_i' (\omega_\nu) = 0 \qquad \text{(D6)}$$

$$1 \le i \le n$$

The above equations are solved by the Newton-Raphson iteration method. The successive solutions are obtained by inverting the Jacobian matrix.

$$\left[\frac{\partial L_i}{\partial \Omega_k} \right] \left\{ \Omega_{k_{\ell+1}} - \Omega_{k_\ell} \right\} = - \left\{ L_{i_\ell} \right\}_{\substack{1 \le i \le n \\ 1 \le k \le n}} \qquad \text{(D7)}$$

The elements of the Jacobian matrix are derived by straightforward differentiation of Equation (D6)

$$\frac{\partial L_i}{\partial \Omega_j} = W1 \sum_{\nu=1}^{m} k_i f_i' (\omega_\nu) \; k_j f_j' (\omega_\nu)$$

$$+ W2 \sum_{\nu=1}^{m} k_i h_i' (\omega_\nu) \; k_j h_j' (\omega_\nu) \qquad \text{(D8)}$$

$$i \neq j$$

and

$$\frac{\partial L_i}{\partial \Omega_i} = -W1 \sum_{\nu=1}^{m} \left[K1_\nu - k_o - \sum_{j=1}^{n} k_j f_j (\omega_\nu) \right] k_i f_i'' (\omega_\nu)$$

$$+ W1 \sum_{j=1}^{n} \left[k_i f_i' (\omega_\nu) \right]^2$$

$$- W2 \sum_{\nu=1}^{m} \left[K2_\nu - c_o \omega - \sum_{j=1}^{n} k_j h_j (\omega_\nu) \right] k_i h_i'' (\omega_\nu) \qquad \text{(D9)}$$

$$+ W2 \sum_{\nu=1}^{m} k_i h_i' (\omega_\nu)^2$$

where

$$f_i'' = \frac{\partial f_i'}{\partial \Omega_i} \quad \text{and} \quad h_i'' = \frac{\partial h_i'}{\partial \Omega_i} .$$

The various derivatives of functions f and h are derivable by the relations defined in Equations

$$f_i' (\omega) = - \frac{2}{\omega} \frac{\frac{\Omega_i}{\omega}}{\left[1 + \left(\frac{\Omega_i}{\omega} \right)^2 \right]^2}$$

$$f_i'' (\omega) = - \frac{2}{\omega^2} \frac{1 - 3\left(\frac{\Omega_i}{\omega} \right)^2}{\left[1 + \left(\frac{\Omega_i}{\omega} \right)^2 \right]^3} \qquad \text{(D10)}$$

and

$$h_i'(\omega) = \frac{1}{\omega} \frac{1 - \left(\frac{\Omega_i}{\omega}\right)^2}{\left[1 + \left(\frac{\Omega_i}{\omega}\right)^2\right]^2}$$

$$h_i''(\omega) = \frac{2}{\omega^2} \frac{\left(\frac{\Omega_i}{\omega}\right)^3 - 3\left(\frac{\Omega_i}{\omega}\right)}{\left[1 + \left(\frac{\Omega_i}{\omega}\right)^2\right]^3} \qquad \text{(D11)}$$

To summarize the iterative solution procedure the linear parameters, k_o, c_o, k_j, $1 \le j \le n$ are solved for any set of iterates Ω_j, $1 \le j \le n$. The new set of iterates $\Omega_{j\,p+1}$, $1 \le j \le n$ are obtained by solving the linear algebraic Equations (D7).

It should be noted that such a least squares analysis may sometimes result in negative coefficients, which are physically meaningless. Under these conditions, it might seem reasonable to guess the possible relaxation frequencies from the trend of the data and determine the linear parameters by carrying out a simple linear regression.

In order to judge the reasonable values of Ω_j, $1 \le j \le n$, the qualitative trends of Equation (D4) must be examined. It is clear that K1 is formed by linear superposition of f_j and K2 is obtained by superposing the functions h_j. The functions f and h are plotted as functions of ω/Ω in Figure D3. Thus, superposing f_j over a static stiffness k_o will result in an increasing K1 as a function of frequency. In the case of K2, some maxima or minima may be observed, depending on the values of Ω_j. If $n = 1$, then clearly K2 will peak at $\omega = \Omega_1$. If $n = 2$ and Ω_1 and Ω_2 are quite far apart, then a minimum will be observed in K2 at ω somewhere between Ω_1 and Ω_2. If $n = 2$ and Ω_1 and Ω_2 are quite close, then a maximum will be observed in K2 at ω somewhere between Ω_1 and Ω_2. A non-zero value for coefficient c_o clearly indicates a linear increase in K2 with frequency. If no such trend is present in the data, c_o may be set equal to zero. These qualitative trends will establish the possible values of Ω_j, $1 \le j \le n$, and also might help determine the number of elements, n, required in a model to fit the experimental data.

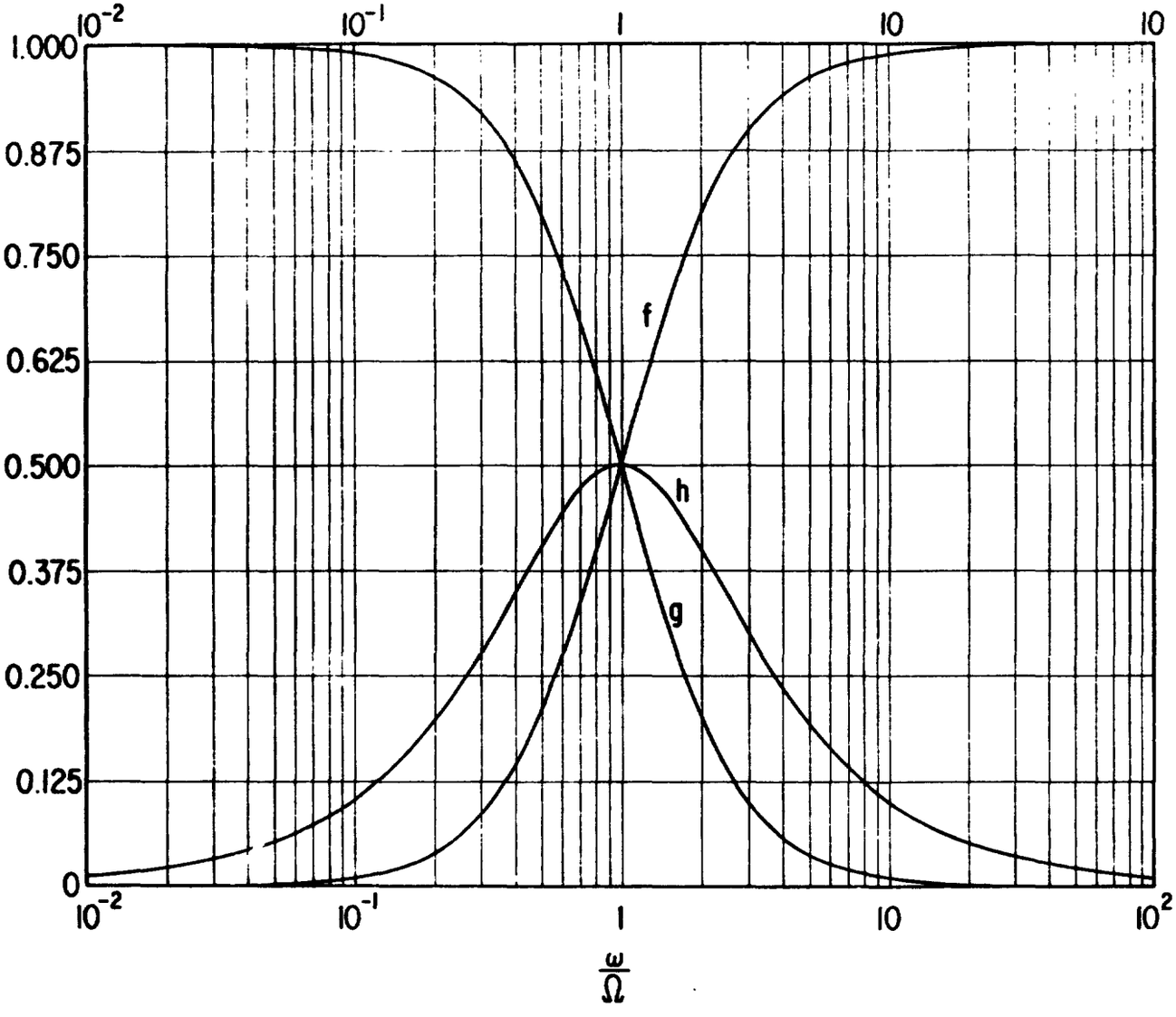

Fig. D3 Characteristic Functions Defining the Behavior of Visco-Elastic Models

2. Voigt Model

As shown in Figure D2 let a generalized Voigt model be defined by n Voigt elements connected in series with a spring of stiffness k_o. Also, let the jth element have a spring of stiffness k_j and a dashpot with damping coefficient c_j. If this model is applied to solid materials, and if the static spring with stiffness k_o is not present then the springs in all elements must have non-zero stiffness. This model is best analyzed in terms of complex compliance $H(\omega)$ which may be expressed as [9].

$$H(\omega) = \left\{ b_o + \sum_{j=1}^{n} \frac{b_j}{1 + \omega^2 \tau_j^2} \right\} - i \left\{ \sum_{j=1}^{n} \frac{b_j \omega \tau_j}{1 + \omega^2 \tau_j^2} \right\} \qquad (D12)$$

where

$$b_o = 1/k_o , \quad b_j = 1/k_j \quad \text{and} \quad \tau_j = c_j/k_j$$

The time τ_j in this case, is generally called retardation time since it is a measure of time required for the extension of the spring, in the Voigt element, to its equilibrium length while retarded by the dashpot.

Equation (D12) for brevity may be expressed as

$$H(\omega) = H1(\omega) - i\, H2(\omega) \qquad (D13)$$

where

$$H1(\omega) = b_o + \sum_{j=1}^{n} b_j\, g_j(\omega)$$

$$H2(\omega) = \sum_{j=1}^{n} b_j\, h_j(\omega) \qquad (D14)$$

$$g_j(\omega) = \frac{1}{1 + \omega^2 \tau_j^2}$$

and h_j is same as defined in Equation (D4).

It is clearly noted that Equation (D14) is similar to Equation (D3) with $c_o = 0$. In fact, if k_o, k_j, f_j, $1 \le j \le n$, and $K1_\nu$, $K2_\nu$, $1 \le \nu \le m$ in Equation (D3) are respectively replaced by b_o, b_j, g_j, $1 \le j \le n$, and $H1_\nu$, $H2_\nu$, $1 \le \nu \le m$, then the resulting equation will be identical to Equation (D14). Thus, all the analysis outlined for the Maxwell model is also applicable in the case of the Voigt model.

The derivatives of the function g_j are easily obtained

$$g_j'(\omega) = \frac{dg_j}{d\Omega_j} = \frac{2}{\omega} \frac{\frac{\Omega_j}{\omega}}{\left[1 + \left(\frac{\Omega_j}{\omega}\right)^2\right]^2}$$

$$g_j''(\omega) = \frac{dg_j'}{d\Omega_j} = \frac{2}{\omega^2} \frac{1 - 3\left(\frac{\Omega_j}{\omega}\right)^2}{\left[1 + \left(\frac{\Omega_j}{\omega}\right)^2\right]^3} \qquad \text{(D15)}$$

All the qualitative features described in the case of the Maxwell model are also relevant here when the experimental data is plotted in terms of complex compliance. However, the function g_j must be used instead of f_j. This is also plotted in Figure D3.

NOMENCLATURE

A	Cross sectional area of elastomer specimen (m^2)
A_1	Input, shaker table amplitude (m)
A_2	Output, resonant mass amplitude (m)
a	Height of elastomer specimen (m)
b	Thickness of shear specimen (m)
c	Damping coefficient (N-sec/m)
c_c	Critical damping (see Equation C1, Appendix C) (N-sec/m)
c_e	Elastomer damping coefficient (N-sec/m)
c_ℓ	Lower cylinder damping coefficients (N-sec/m)
c_o	Damping as defined in viscoelastic models in Appendix D (N-sec/m)
c_u	Upper cylinder damping coefficient (N-sec/m)
c_1, c_2	Variable damping coefficients as defined in Table 1 (N-sec/m)
d	Diameter of compression specimen (m)
E	Young's Modulus of Elasticity (N/m^2)
F	Static Force (N)
f,g,h	Characteristic functions defined in Appendix D
G	Shear modulus of the material (N/m^2)
H	Complex compliance ($= H1 - iH2$) (m/N)
i	Imaginary unit ($= \sqrt{-1}$)
K	Complex stiffness ($= K1 + iK2$) (N/m)
k	Dynamic stiffness (N/m)
k_e	Elastomer dynamic stiffness (N/m)
k_ℓ	Stiffness of lower cylinder (N/m)
k_m	Stiffness of mechanical spring (N/m)

k_o	Static stiffness defined in viscoelastic models in Appendix D (N/m)
k_u	Stiffness of upper cylinder (N/m)
k_s	Stiffness of guide bearings (N/m)
k_{st}	Static stiffness of elastomer specimen (N/m)
m	Resonant mass (kg)
m_{acc}	Equivalent mass of accelerometer (kg)
m_m	Equivalent mass of mechanical spring (kg)
$m_{p\ell}$	Equivalent mass of lower piston (kg)
m_{pu}	Equivalent mass of upper piston (kg)
m_s	Mass of the hub in the guide bearing (kg)
S	Shape factor
s	Shore A hardness
t	Time (sec)
u	Dimensionless stiffness
v	Dimensionless damping
W1,W2	Weights used in least squares analysis
w	Width of shear specimen (m)
z	Height of shear specimen (m)
α	Transmissibility (= $\left\|A_2/A_1\right\|$)
β	Defined in Equation (C5) of Appendix C
δ	Static deflection (m)
ϵ	Strain (= 1 - λ)
ζ	Damping ratio as defined in Equation (C1) of Appendix C
λ	Ratio of strained to unstrained length
σ	Stress (N/m^2)

τ	Relaxation or retardation time (sec)
φ	Phase angle (degree)
$\bar{\Omega}$	Dimensionless frequency
ω_m	Natural frequency of mechanical spring (rad/sec)
ω_n	Natural frequency (rad/sec)
ω_s	Natural frequency of guide bearings (rad/sec)
ω,Ω	Frequency (rad/sec)

REFERENCES

1. Chiang, T., Tessarzik, J.M., and Badgley, R.H., "Development of Procedures for Calculating Stiffness and Damping Properties of Elastomers in Engineering Applications - Part I: Verification of Basic Methods, NASA Contractor Report CR-120965, Prepared by Mechanical Technology Incorporated for NASA-Lewis Research Center under Contract NAS3-15334, March 1972.

2. Miller, H.E., "Dynamic Property Measurement of Elastomers and Elastomeric Mounts-Past, Present, and Future", Paper No. 730256, SAE/ASTM Sym., "The Measurement of the Dynamic Properties of Elastomer Properties of Elastomer and Elastomeric Mounts" Det., Michigan, January 1973.

3. Larsen, R.T., "Dynamic Versus Static Spring Rates for Vibration Mounts", SAE Trans. Paper No. 660599, 1966, 193-200.

4. Cardillo, R.M., "Dynamic Testing of Elastomer Mountings", J. Appl. Poly. Sc. 8, 1964, 53-71.

5. Meyer, D.A. and Sommer, J.G., "The Effect of Compositional and Testing Variations on the Dynamic Properties of Compounds Based on Styrene-Butadiene and Polybutadiene Elastomers", Rubber Chem. Tech. 44, 1971, 258-270.

6. Sommer, J.G., and Meyer, D.A., "Factors Controlling the Dynamic Properties of Elastomeric Products", Paper No. 730267 SAE/ASTM Sym., "The Measurement of the Dynamic Properties of Elastomer and Elastomeric Mounts", Detroit, Michigan, January 1973.

7. Hodgman, C.D., Editor, HANDBOOK OF CHEMISTRY AND PHYSICS, Chemical Rubber Publishing Co., 40th Edition, 1958-59, 1553.

8. DenHartog, J.P., MECHANICAL VIBRATIONS, McGraw-Hill Book Company, 1965.

9. Ferry, J.D., VISCOELASTIC PROPERTIES OF POLYMERS, John Wiley and Sons, 1970.

10. Payne, A.R., and Scott, J.R., ENGINEERING DESIGN WITH RUBBER, Interscience Publishers, New York.

11. Gent, A.N., "On the Relation Between Indenation Hardness and Youngs Modulus", Rubber Chem. Tech., 31, 1958, 896-905.

12. Thompson, W.T., VIBRATION THEORY AND APPLICATIONS, Prentice Hall, 1965.

13. Lazan, B.J., DAMPING OF MATERIALS AND MEMBERS IN STRUCTURAL MECHANICS, Pergamon Press, 1968.

14. Hald, A., STATISTICAL THEORY WITH ENGINEERING APPLICATIONS, John Wiley and Sons, 1952.

NASA-Lewis Research Center
21000 Brookpark Road
Cleveland, OH 44135

Attention: Project Manager, M.S. 6-1
A. Ginsburg, M.S. 5-3
W. Loomis, M.S. 23-2
W. Anderson, M.S. 23-2
R. Johnson, M.S. 23-2
S. Himmel, M.S. 3-5
B. Lubarsky, M.S. 3-3
L. Schopen, M.S. 500-206
C. H. Wintig, M.S. 5-3
N. Musial, M.S. 500-113
Report Control Office, M.S. 505
Library, M.S. 60-3 (2 copies)
Reliability & Quality Assurance
Office, M.S. 500-111
Technology Utilization Office, M.S. 3-19
Plans & Programs Office, M.S. 3-15

NASA Scientific & Technical
Information Facility (10 copies)
Attn: Acquisitions Branch (SQT-34054)
P. O. Box 33
College Park, MD 20740

NASA Ames Research Center
Attn: Library
Moffett Field, CA 94035

NASA Flight Research Center
Attn: Library
P. O. Box 273
Edwards, CA 93523

NASA Goddard Space Flight Center
Attn: Library
Greenbelt, MD 20771

Jet Propulsion Laboratory
Attn: Library
4800 Oak Grove Drive
Pasadena, CA 91103

NASA Langley Research Center
Attn: Library
Langley Station
Hampton, VA 23365

NASA Manned Spacecraft Center
Attn: Library
Houston, TX 77058

NASA Marshall Space Flight Center
Attn: Library
Marshall Space Flight Center, AL 35812

NASA Headquarters
Washington, D.C 20546
Attn: RLC/D. Miller (2 copies)
RLC/N.F. Rekos

Atomic Energy Commission
Attn: N. Gerstein
AEC-NASA Space Nuclear Propulsion Office
Washington, DC 20545

Battelle Memorial Institute
Columbus Laboratories
505 King Avenue
Columbus, OH 43201
Attn: C.M. Allen
J.W. Kannel
Library

General Electric Company
Attn: C. C. Moore
Gas Turbine Engineering Division
Schenectady, NY 12306

Industrial Tectonics, Inc.
18301 Santa Fe Avenue
Compton, CA 90024
Attn: H. Hanau
H. Signer (6 copies)

Mechanical Technology Incorporated
Attn: Library
968 Albany-Shaker Road
Latham, NY 12110

Pure Carbon Company
Attn: J. J. Sherlock
MAIC Division
441 Hall Avenue
St. Mary, PA 15857

National Science Foundation
Attn: Library
Engineering Division
1800 G. Street, N.W.
Washington, DC 20540

Naval Ship Engineering Center
Attn: W. C. Lindstrom NSC 613D4B
Washington, DC 20360

Naval Ship Research & Development Center
Attn: W. V. Smith
Annapolis Division
Annapolis, MD 21402

Naval Ship Systems Command
Attn: J. E. Dray SNHIP 6148
Washington, DC 20360

North American Rockwell
Attn: Myles Butner
Power Systems Divisions
6633 Canoga Avenue
Canoga Park, CA 91304

North American Rockwell Corporation
Attn: Library
Space Division
12214 Lakewood Boulevard
Downey, CA 90241

Office of Naval Research
Attn: S. W. Doroff ONR/463
Washington, D.C. 20360

Rensselaer Polytechnic Institute
Attn: F. F. Ling
Mechanics Division
Troy, NY 12181

AVSCOM
Attn: E. J. Hollman, AMSAV-11
Director Product Assurance
P. O. Box 209
St. Louis, MO 63012

SKF Industries, Incorporated
Engineering and Research Center
1100 First Avenue
King of Prussia, PA 19406
Attn: T. Tallian
A. Troiani
L. Sibley

TRW Marlin Rockwell Division
Attn: A. S. Irwin
402 Chandler Street
Jamestown, NY 14701

United Aircraft Corporation
Pratt & Whitney Aircraft Division
400 Main Street
East Hartford, CT 06108
Attn: F. H. Mahler
P. Holmes
Library
P. Brown
R. Shevchenko

U. S. Army Air Mobility R&D Laboratory
Eustis Directorate
Commanding Officer (SAV DL-EU-PP)
Fort Eustis, VA 23604
Attn: J. White
L. Bartone
R. Givens

NAVAIRSYSCOMHQ
Attn: H. Lewis, AIR 53645A
Department of the Navy
Washington, DC 20360

AVCO Lycoming Division
Attn: R. P. Cuny
Manager, Machanical Components
Stratford, CT 06497

AFAPL-SFL
Wright-Patterson Air Force Base, OH 45433
Attn: J. Jenkins
E. Lake

Office of Naval Research
Attn: Lt. Richard Miller, Code 463
800 N. Quincy Street
Arlington, VA 22217

Northwestern University
Department of Mechanical Engineering
and Astronautical Science
Evanston, IL 60201
Attn: Dr. R. Burton
Dr. H.S. Cheng

Sunstrand Denver
Attn: Library
2480 West 70 Avenue
Denver, CO 80221

TRW Accessories Division
Attn: Library
2355 Euclid Avenue
Cleveland, OH 44117

U.S. Army Engineering R&D Labs
Atten: W. Crim
Gas Turbine Test Facility
Fort Belvoir, VA 22060

United Aircraft Corporation
Sikorsky Aircraft Division
Attn: Lester Burroughs
Stratford, CT 06497

Southwest Research Institute
Attn: P. M. Ku
Technical Vice President
P. O. Drawer 28510
San Antonio, TX 78284

Aerospace Corporation
Attn: Library
P. O. Box 95085
Los Angeles, CA 91745

AiResearch Manufacturing Company
402 South 36 Street
Phoenix, AZ 85034
Attn: Library
Lyle Six

Bendix Research Labs Division
Attn: Library
Detroit, MI 48232

Boeing Company
Aerospace Division
Attn: Library
P. O. Box 3707
Seattle, WA 98124

Boeing Company
Vertol Division, Boeing Center
P. O. Box 16858
Philadelphia, PA 19142
Attn: Library
A. J. Lemanski

Continental Aviation & Engineering Corp.
Attn: Library
12700 Kercheval Avenue
Detroit, MI 48215

Curtiss-Wright Corporation
Wright Aero Division
Attn: Library
Main & Passaic Streets
Woodridge, NJ 07075

Fafnir Bearing Company
Attn: R. J Matt
37 Booth Street
New Britain, CT 06050

Franklin Institute Research Labs
Benjamin Franklin Pkwy, at 20th Street
Philadelphia, PA 19103
Attn: W. Shapiro
J. Rumbarger

General Electric Company
Attn: Library
Mechanical Technology Laboratory
R&D Center
Schenectady, NY 12301

General Motors Corporation
Attn: Library
Detroit-Allison Division
Indianapolis, IN 46206

General Motors Corporation
Attention: W. Kacmarsky
New Departure-Hyatt Division
Hayes Avenue (Route 4)
Sandusky, OH 44871

Hughes Aircraft Corporation
Attn: Library
Centinela & Teale Avenue
Culver City, CA 90230

Institute for Defense Analyses
Attn: Library
400 Army-Navy Drive
Arlington, VA 22202

Lockheed Missiles & Space Company
Attn: Library
P. O. Box 504
Sunnyvale, CA 94088

Massachusetts Institute of Technology
Attn: Library
Cambridge, MA 02139

AiResearch Manufacturing Company
Attn: Library
9851 Sepulveda Boulevard
Los Angeles, CA 90009

Materials Science Copr.
Blue Bell Office Campus
Merion Tower Building
Blue Bell, PA 19422

Shaker Research Corp.
Attn: Dr. C.H.T. Pan
Northway 10 Executive Park
Ballston Lake, NY 12019

Marlin-Rockwell Company
Attn: Anthony T. Galbato
Division of TRW, Inc.
402 Chandler Street
Jamestown, NY 14701

General Electric Co.
Attn: Dr. Alfred J. Martenson
P. O. Box 8, Malta Site
Schenectady, NY 12301

Naval Air Systems Command
Attn: S. M. Collegeman AIR 5365A
Washington, DC 20360